PROCEEDINGS OF SCIENCE

The IceCube Neutrino Observatory

Contributions to ICRC 2015 Part IV: Searches for Dark Matter and Exotic Particles

The IceCube Collaboration

Contents

The 34th International Cosmic Ray Conference,
30 July- 6 August, 2015
The Hague, The Netherlands

IceCube Collaboration Member List

M. G. Aartsen[2], K. Abraham[32], M. Ackermann[48], J. Adams[15], J. A. Aguilar[12], M. Ahlers[29], M. Ahrens[39], D. Altmann[23], T. Anderson[45], I. Ansseau[12], M. Archinger[30], C. Arguelles[29], T. C. Arlen[45], J. Auffenberg[1], X. Bai[37], S. W. Barwick[26], V. Baum[30], R. Bay[7], J. J. Beatty[17,18], J. Becker Tjus[10], K.-H. Becker[47], E. Beiser[29], S. BenZvi[29], P. Berghaus[48], D. Berley[16], E. Bernardini[48], A. Bernhard[32], D. Z. Besson[27], G. Binder[8,7], D. Bindig[47], M. Bissok[1], E. Blaufuss[16], J. Blumenthal[1], D. J. Boersma[46], C. Bohm[39], M. Börner[20], F. Bos[10], D. Bose[41], S. Böser[30], O. Botner[46], J. Braun[29], L. Brayeur[13], H.-P. Bretz[48], N. Buzinsky[22], J. Casey[5], M. Casier[13], E. Cheung[16], D. Chirkin[29], A. Christov[24], K. Clark[42], L. Classen[23], S. Coenders[32], D. F. Cowen[45,44], A. H. Cruz Silva[48], J. Daughhetee[5], J. C. Davis[17], M. Day[29], J. P. A. M. de André[21], C. De Clercq[13], E. del Pino Rosendo[30], H. Dembinski[33], S. De Ridder[25], P. Desiati[29], K. D. de Vries[13], G. de Wasseige[13], M. de With[9], T. DeYoung[21], J. C. Díaz-Vélez[29], V. di Lorenzo[30], J. P. Dumm[39], M. Dunkman[45], R. Eagan[45], B. Eberhardt[30], T. Ehrhardt[30], B. Eichmann[10], S. Euler[46], P. A. Evenson[33], O. Fadiran[29], S. Fahey[29], A. R. Fazely[6], A. Fedynitch[10], J. Feintzeig[29], J. Felde[16], K. Filimonov[7], C. Finley[39], T. Fischer-Wasels[47], S. Flis[39], C.-C. Fösig[30], T. Fuchs[20], T. K. Gaisser[33], R. Gaior[14], J. Gallagher[28], L. Gerhardt[8,7], K. Ghorbani[29], D. Gier[1], L. Gladstone[29], M. Glagla[1], T. Glüsenkamp[48], A. Goldschmidt[8], G. Golup[13], J. G. Gonzalez[33], D. Góra[48], D. Grant[22], J. C. Groh[45], A. Groß[32], C. Ha[8,7], C. Haack[1], A. Haj Ismail[25], A. Hallgren[46], F. Halzen[29], B. Hansmann[1], K. Hanson[29], D. Hebecker[9], D. Heereman[12], K. Helbing[47], R. Hellauer[16], D. Hellwig[1], S. Hickford[47], J. Hignight[21], G. C. Hill[2], K. D. Hoffman[16], R. Hoffmann[47], K. Holzapfel[32], A. Homeier[11], K. Hoshina[29,a], F. Huang[45], M. Huber[32], W. Huelsnitz[16], P. O. Hulth[39], K. Hultqvist[39], S. In[41], A. Ishihara[14], E. Jacobi[48], G. S. Japaridze[4], K. Jero[29], M. Jurkovic[32], B. Kaminsky[48], A. Kappes[23], T. Karg[48], A. Karle[29], M. Kauer[29,34], A. Keivani[45], J. L. Kelley[29], J. Kemp[1], A. Kheirandish[29], J. Kiryluk[40], J. Kläs[47], S. R. Klein[8,7], G. Kohnen[31], R. Koirala[33], H. Kolanoski[9], R. Konietz[1], A. Koob[1], L. Köpke[30], C. Kopper[22], S. Kopper[47], D. J. Koskinen[19], M. Kowalski[9,48], K. Krings[32], G. Kroll[30], M. Kroll[10], J. Kunnen[13], N. Kurahashi[36], T. Kuwabara[14], M. Labare[25], J. L. Lanfranchi[45], M. J. Larson[19], M. Lesiak-Bzdak[40], M. Leuermann[1], J. Leuner[1], L. Lu[14], J. Lünemann[13], J. Madsen[38], G. Maggi[13], K. B. M. Mahn[21], R. Maruyama[34], K. Mase[14], H. S. Matis[8], R. Maunu[16], F. McNally[29], K. Meagher[12], M. Medici[19], A. Meli[25], T. Menne[20], G. Merino[29], T. Meures[12], S. Miarecki[8,7], E. Middell[48], E. Middlemas[29], L. Mohrmann[48], T. Montaruli[24], R. Morse[29], R. Nahnhauer[48], U. Naumann[47], G. Neer[21], H. Niederhausen[40], S. C. Nowicki[22], D. R. Nygren[8], A. Obertacke[47], A. Olivas[16], A. Omairat[47], A. O'Murchadha[12], T. Palczewski[43], H. Pandya[33], L. Paul[1], J. A. Pepper[43], C. Pérez de los Heros[46], C. Pfendner[17], D. Pieloth[20], E. Pinat[12], J. Posselt[47], P. B. Price[7], G. T. Przybylski[8], J. Pütz[1], M. Quinnan[45], C. Raab[12], L. Rädel[1], M. Rameez[24], K. Rawlins[3], R. Reimann[1], M. Relich[14], E. Resconi[32], W. Rhode[20], M. Richman[36], S. Richter[29], B. Riedel[22], S. Robertson[2], M. Rongen[1], C. Rott[41], T. Ruhe[20], D. Ryckbosch[25], S. M. Saba[10], L. Sabbatini[29], H.-G. Sander[30], A. Sandrock[20], J. Sandroos[30], S. Sarkar[19,35], K. Schatto[30], F. Scheriau[20], M. Schimp[1], T. Schmidt[16], M. Schmitz[20], S. Schoenen[1], S. Schöneberg[10], A. Schönwald[48], L. Schulte[11], D. Seckel[33], S. Seunarine[38], R. Shanidze[48], M. W. E. Smith[45], D. Soldin[47], M. Song[16], G. M. Spiczak[38], C. Spiering[48], M. Stahlberg[1], M. Stamatikos[17,b], T. Stanev[33], N. A. Stanisha[45], A. Stasik[48], T. Stezelberger[8], R. G. Stokstad[8], A. Stößl[48], R. Ström[46], N. L. Strotjohann[48], G. W. Sullivan[16], M. Sutherland[17], H. Taavola[46], I. Taboada[5], S. Ter-Antonyan[6], A. Terliuk[48], G. Tešić[45], S. Tilav[33], P. A. Toale[43], M. N. Tobin[29], S. Toscano[13], D. Tosi[29], M. Tselengidou[23], A. Turcati[32], E. Unger[46], M. Usner[48], S. Vallecorsa[24], J. Vandenbroucke[29], N. van Eijndhoven[13],

S. Vanheule[25], J. van Santen[29], J. Veenkamp[32], M. Vehring[1], M. Voge[11], M. Vraeghe[25], C. Walck[39], A. Wallace[2], M. Wallraff[1], N. Wandkowsky[29], Ch. Weaver[22], C. Wendt[29], S. Westerhoff[29], B. J. Whelan[2], N. Whitehorn[29], C. Wichary[1], K. Wiebe[30], C. H. Wiebusch[1], L. Wille[29], D. R. Williams[43], H. Wissing[16], M. Wolf[39], T. R. Wood[22], K. Woschnagg[7], D. L. Xu[43], X. W. Xu[6], Y. Xu[40], J. P. Yanez[48], G. Yodh[26], S. Yoshida[14], M. Zoll[39]

[1]III. Physikalisches Institut, RWTH Aachen University, D-52056 Aachen, Germany
[2]Department of Physics, University of Adelaide, Adelaide, 5005, Australia
[3]Dept. of Physics and Astronomy, University of Alaska Anchorage, 3211 Providence Dr., Anchorage, AK 99508, USA
[4]CTSPS, Clark-Atlanta University, Atlanta, GA 30314, USA
[5]School of Physics and Center for Relativistic Astrophysics, Georgia Institute of Technology, Atlanta, GA 30332, USA
[6]Dept. of Physics, Southern University, Baton Rouge, LA 70813, USA
[7]Dept. of Physics, University of California, Berkeley, CA 94720, USA
[8]Lawrence Berkeley National Laboratory, Berkeley, CA 94720, USA
[9]Institut für Physik, Humboldt-Universität zu Berlin, D-12489 Berlin, Germany
[10]Fakultät für Physik & Astronomie, Ruhr-Universität Bochum, D-44780 Bochum, Germany
[11]Physikalisches Institut, Universität Bonn, Nussallee 12, D-53115 Bonn, Germany
[12]Université Libre de Bruxelles, Science Faculty CP230, B-1050 Brussels, Belgium
[13]Vrije Universiteit Brussel, Dienst ELEM, B-1050 Brussels, Belgium
[14]Dept. of Physics, Chiba University, Chiba 263-8522, Japan
[15]Dept. of Physics and Astronomy, University of Canterbury, Private Bag 4800, Christchurch, New Zealand
[16]Dept. of Physics, University of Maryland, College Park, MD 20742, USA
[17]Dept. of Physics and Center for Cosmology and Astro-Particle Physics, Ohio State University, Columbus, OH 43210, USA
[18]Dept. of Astronomy, Ohio State University, Columbus, OH 43210, USA
[19]Niels Bohr Institute, University of Copenhagen, DK-2100 Copenhagen, Denmark
[20]Dept. of Physics, TU Dortmund University, D-44221 Dortmund, Germany
[21]Dept. of Physics and Astronomy, Michigan State University, East Lansing, MI 48824, USA
[22]Dept. of Physics, University of Alberta, Edmonton, Alberta, Canada T6G 2E1
[23]Erlangen Centre for Astroparticle Physics, Friedrich-Alexander-Universität Erlangen-Nürnberg, D-91058 Erlangen, Germany
[24]Département de physique nucléaire et corpusculaire, Université de Genève, CH-1211 Genève, Switzerland
[25]Dept. of Physics and Astronomy, University of Gent, B-9000 Gent, Belgium
[26]Dept. of Physics and Astronomy, University of California, Irvine, CA 92697, USA
[27]Dept. of Physics and Astronomy, University of Kansas, Lawrence, KS 66045, USA
[28]Dept. of Astronomy, University of Wisconsin, Madison, WI 53706, USA
[29]Dept. of Physics and Wisconsin IceCube Particle Astrophysics Center, University of Wisconsin, Madison, WI 53706, USA
[30]Institute of Physics, University of Mainz, Staudinger Weg 7, D-55099 Mainz, Germany

[31]Université de Mons, 7000 Mons, Belgium
[32]Technische Universität München, D-85748 Garching, Germany
[33]Bartol Research Institute and Dept. of Physics and Astronomy, University of Delaware, Newark, DE 19716, USA
[34]Dept. of Physics, Yale University, New Haven, CT 06520, USA
[35]Dept. of Physics, University of Oxford, 1 Keble Road, Oxford OX1 3NP, UK
[36]Dept. of Physics, Drexel University, 3141 Chestnut Street, Philadelphia, PA 19104, USA
[37]Physics Department, South Dakota School of Mines and Technology, Rapid City, SD 57701, USA
[38]Dept. of Physics, University of Wisconsin, River Falls, WI 54022, USA
[39]Oskar Klein Centre and Dept. of Physics, Stockholm University, SE-10691 Stockholm, Sweden
[40]Dept. of Physics and Astronomy, Stony Brook University, Stony Brook, NY 11794-3800, USA
[41]Dept. of Physics, Sungkyunkwan University, Suwon 440-746, Korea
[42]Dept. of Physics, University of Toronto, Toronto, Ontario, Canada, M5S 1A7
[43]Dept. of Physics and Astronomy, University of Alabama, Tuscaloosa, AL 35487, USA
[44]Dept. of Astronomy and Astrophysics, Pennsylvania State University, University Park, PA 16802, USA
[45]Dept. of Physics, Pennsylvania State University, University Park, PA 16802, USA
[46]Dept. of Physics and Astronomy, Uppsala University, Box 516, S-75120 Uppsala, Sweden
[47]Dept. of Physics, University of Wuppertal, D-42119 Wuppertal, Germany
[48]DESY, D-15735 Zeuthen, Germany
[a]Earthquake Research Institute, University of Tokyo, Bunkyo, Tokyo 113-0032, Japan
[b]NASA Goddard Space Flight Center, Greenbelt, MD 20771, USA

Acknowledgment: We acknowledge the support from the following agencies: U.S. National Science Foundation-Office of Polar Programs, U.S. National Science Foundation-Physics Division, University of Wisconsin Alumni Research Foundation, the Grid Laboratory Of Wisconsin (GLOW) grid infrastructure at the University of Wisconsin - Madison, the Open Science Grid (OSG) grid infrastructure; U.S. Department of Energy, and National Energy Research Scientific Computing Center, the Louisiana Optical Network Initiative (LONI) grid computing resources; Natural Sciences and Engineering Research Council of Canada, WestGrid and Compute/Calcul Canada; Swedish Research Council, Swedish Polar Research Secretariat, Swedish National Infrastructure for Computing (SNIC), and Knut and Alice Wallenberg Foundation, Sweden; German Ministry for Education and Research (BMBF), Deutsche Forschungsgemeinschaft (DFG), Helmholtz Alliance for Astroparticle Physics (HAP), Research Department of Plasmas with Complex Interactions (Bochum), Germany; Fund for Scientific Research (FNRS-FWO), FWO Odysseus programme, Flanders Institute to encourage scientific and technological research in industry (IWT), Belgian Federal Science Policy Office (Belspo); University of Oxford, United Kingdom; Marsden Fund, New Zealand; Australian Research Council; Japan Society for Promotion of Science (JSPS); the Swiss National Science Foundation (SNSF), Switzerland; National Research Foundation of Korea (NRF); Danish National Research Foundation, Denmark (DNRF)

PROCEEDINGS OF SCIENCE

Search for Gravitino Dark Matter Decay with IceCube Data

The IceCube Collaboration[†]

[†] *http://icecube.wisc.edu/collaboration/authors/icrc15_icecube*

E-mail: japepper@crimson.ua.edu

The IceCube Neutrino Observatory has recently observed a flux of TeV-PeV neutrinos that corresponds to a highly significant excess over atmospheric backgrounds. It has been suggested that these events could originate from the decay of very heavy dark matter. We outline here an analysis of the IceCube data observed in 2011 with respect to the neutrino emission from heavy gravitino dark matter decay in the Galactic Halo.

Corresponding authors: J. Pepper[1]*

[1] *Department of Physics and Astronomy, University of Alabama, Tuscaloosa, AL 35487, USA*

The 34th International Cosmic Ray Conference,
30 July- 6 August, 2015
The Hague, The Netherlands

*Speaker.

1. Introduction

The observational evidence for Dark Matter (DM) is overwhelming, but its true nature remains elusive. One often invoked explanation comes in the form of Weakly Interacting Massive Particles (WIMPs) which have masses in the GeV - 10 TeV range. These particles are expected to accumulate in the center of massive celestial objects like the Earth, the Sun, galaxies or galaxy clusters. As these particles annihilate with each other or decay, an indirect detection is possible via the observation of secondary particles, such as gamma-rays, cosmic rays, or neutrinos.

IceCube is a cubic-kilometer neutrino detector installed in the ice at the geographic South Pole [1] between depths of 1450 m and 2450 m. Detector construction started in 2005 and finished in 2010. Neutrino reconstruction relies on the optical detection of Cherenkov radiation emitted by secondary particles produced in neutrino interactions in the surrounding ice or the nearby bedrock. IceCube has previously conducted searches for WIMP annihilation in various astrophysical objects such as the Sun [2], Galactic Halo [3], and galaxy clusters [4].

However, it has been speculated [5–9] that the recent observed flux of extraterrestrial neutrinos with energies ranging from 30 TeV to 2 PeV [10, 11] could originate from the decay of Very Heavy Dark Matter (VHDM). The observed abundance of DM can be reached if VHDM is produced non-thermally in the early Universe [12, 13]. This type of DM could decay with lifetimes much longer than the age of the Universe, producing neutrinos in the same energy range as the high energy events observed by IceCube [5–9]. One such candidate for VHDM is a heavy gravitino [14]. Neutrinos from decaying gravitino dark matter should arrive with a unique energy spectrum and directional distribution proportional to the dark matter density of the galaxy.

2. Simulation

The observed flux of neutrinos from DM decay depends on the distribution of DM in the Milky Way, its lifetime, and decay spectrum. In the following we will focus on the decay of gravitino DM as outlined in [14] and consider decays into $\gamma\nu$, $Z\nu$, $h\nu$, and $W^+\tau^-$ following the procedure outlined in [14]. Whereas the neutrino from the primary gravitino decay involving a neutral boson produces a line spectrum, the decay of the Z and W bosons as well as the Higgs h and tau τ produces a continuum emission. We consider 100% branching into each decay channel, and model the decay with PYTHIA 6 [15]. The neutrino flux at IceCube resulting from gravitino dark matter is shown in Figure 1 for a dark matter mass of 2 PeV and a lifetime of 10^{28} s.

Simulated neutrino events in IceCube were weighted to represent the spectrum that would result from gravitino decay. This weighting was performed according to the equation for differential flux:

$$\frac{d\Phi}{dE_\nu} = \frac{1}{\tau}\frac{R_{sc}\rho_{sc}}{4\pi m_\chi} J(\psi)\frac{dN}{dE_\nu} \tag{2.1}$$

where τ is the lifetime of the dark matter particle, and dN/dE_ν is the differential neutrino flux produced with PYTHIA. R_{sc} and ρ_{sc} represent the radius of the solar circle and the local dark matter density respectively. The dimensionless factor $J(\psi)$ corresponds to the integral over the line of sight of the dark matter density ρ :

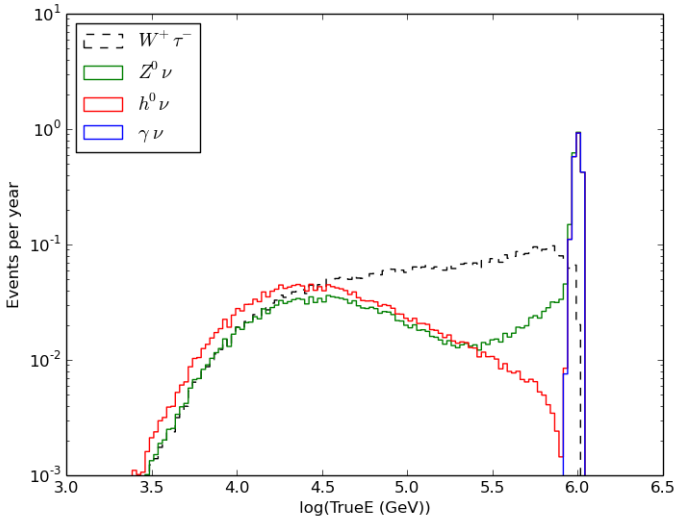

Figure 1: Neutrino spectrum at IceCube produced by 2 PeV decaying gravitino dark matter assuming a lifetime of 10^{28} s and 100% branching into each decay mode.

$$J(\psi) = \int_0^{l_{max}} \frac{\rho(\sqrt{R_{sc}^2 - 2lR_{sc}cos(\psi) + l^2})}{R_{sc}\rho_{sc}} dl \tag{2.2}$$

with

$$l_{max} = \sqrt{R_{MW}^2 - R_{sc}^2 \cdot sin^2(\psi) + R_{sc} \cdot cos(\psi)} \tag{2.3}$$

where R_{MW} is the extent of the Milky Way dark matter halo (40 kpc used in this analysis) and ψ is the angular distance from the galactic center. For this analysis we use the Burkert dark matter profile, as parameterized in [16] to model the matter distribution in the Milky Way:

$$\rho_{Bur} = \rho_H \frac{1}{(1+\frac{r}{R_H})(1+\frac{r^2}{R_H^2})} \tag{2.4}$$

The initial neutrino flavor composition from the decay is not directly observable. One has to account for neutrino oscillation over cosmic distances that result in an oscillation-averaged flavor composition. In general, an arbitrary initial flavor ratio will lead to an oscillation average that is close to an equal distribution between all flavors [17]. For simplicity, we will assume in the following that each neutrino flavor in the gravitino decay spectrum carries 1/3 of the total flux calculated by PYTHIA.

3. Event Selection & Reconstruction

This analysis is based on events that have been previously selected by the High Energy Starting Event (HESE) analysis [10, 11]. The sample consists of events with no more than three photoelectrons (p.e.) out of the first 250 recorded in an outer veto layer of optical modules, as described in [10]. This veto region includes the top 90 m, bottom 10 m, and outermost strings of the detector

as well as a region of high dust concentration known as the “dust layer". Additionally, the event must also produce at least 6000 p.e. to ensure (to 99.999%) that cosmic ray muons would produce enough light in the veto region to be excluded. The HESE sample after three years of observation consists of 36 events (+1 coincident event removed from the sample), whereas only one event per year is expected from atmospheric backgrounds. Assuming an astrophysical E^{-2} power-law spectrum, the excess has a significance of 5.7σ [11].

In order to identify possible spectral features and an anisotropic event arrival distribution expected from gravitino decay in the Galactic Halo, it is necessary to measure the energy and direction of the neutrino flux as accurately as possible. To this end, IceCube has many different methods of reconstructing the energy, position, and direction of the incoming neutrino from the timing and amount of light deposited in the detector at various positions.

At energies in and above the TeV range, neutrinos primarily interact via deep-inelastic scattering, which produces a hadronic shower (cascade) at the interaction vertex. Charged-current interactions, where a charged boson is exchanged, produce a hadronic cascade accompanied by an outgoing lepton. This lepton can trigger an additional electromagnetic cascade in the detector, created by the outgoing electron, tau decay, muon bremsstrahlung, and/or pair production. All neutrino interactions produce cascades with the exception of ν_μ charged-current interactions, which produce a hadronic cascade and an accompanying ‘track’ of light from the bremsstrahlung radiation of the outgoing muon.

The specific cascade reconstruction used in this analysis started with a basic line fit, which reconstructs a track under the assumption that the cascade vertex would lie somewhere along this track. Using this track as a seed, a cascade fitter positioned the vertex along this line to find the most likely position where the interaction occurred in the detector. The best fit vertex was then used as the seed for a more complex reconstruction algorithm which uses a likelihood method for fitting energy, direction, and position simultaneously in order to find the best fit values of these parameters [18].

4. Binned Likelihood Analysis & Sensitivity

The neutrino flux from dark matter decay should be distinguishable from the atmospheric and astrophysical backgrounds by its unique energy spectrum and anisotropic arrival direction. While a limit could be set by counting the neutrinos in regions of energy and direction chosen so as to increase the signal to background ratio, greater sensitivity can be achieved by analyzing the overall shape of the reconstructed energy and direction simultaneously.

For a given two-dimensional histogram of data with respect to reconstructed energy and direction, the event distribution in each bin follows a Poisson distribution. The likelihood is then simply the product of Poisson probabilities for each bin, representing the total probability that the data was produced by the hypothesis. For a given distribution of data, the best-fit hypothesis is the one that maximizes the likelihood.

In order to calculate the sensitivity, the reconstructed energies and directions were binned with bin sizes equal to the width of the resolutions (Figure 2). Pseudodata was generated by sampling of Poisson distributions in each bin, with means given by the particular hypothesis. Using this pseu-

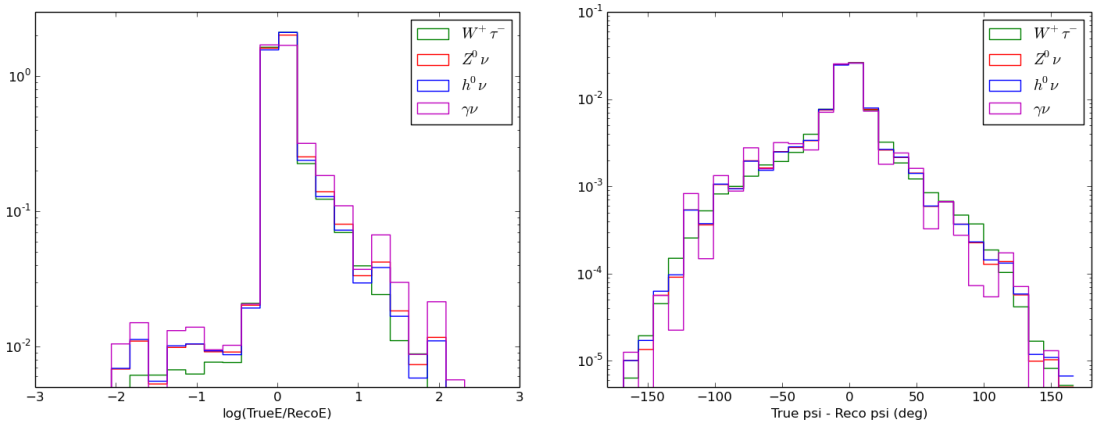

Figure 2: **Left:** Normalized histogram of the energy resolution for the two-body decay modes of a 2 PeV gravitino. The standard deviation was used as the bin size in log(E) for the binned-likelihood sensitivity calculation. **Right:** Similarly to the energy resolution, this plot shows the distribution of angular resolution around the galactic center for a 2 PeV gravitino. Optimal binning for this analysis is currently under study.

dodata, the best fit background-only hypothesis was compared to the best fit background+signal hypothesis using the test statistic (TS):

$$\Lambda = \frac{\mathscr{L}_{sig+bg}}{\mathscr{L}_{bg}} \qquad TS = -2 \cdot ln(\Lambda) \tag{4.1}$$

For this analysis, three likelihoods are considered (described below), which differ only in their interpretation of the background. For each likelihood, pseudodata representing background only sources as well as pseudodata representing background plus a given dark matter signal were generated 1000 times each. For each pseudoexperiment, a test statistic was calculated. This resulted in a distribution of test statistics for background-only pseudodata as well as a distribution of test statistics for background with injected signal. If 90% of the signal+bg TS distribution is above the median of the background-only TS distribution, the detector is said to be sensitive to that signal.

In the first likelihood method, the HESE power law fit to the astrophysical flux ($\Phi_{astro} \propto E^{-2.3\pm0.3}$) is considered to be the background along with neutrinos produced in the atmosphere. The astrophysical flux was allowed to vary within the HESE uncertainties to result in the best fit. This interpretation leads to a sensitivity/limit for the case where none of the events were caused by dark matter decay.

For the second method, the astrophysical background is assumed to be a power law with an unknown spectral index and normalization. This background is then allowed to take on the values which lead to the best fit. This interpretation allows for events to have been created by both the astrophysical flux as well as dark matter decay, and sets the sensitivity/limit accordingly.

Lastly, the third likelihood considers only atmospheric background, and 100% of the events

detected are assumed to be from dark matter decay. The resulting sensitivities for each likelihood method are shown below in Table 1. As expected, decay modes with spectral lines perform better due to the distinct shape of their energy distribution with respect to background sources. The gravitino decay into $\gamma\nu$ gives slightly worse sensitivity than decay into $Z^0\nu$ or $h^0\nu$, which is currently thought to be due to the lack of neutrinos at lower energies.

Table 1: Preliminary sensitivities for 2 PeV gravitino DM using the three likelihood methods

	Lifetime Sensitivity		
Decay Mode	HESE flux + DM	Power law + DM	DM only
$W^+ + \tau^-$	$10^{27.8}$ s	$10^{27.6}$ s	$10^{27.6}$ s
$Z^0 + \nu$	$10^{27.9}$ s	$10^{27.8}$ s	$10^{27.8}$ s
$h^0 + \nu$	$10^{27.9}$ s	$10^{27.7}$ s	$10^{27.8}$ s
$\gamma + \nu$	$10^{27.9}$ s	$10^{27.8}$ s	$10^{27.8}$ s

5. Conclusions

The decay of very heavy dark matter is an interesting hypothesis of the recently observed flux of high-energy neutrinos by IceCube. We have outlined our analysis to study this decay via a maximum likelihood test taking into account the energy and arrival direction of events. For all decay modes, the resulting lifetime sensitivities are approximately 10^{28} s, with the most sensitive decay modes being the ones that produce spectral lines. The next step for this analysis will be to set a limit on the gravitino lifetime using the Feldman-Cousins method for DM masses in the PeV - 10 PeV range.

References

[1] A. Achterberg et al., Astropart. Phys. 26 (2006) 155.

[2] M. G. Aartsen et al. [IceCube Collaboration], Phys. Rev. Lett. 110, 131302 (2013)

[3] R. Abbasi et al. [IceCube Collaboration], Phys. Rev. D 84, 022004 (2011).

[4] M. G. Aartsen et al. [IceCube Collaboration], Phys. Rev. D88 (2013) 122001 (2014).

[5] Arman Esmaili and Pasquale Dario Serpico, JCAP 1311 (2013) 054 [arXiv:1308.1105 [hep-ph]].

[6] Arman Esmaili, Sin Kyu Kang, and Pasquale Dario Serpico, JCAP 12 (2014) 054 [arXiv:1410.5979 [hep-ph]].

[7] Brian Feldstein, Alexander Kusenko, Shigeki Matsumoto, and Tsutomu T. Yanagida, Phys. Rev. D 88, 015004 (2013) [arXiv:1303.7320 [hep-ph]].

[8] Joachim Kopp, Jia Liu, and Xiao-Ping Wang, JHEP 04 (2015) 105 [arXiv:1503.02669 [hep-ph]].

[9] Jesus Zavala Phys. Rev. D 89, 123516 (2014) [arXiv:1404.2932 [astro-ph.HE]].

[10] M. G. Aartsen et al. [IceCube Collaboration], Science 342, 1242856 (2013) [arXiv:1311.5238 [astro-ph.HE]].

[11] M. G. Aartsen et al. [IceCube Collaboration], arXiv:1405.5303 [astro-ph.HE].

[12] M. Cirelli, Pramana 79, 1021 (2012), 1202.1454.

[13] A. Ibarra, D. Tran, and C. Weniger, Int.J.Mod.Phys. A28, 1330040 (2013), 1307.6434.

[14] M. Grefe, arXiv:1111.6779 [astro-ph.HE].

[15] T. Sjöstrand, S. Mrenna, and P. Skands, JHEP 05 (2006) 026 [hep-ph/0603175].

[16] F. Nesti and P. Salucci, arXiv:1304.5127 [astro-ph.GA].

[17] M. G. Aartsen et al. [IceCube Collaboration], Phys. Rev. Lett. 114, 171102 (2015).

[18] M. G. Aartsen et al. [IceCube Collaboration], arXiv:1311.4767 [astro-ph.HE].

PROCEEDINGS OF SCIENCE

New limit for mildly relativistic magnetic monopoles obtained with IceCube

The IceCube Collaboration[†]

[†] *http://icecube.wisc.edu/collaboration/authors/icrc15_icecube*

E-mail: obertacke@uni-wuppertal.de

The existence of magnetic monopoles is a generic prediction of Grand Unified Theories (GUTs). Produced shortly after the Big Bang, these particles carry magnetic charge. Depending on the GUT model, the predicted monopole mass varies from $10^7\,\mathrm{GeV}/c^2$ to $10^{17}\,\mathrm{GeV}/c^2$. Magnetic monopoles could be accelerated to relativistic velocities by intergalactic magnetic fields. Due to these kinetic energies in combination with a moderate energy loss, they can pass through massive objects, such as the Earth, and remain relativistic.

Analogous to an electrical charge, a monopole traveling through IceCube with a velocity above $0.76\,c$ produces direct Cherenkov light. Above $\sim 0.4\,c$, also indirect Cherenkov light is produced via δ-electrons knocked off by the monopole. The Cherenkov light can be detected by the IceCube sensors.

The analysis presented here is distinct from previous searches for relativistic and non-relativistic magnetic monopoles performed by IceCube as it focuses on the intermediate velocity region, $0.4\,c < \beta < 0.76\,c$, using indirect Cherenkov light. We describe the method used in this search, and present the best limit to date in this velocity region, using one year of IceCube data from 2011.

Corresponding author: A. Obertacke Pollmann[*1]

[1] *Dept. of Physics, University of Wuppertal, 42119 Wuppertal, Germany*

The 34th International Cosmic Ray Conference,
30 July- 6 August, 2015
The Hague, The Netherlands

[*]Speaker.

1. Introduction

Magnetic monopoles are particles carrying an isolated magnetic charge, a multiple of the Dirac charge [1] $g = \frac{e}{2\alpha} \approx 68.5e$ where e is the elementary electric charge and α is the fine structure constant. Magnetic monopoles are generic solutions of Grand Unified Theories (GUT) [2, 3]. In this context they would be created in the GUT phase of the universe shortly after the Big Bang. They are one of the most promising candidates for physics beyond the standard model. GUT theories predict particle masses reaching from $10^7\,\mathrm{GeV}/c^2$ to $10^{17}\,\mathrm{GeV}/c^2$. Magnetic monopoles can be accelerated to relativistic velocities in intergalactic magnetic fields.

Water or ice neutrino telescopes, such as IceCube, instrument a large volume and are therefore able to detect rare events. This analysis searches for light signals from magnetic monopoles in the IceCube data recorded from May 2011 to May 2012.

IceCube is a cubic-kilometer neutrino detector installed in the ice at the geographic South Pole [4] between depths of 1450 m and 2450 m. Detector construction started in 2005 and was completed in 2010. Neutrino reconstruction relies on the optical detection of Cherenkov radiation emitted by secondary particles produced in neutrino interactions in the surrounding ice or the nearby bedrock.

Magnetic monopoles faster than the Cherenkov threshold in ice, $v_C \approx 0.76\,c$, emit Cherenkov light. In addition monopoles ionize the surrounding matter, and most of the knocked-off δ-electrons are ejected with energies sufficient to produce Cherenkov light. This mechanism is called indirect Cherenkov light emission and produces light down to a monopole velocity of $\sim 0.4\,c$. The yield of direct and indirect Cherenkov light along a monopole track is shown in Fig. 1.

Monopoles were simulated in a velocity range of $0.4\,c \leq v_M \leq 0.995\ c$. The simulation of monopoles uses the standard IceCube software adjusted to generate and propagate monopoles as well as generating and propagating the Cherenkov light that they emit. For further details, see [5]. The characteristic signature of a (mildly) relativistic monopole in IceCube is a through-going track with very high, but constant brightness. An event view of the signal from a monopole simulated in IceCube is shown in Fig. 2.

2. Event selection

The most abundant background type in this analysis are muons or muon bundles produced in cosmic ray air showers. Since they traverse the detector from above, but monopoles are expected to come from every direction. A cut on the reconstructed zenith angle of a recorded IceCube event removes most of the background while keeping a substantial portion of the signal. When two or more air showers hit the detector at the same time, a time/space clustering algorithm is used to separate them into different events. This improves reconstruction quality by rejecting most of the coincident events, however there still remain many coincident events left to be discarded with other methods, for example with a cut on the length of the longest track segment without any hits closer than 100 m.

A boosted decision tree (BDT) is trained to remove the remaining background. To focus on low monopole velocities $\leq v_C$ and improve the final sensitivity in this parameter range, just this kind of signal simulation is used to train the BDT.

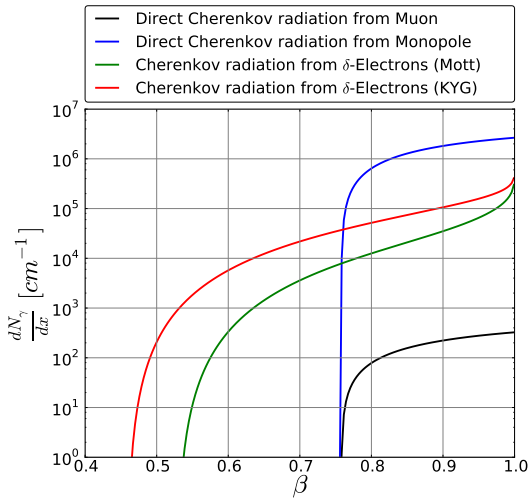

Figure 1: The number of photons per cm produced by a bare relativistic monopole (blue) is 4700 times higher than the light yield of a bare muon (black) producing direct Cherenkov light.
The light yield of all δ-electrons calculated using the KYG cross section [6] (red) is used in this analysis in comparison to the simple Mott cross section [7] (green). Above the Cherenkov threshold indirect and direct light are summed up in simulation.

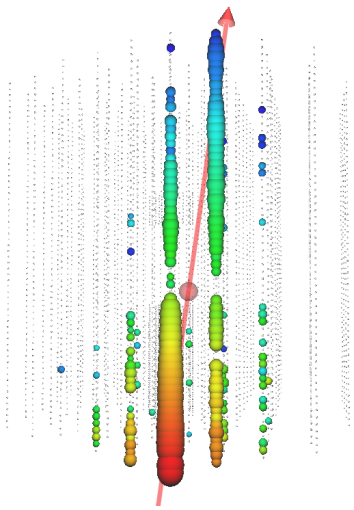

Figure 2: A view of a simulated magnetic monopole event with a velocity of $0.83c$ and a zenith angle of $\sim$ 170 degrees, using both direct and indirect Cherenkov light. The positions of IceCube DOMs are shown with gray dots, hit DOMs with colored spheres. Their size is scaled with the number of recorded photons. The color denotes the time development from red to blue. The red line shows the reconstructed track.

After all cuts, including the BDT cut, the remaining background are charged particles produced in interactions of atmospheric neutrinos. The energies reach from $3.3 \cdot 10^2$ GeV to $2.6 \cdot 10^4$ GeV.

IceCube analyses are performed in a blind way to avoid bias. This is done by using only simulated background and signal. To validate the simulations, 10% of the recorded data are used. However, at this point there was not sufficient background simulation available. Therefore pull-validation was used, which is a re-sampling method inspired by bootstrapping. This method enables the estimation of the uncertainties of the background rate at low-statistics and is described in detail in [8]. Finally, the BDT cut, shown in Fig. 3, in its re-sampled distribution was optimized using a modified Feldman-Cousin approach which also considerates uncertainties [9].

The velocity distribution of background after the last cut, estimated with pull-validation, is shown in Fig. 4. The total uncertainties of this analysis are also shown. The detector simulation gives an uncertainty of 3.0% on the monopole rate. The theoretical flux model is taken into account for the uncertainty of the neutrino flux in addition to the detector simulation which gives 16.9% of total systematic uncertainty. The variation in the background rate estimate obtained with re-sampled BDTs was used as an additional, largest source of uncertainty.

This results in a background rate of 0.55 events with a 90% confidence upper limit of 3.61 events.

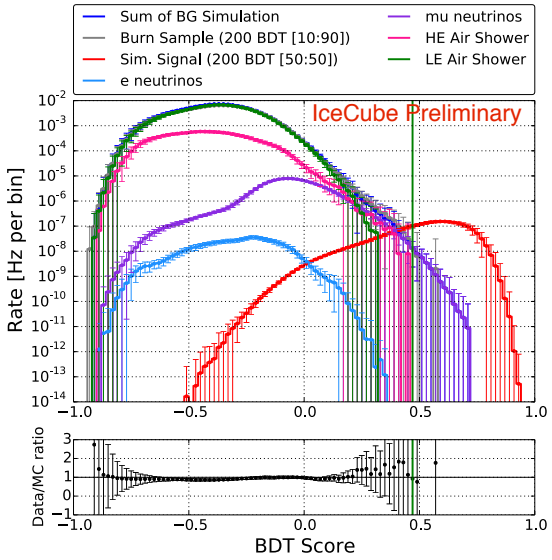

Figure 3: 200 BDTs are trained on a random subsample of 10% of IceCube data. The mean and standard deviation per bin is shown and compared with different types of background simulation. In the signal region atmospheric neutrinos dominate the background contribution.

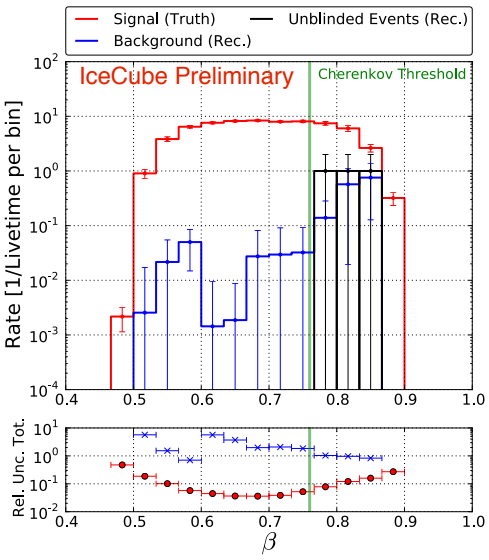

Figure 4: Velocity distribution used to calculate the final differential limit. Reconstructed velocity is used for background and true simulated velocity for signal. The lower part of the plot shows the velocity dependence of the total uncertainties including resampling.

3. Result

After the analysis procedure was finalized and all selection criteria fixed, the remaining 90% of available data from the IceCube season 2011/2012 was used to derive the result. Three events with velocities $\geq v_C$ survived the event selection. This is consistent with background. Fig. 4 shows these events in comparison to the expectation.

Two events have a clear background signature, when inspected visually, because they stop in the detector. One event traverses the whole detector but has light output fainter than expected from a monopole of this velocity. All three events are therefore treated as an upward fluctuation of the background weakening the limit.

The limit for different velocities at the detector is shown in Fig. 6. It extends from $0.51\,c$ to $0.877\,c$ and for most of this range improves previous limits by a factor of almost two orders of magnitude. For a more detailed description of this analysis see [5].

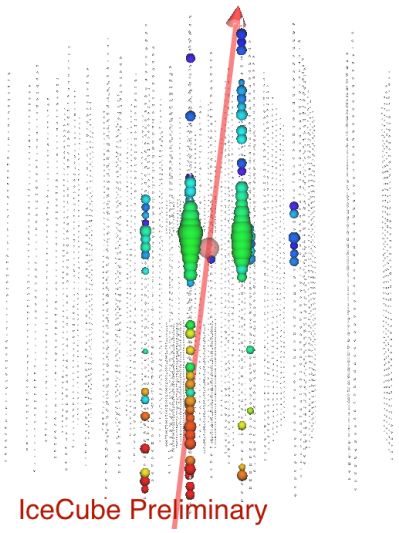

Figure 5: One of three events which passed all cuts in this analysis with a BDT Score of 0.53. 110 optical sensors are hit as opposed to an expectation of 196 ± 11 for a monopole with the velocity and direction as shown in Fig. 2.

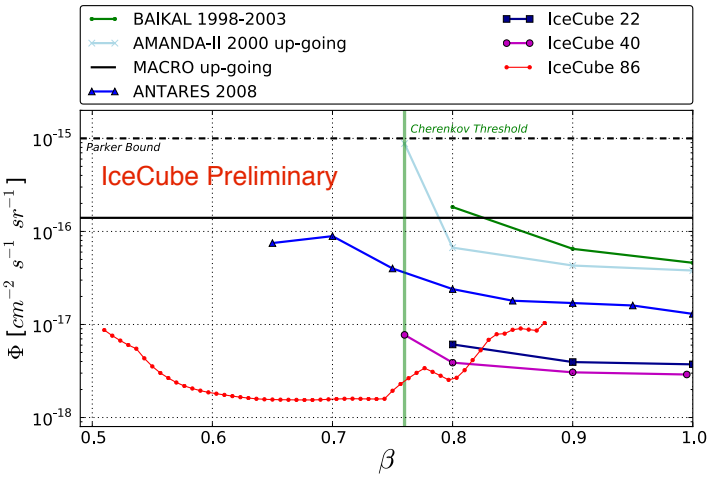

Figure 6: Limit of this analysis (red) compared to other analyses. The lines of all limits are only drawn to guide the eyes. This analysis compares directly with limits from ANTARES [10] and MACRO [11]. Other limits are from BAIKAL [12], AMANDA [13], and IceCube in its 22 [14] and 40 [15] string configuration.

References

[1] P. Dirac, *Proc. Roy. Soc.* **A 133** (1931) 60–73.

[2] G. 't Hooft, *Nucl. Phys. B* **79** (1974) 276–284.

[3] A. M. Polyakov, *JETP Lett.* **20** (1974) 194–195.

[4] A. Achterberg et al., *Astropart. Phys.* **26** (2006) 155–173.

[5] A. Obertacke Pollmann, PhD thesis, University of Wuppertal. In Preparation.

[6] Y. Kazama, C. N. Yang, and A. S. Goldhaber, *Phys. Rev. D* **15** (1977) 2287–2299.

[7] S. P. Ahlen, *Phys. Rev. D* **14** (1975) 2935–2940.

[8] IceCube Collaboration, in these proceedings, no. PoS(ICRC2015)1211.

[9] G. J. Feldman and R. D. Cousins, *Phys. Rev. D* **57** (1998) 3873–3889.

[10] S. Adrián-Martínez et al., *Astropart. Phys.* **35** (2012) 634–640.

[11] M. Ambrosio et al., *Eur. Phys. J. C* **25** (2002) 511–522.

[12] V. Aynutdinov et al., *Astrophys. J.* **29** (2008) 366–372.

[13] R. Abbasi et al., *Eur. Phys. J. C* **69** (2010) 361–378.

[14] R. Abbasi et al., *Phys. Rev. D* **87** (2013) 022001 1–11.

[15] J. Posselt, PhD thesis, University of Wuppertal, 2013.

PROCEEDINGS OF SCIENCE

Improved methods for solar Dark Matter searches with the IceCube neutrino telescope

The IceCube Collaboration[†]
[†] *http://icecube.wisc.edu/collaboration/authors/icrc15_icecube*
E-mail: marcel.zoll@fysik.su.se

Gravitationally captured Dark Matter in the form of Weakly Interacting Massive Particles (WIMPs) can annihilate into standard-model particles, such as neutrinos. The IceCube neutrino detector at the South Pole is an excellent instrument to search for such a neutrino signal from the Sun. We present an alternative analysis which improves on previous approaches, in particular in background-dominated regions. Newly developed techniques based on hit clustering and hit-based vetos allow a more accurate reconstruction and identification of events in the detector and thereby a stronger rejection of background. These techniques are also applicable to other IceCube analyses and event filters. We present results for a solar WIMP search using the first year of data taken with the completed IceCube detector with 86 strings.

Corresponding authors: Marcel Zoll[*1]
[1] *Fysikum, Stockholm Universitet, 11419 Stockholm, Sweden*

The 34th International Cosmic Ray Conference,
30 July- 6 August, 2015
The Hague, The Netherlands

[*]Speaker.

1. Introduction

There is strong observational evidence for the existence of Dark Matter in the universe, including our own galaxy[1], which could possibly have a particle manifestation. Examination of this possibility to date has not revealed the exact constituents of Dark Matter. One intriguing candidate is a Weakly Interacting Massive Particle (WIMP) [2], which could for example emerge in a super-symmetric extension of the Standard Model (SM). If Dark Matter indeed exists in the form of WIMPs, they should reveal their presence through their annihilation into lighter detectable SM particles. Still, with a low local density of about 0.3 GeV/cm^3 and preferred WIMP masses in the range from a few GeV up to the TeV scale, as well as the cross-section limits obtained, their annihilation processes remain rarely accesible for our observation.

Due to their gravitational interaction, it is probable that WIMPs get gravitationally trapped inside heavy bodies of ordinary matter. The Sun represents the best nearby candidate for this capture process which is driven by the scattering of the WIMPs on nuclei of the Sun, binding them to the system, and subsequent gradual energy losses while sinking towards the Sun's centre. The resultant over-density of WIMPs in a sphere at the centre of the Sun increases the rate of self-annihilation processes so that it is competitive with the capture rate. Considering the lifetime of the Sun, we assume that these processes have reached equilibrium[3]. The annihilations will result in a variety of SM particles, with further particles produced in secondary decay processes, of which only neutrinos can possibly escape the Sun without absorption. The detection of a neutrino flux from the Sun at energies similar to the rest-mass of the WIMP would therefore provide evidence of the presence of Dark Matter and indicate some of its properties.

We present a search for solar WIMPs with the IceCube neutrino telescope. We use one year of data recorded in 2011/12 with the fully completed detector (IC86). A second independent solar WIMP analysis has been carried out on the same data set. It achieved a consistent result and is presented as a separate contribution (ICRC 1209[4]).

2. The IceCube Neutrino Detector

IceCube is a cubic-kilometer sized neutrino detector installed in the ice at the geographic South Pole [5] between depths of 1450 m and 2450 m. Detector construction started in 2005 and finished in 2010. The detector consists of an array of 5160 digital optical modules (DOMs) assembled on 86 so-called strings. The DOMs detect the light emitted whenever a neutrino undergoes a neutral current (NC) or charged current (CC) interaction on a nucleus in the ice. Only the CC interaction of a muon neutrino creates an energetic and therefore long-ranged muon, whereas the products of all other interactions lose all their energy in particle showers with a typical size of a few meters. Events in IceCube thus leave two distinct hit patterns in the detector: tracks, identified by the extended pattern of Cherenkov-light emitted as the muon propagates O(km), and spherical cascades, caused by particle showers in NC and CC interactions, as well as by stochastic losses along a muon-track, which can dominate in terms of the amount of light emitted. All IceCube analyses reconstruct events recorded in the detector by fits to these two very distinct light distribution patterns.

In IceCube data at trigger level two effects of nuisance are found: detector noise (500-700 Hz per DOM) and event coincidences, where two or more events are simultaneously present inside the

detector ($\sim$10% of the events). Both effects lead to errors in event reconstructions and need to be removed by algorithms performing *noise/hit-cleaning* and *event-splitting*.

3. The IceHive Event-splitter

In this analysis a novel event-splitter named IceHive was developed, which is based on clustering of DOM-*hits* in space and time with an imposed multiplicity requirement. This clustering routine is based on the determination of whether any two hits are causally connected and are therefore caused by a common source of light (*physics hit*), different from stochastic noise (*noise hit*). Collecting physics hits into clusters while excluding noise hits allows the separation of individually developing sub-events in the detector.

The relation between two physics hits can be described by one of the following causes:

1. hits are located on different geometrical/topological sites of the same light-front (Cherenkov-cone), thus are spatially separated with no or little time separation
2. hits are caused by photons of the same light-front travelling between DOMs, thus hits are connected by the speed of photon propagation
3. hits are caused by light-emission at different positions along a muon-track, thus hits are connected by the speed of particle propagation

A graphical impression of this can be found in Figure 1.

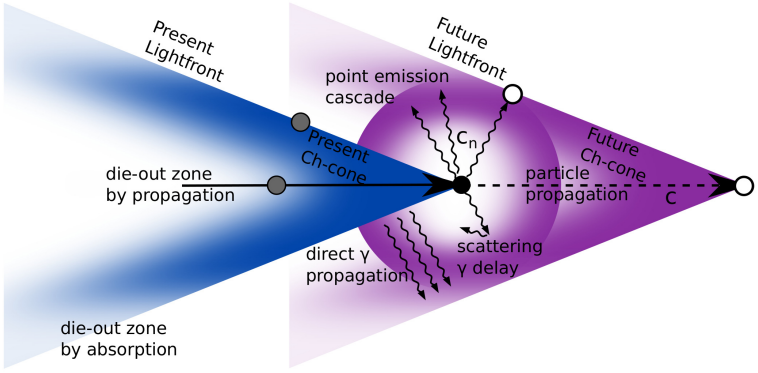

Figure 1: Possible light emission topologies for tracks and cascades at the present (blue) and future (pink) after photon-propagation for a particle (arrow) traversing the detector volume. Hits are registered on DOMs (circles); their relation is governed by the causal arguments of spatial separation, photon propagation and particle propagation.

This allows the construction of a binary causal connection estimator between hits $h_1(\vec{r}_1,t_1)$ and $h_2(\vec{r}_2,t_2)$ with three dedicated terms (without restriction of generality: $t_1 < t_2$):

$$E(h_1,h_2) = \quad [(h_2 \in EV_{\text{static}}(h_1)) \wedge (\alpha_\infty^- \leq R_\infty(h_1,h_2) \leq \alpha_\infty^+)] \tag{3.1}$$

$$\vee \left[(h_2 \in EV_{\text{photon}}(h_1)) \wedge (\alpha_{c_{\text{ice}}}^- \leq R_{c_{\text{ice}}}(h_1,h_2) \leq \alpha_{c_{\text{ice}}}^+)\right] \tag{3.2}$$

$$\vee \left[(h_2 \in EV_{\text{particle}}(h_1)) \wedge (\alpha_{c_{\text{vac}}}^- \leq R_{c_{\text{vac}}}(h_1,h_2) \leq \alpha_{c_{\text{vac}}}^+)\right] \tag{3.3}$$

where $R_v = (t_1 - t_2) - |\vec{r}_1 - \vec{r}_2|/v$ is the time-residual of a messenger particle travelling with speed v between hits, the $\alpha_v^{\pm}$ are adjustable parameters, and EV_{relation} is the eligibility volume (EV) containing all DOMs to which a specific hit can possibly connect. The EV needs to be selected according to the typical range of the messenger and the imposed multiplicity criterion. In contrast to previous solutions IceHive explicitly takes the detector geometry into account when the EV is constructed[1]. These equations with careful selection of the involved parameters make IceHive very robust against the influence of noise, so that its application on the raw detector readout becomes possible. Figure 2 shows the ability of IceHive to select the correct physics hits. Applied before online reconstructions and filters, IceHive could demonstrate an additional background reduction of 30% for muon topologies and 65% for cascades. Coincident events, which are expected to be found at an abundance of 10% in the recorded data, were separated at a success rate of 87%.

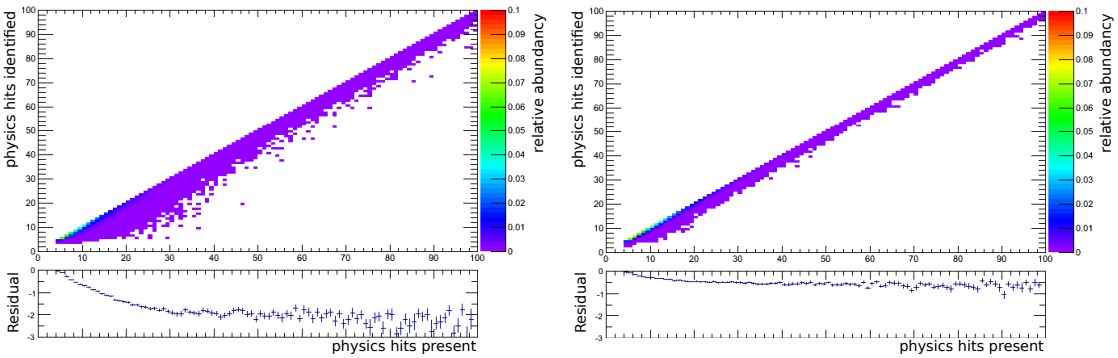

Figure 2: Comparing the selection of physics hits for the previous event-splitter solution based on spatial clustering (left) and the improved IceHive algorithm (right). Optimal performance is indicated along the diagonal. The residual plots show the average number of missed physics hits for events with different number of physics hits present in total.

4. Event Selection

For this analysis we produce dedicated signal simulation using WimpSim [6, 7] for several WIMP masses. We pick the annihilation into W^+W^- and $\tau^+\tau^-$ to represent a hard neutrino spectrum and annihilation into $b\bar{b}$ for a soft one and thereby bracket other conceivable branching scenarios. Depending on the WIMP mass and annihilation channel, the expected signal neutrinos at the detector range in energy from just a few GeV up to some TeV. This analysis focuses exclusively on a signal in muon neutrinos creating tracks in the detector, as these in general yield the best pointing. Compared to previous WIMP analyses in IceCube, the detector simulation has been substantially improved; in particular, the description of the particle/photon propagation and detection in ice, as well as the detector response.

The regular IceCube (IC) array has a threshold on the neutrino energy $\sim$100 GeV while the more densely instrumented region DeepCore (DC) lowers this threshold to $\sim$10 GeV. All IceCube neutrino analyses suffer from a strong background of down-going muons and neutrinos created

[1]The detector geometry resembles regular hexagons similar to a bee hive, hence the naming of the algorithm.

from cosmic ray showers in the upper atmosphere. Atmospheric muons will be observed only as down-going while atmospheric neutrinos are found at all directions. This greatly influences the approach to the event selection.

As the event-splitter IceHive shows better performance compared to the methods used traditionally, it is initially applied to all available detector data selected by any of the online filters ($\sim$800 Hz) during one year of live-time (337.4 d). Thereafter event reconstructions are performed on the split physics hit selection and minimum quality cuts are enforced.

The event sample is then split into four sub-samples: if the hits of an event are predominantly found in the denser instrumented region of DeepCore they are classified as *DC-dominated*, otherwise they are classified as *IC-dominated*. Another subdivision is performed according to the incident zenith angle, where events originating from above the horizon are dominated by through-going atmospheric muons (referred to as *BG-dominated*).

In the further treatment we require that events in the BG-dominated sample are starting within the detector, which can only be fulfilled by true neutrino events; the detector's outer layer of strings act as an active veto. No such requirement is applied for the up-going (not BG-dominated) sample, because the Earth acts as a natural filter for the atmospheric muon background.

At this level of about 1 Hz we apply two dedicated Boosted Decision Trees (BDT), one for DC-dominated and another one for IC-dominated events, thus the different background samples are treated conjointly. These BDTs are trained solely on variables expressing the containment of events in the detector, thus explicitly ignore any energy dependence. This reduces the background by another factor of $\sim$10. Thereafter another four now energy-sensitive BDTs are applied, one to each of the four sub-samples. The second stage BDTs are trained on a signal sample which is typical for the respective selection: 1 TeV WIMPs annihilating into W^+W^- for the IC-dominated samples and an equal mixture of 100 GeV WIMPs into W^+W^- and $b\bar{b}$ and 50 GeV WIMPs into $\tau^+\tau^-$ for the DC-dominated samples. The BDT-classifiers at this point are sensitive to the specific energy spectrum and zenith distribution of the signal expectation and can now be used as tuning parameters. Figure 3 shows the classifier distributions for the up-going subsamples. A loose cut on the BDT-classifier at zero brings the data rate down to about 20 mHz.

Up to this level the background has been reduced by a factor of $4 \cdot 10^4$ while, depending on chosen mass and annihilation channel, between 11% and 20% of the signal could be retained.

5. Analysis method

We use a shape likelihood based on the opening angle Ψ of the observed event direction compared to the current position of the Sun. The probability density function for an event $\vec{e}_i$ as a set of observable quantities in a sample containing μ signal events in a total of N_{obs} events is given by

$$g(\vec{e} = (\Psi)|\mu) = \frac{\mu}{N_{\text{obs}}} f_{\text{s}}(\Psi) + (1 - \frac{\mu}{N_{\text{obs}}}) f_{\text{bg}}(\Psi) \tag{5.1}$$

where $f_{\text{s}}(\Psi)$ and $f_{\text{bg}}(\Psi)$ are the probability distribution function (PDF) for signal and background. The signal PDF can be obtained by direct tabulation from WIMP simulation of any specific mass-channel combination; in contrast the background PDF is obtained from experimental data by scram-

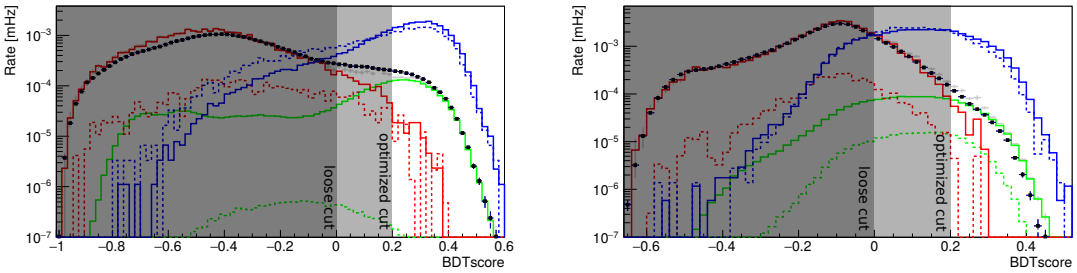

Figure 3: The energy-sensitive BDT-classifier score for the up-going subsamples of IC-dominated (left) and DC-dominated events (right). Events scored to high values are most signal-like. Shown is experimental data (black) and the simulation of atm. ν_μ (solid green) and atm. ν_e (dashed green), as well as atm. μ from CORSIKA at low (solid red) and high primary energies (dashed red). The simulation total is shown in gray. The signal expectation (blue) scaled to the data-rate is shown for a representative of a hard (solid) and soft (dashed) spectrum in the respective sample.

bling the apparent Sun azimuth, thereby removing any possible signal traits in Ψ; see figure 4 for some examples.

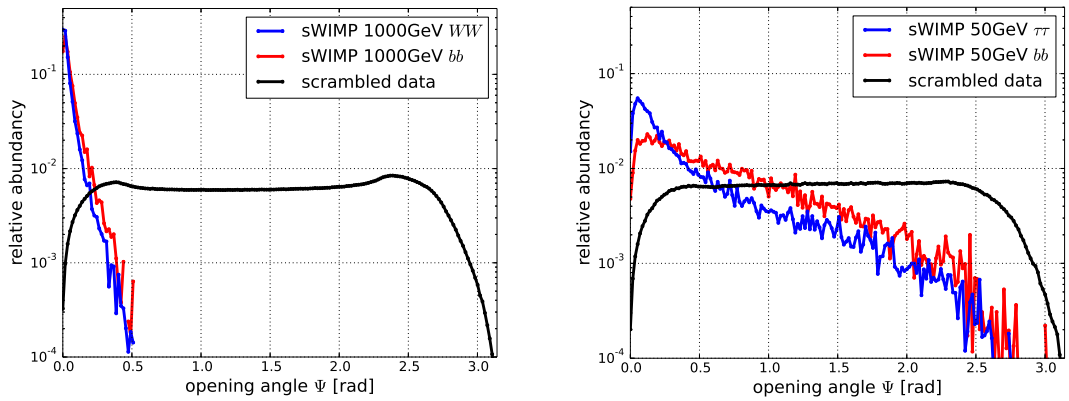

Figure 4: The obtained PDFs for background by scrambled experimental data and a hard and soft signal expectation in the IceCube-dominated (left) and DeepCore-dominated (right) sample. Only the winter months and up-going events are considered. The different structure in the background is caused by selection and geometrical effects in the respective sample.

The likelihood value for μ signal events in the complete sample is then given by

$$\mathscr{L}(\mu) = \prod_i^{N_{\text{obs}}} g(\vec{e}_i|\mu) \tag{5.2}$$

We use the prescription from Feldman and Cousins[8] to construct a test statistic and extract sensitivities and limits for the number of observed signal events in the sample at 90% confidence level. This number can then be converted to a WIMP annihilation rate in the Sun and finally to a limit on the WIMP-nucleon scattering cross-section.

In the evaluation of our data sample, we limit ourselves to data obtained in the winter months (174 days of live-time) when the Sun is below the horizon and all sensitivity is obtained from up-going neutrino events. Furthermore we tighten the last cut on the BDT-classifier to obtain the best

sensitivity from the respective sample. The final event rate is 1.4 mHz in the IC-dominated sample and 0.4 mHz in the DC-dominated sample.

6. Results and discussion

This analysis found no significant excess in muon neutrinos from the direction of the Sun in the search for a possible solar WIMP signal. This allows us to set stringent limits on the muon neutrino-flux from the Sun for energies in the GeV-TeV range. Under the assumption of a local DM density at 0.3 GeV/cm^3, a standard Maxwellian velocity distribution in the galactic WIMP halo and the Standard Solar Model this limit can be converted to a limit on the WIMP-nucleon scattering cross-section for each such probed WIMP model. Figure 5 shows the obtained sensitivities and limits of this analysis for the spin-dependent and spin-independent scattering cross-section.

Compared to the previous IceCube solar WIMP analysis[9] conducted with 79 deployed strings, the improvement ranges from a factor up to 10 at the lowest WIMP mass at 20 GeV to a factor 2 for higher WIMP masses up to 10 TeV. The improvement over just the added detector volume can be attributed to the refinement of the analysis methods and a better hit selection with IceHive. The so obtained limits make IceCube very competitive compared to the reported limits from other experiments for WIMP masses above $\sim$150 GeV.

Note: We have carried out a second independent solar WIMP analysis on the same dataset. The results of the two analyses are consistent with each other and are described as separate contributions to this conference (see [4]). At a later time we will combine the two analyses.

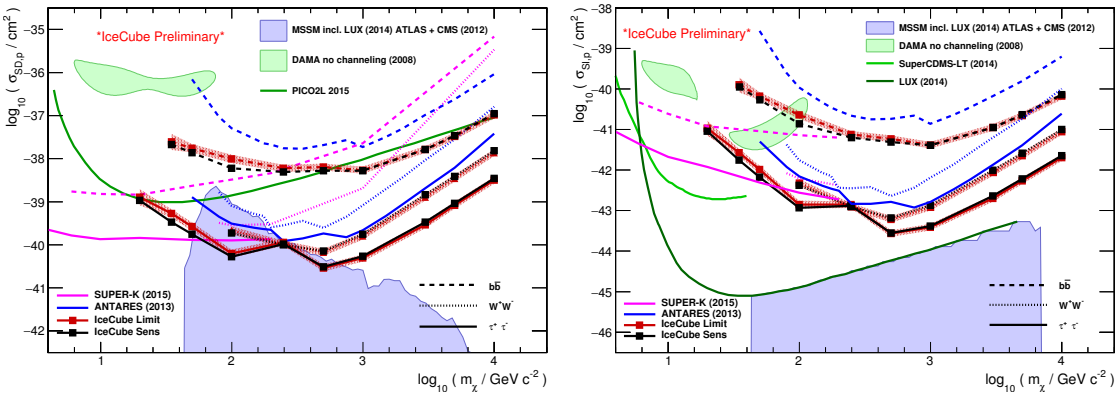

Figure 5: Limits of this analysis on the spin dependent (left) and spin independent (right) WIMP-nucleon scattering cross-section as a function of the WIMP mass derived from this analysis. Systematic uncertainties are shown as a red band. Also shown are reported limits from other experiments [10, 11, 12, 13, 14, 15, 16, 17, 18].

References

[1] M. Pato, F. Iocco, G. Bertone, Nature 11 (2015) p.245-248

[2] G. Bertone *et al.*, Phys. Rep. 405 (2005) p.279

[3] K. Choi *et al.*, JCAP 05, 049 (2014)

[4] IceCube Coll., PoS(ICRC2015)1209 these proceedings

[5] A. Achterberg *et al.*, [IceCube Coll.], Astropart. Phys. 26 (2006) 155

[6] M. Blennow, J. Edsjö and T. Ohlsson, JCAP 01, 021 (2008), http://www.fysik.su.se/~edsjo/wimpsim/

[7] P. Gondolo, J. Edsjö, P. Ullio, L. Bergström, M. Schelke and E.A. Baltz, JCAP 07, 008 (2004)

[8] G.J. Feldman, R. D. Cousins, Phys. Rev. D 57:3873 (1998)

[9] M.G. Aartsen *et al.* [IceCube Coll.], Phys. Rev. Lett. 110, 131302 (2013)

[10] D.S. Akerib *et al.* [LUX Coll.], Phys. Rev. Lett. 112, 091303 (2013)

[11] R. Agnese *et al.* [SuperCDMS Coll.], Phys. Rev. Lett. 112, 241302 (2014)

[12] R. Bernabei *et al.*, Eur. Phys. J. C 53 (2008), 205

[13] H. Silverwood *et al.*, arXiv:1210.0844v1 (2012)

[14] The ATLAS Collaboration, Phys. Lett. B 701 (2013) 186

[15] The CMS Collaboration, arXiv:1207.1798 (2012)

[16] K. Choi *et al.* [Super-Kamiokande Coll.], Phys. Rev. Lett. 114, 141301 (2015)

[17] C. Amole *et al.* [PICO Coll.], Phys. Rev. Lett. 114, 231302 (2015)

[18] The ANTARES Collaboration, JCAP 11 (2013) 032

PROCEEDINGS OF SCIENCE

Search for Neutrino-Induced Double Tracks as an Exotic Physics Signature in IceCube

The IceCube Collaboration[1]**,**

[1] *http://icecube.wisc.edu/collaboration/authors/icrc15_icecube*

E-mail: sandro@kopper.info

Physics theories beyond the Standard Model, like Supersymmetry and models with extra dimensions, often invoke $\mathbb{Z}_2$-symmetries in order to avoid new couplings that lead to unobserved new physics, like unnaturally fast proton decay. This gives rise to the possibility of heavy new particles being produced in pairs with the lightest of them being (meta-)stable. Thus, under favorable conditions, neutrinos in the PeV range - like those observed by IceCube - can produce pairs of exotic, charged particles that can be seen in a km^3-sized detector as two parallel, muon-like tracks with a track separation of a few hundred meters. We discuss the methods of reconstructing double tracks and how to separate them from other air shower or neutrino-induced (coincident) muon events in a model independent way.
The first search for such events with the IceCube detector in its 79-string configuration resulted in no candidate events. This result can be used to derive limits that can be applied to explicit exotic models.

Corresponding author: Sandro Kopper*†

† *Dept. of Physics, University of Wuppertal, 42119 Wuppertal, Germany*

The 34th International Cosmic Ray Conference,
30 July- 6 August, 2015
The Hague, The Netherlands

*Speaker.

1. Physics Beyond the Standard Model

With the observation of the Higgs boson [1], the last of the particles predicted by the Standard Model (SM) has been found. Yet there are some problems that lead to the conclusion that the SM can not be a fundamental description of nature: firstly, gravity is not part of the model and its apparent extreme weakness compared to the weak force gives rise to the *hierarchy problem* when trying to extend the Standard Model to the energy scale where gravity becomes important; secondly, experimental observations like a non-zero neutrino mass [2] and the existence of *dark matter* are direct evidence of physics not included in the Standard Model. Many models of new physics trying to explain these facts predict new particles at the TeV scale.

Pair Production of long-lived, exotic particles

Additionally, theories beyond the Standard Model like *Supersymmetry* or the assumption of *additional compact dimensions* are generally required to have a $\mathbb{Z}_2$-symmetry within the theory (like R-parity in Supersymmetry) in order not to spoil precision electroweak observations. This discrete symmetry leads to two important phenomenological aspects: most new particles can only be produced in pairs and the lightest of them will be stable - making it an excellent dark matter candidate. Unless the $\mathbb{Z}_2$-symmetry is (slightly) violated this particle has to be neutral but the next-lightest particle can possibly be both charged and long-lived. The latter is usually the result of the lightest exotic particle interacting only extremely weakly like in the case of *gravitinos* for Supersymmetry or Kaluza-Klein excitations of right-handed neutrinos in models with extra dimensions. Long-lived, charged and massive particles like this are often called *CHAMPs*.

Mass Suppression of Energy-Losses

An interesting aspect of CHAMPs is how their mass influences their radiative energy losses in matter. Bremsstrahlung is naturally suppressed by mass and becomes sub-dominant for any heavy particle, but photonuclear and pair production processes can also be shown to be similarly affected [3]. In particular particles that mostly behave like *heavy leptons* exhibit a suppression of energy losses. The scaling for very heavy particles goes inversely with mass [3, 4]. The radiative energy losses of a CHAMP with $m_{\text{CHAMP}} > 100$ GeV are at least three orders of magnitude lower when compared to a muon - the most penetrating charged SM particle [5]. While even muons at the highest energies produced in air showers only have ranges of tens of kilometers, such a CHAMP can potentially traverse the whole Earth. On a smaller scale $\mathcal{O}(1\text{ km})$ they will mostly look like comparatively lower energy ($\approx$ few hundred GeV) muons. Ideal detectors for particles like this are cubic-kilometer neutrino telescopes like IceCube.

Neutrino-Induced Double Tracks

Production of pairs of exotic particles is possible directly in cosmic ray interactions in the atmosphere, but the observable flux is expected to be rather low (i.e. below ≈ 0.02 - 3 year^{-1} km^{-2} [6]). A more prominent way to produce CHAMPs is neutrino interactions within the Earth [7]. For heavy, exotic particles to be produced these neutrinos need to be in the PeV range [8] or higher. The CHAMPs can be produced far from the detector site due to their long range and thus have an

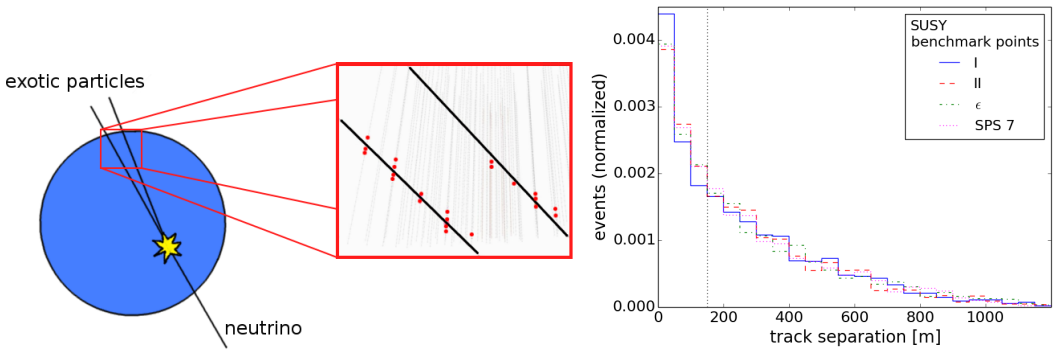

Figure 1: Scheme of a double track signal in a neutrino telescope like IceCube *(left)* and track distance distribution in SUSY models *(right)* (SUSY parameter points adopted from [10]) with a simplified energy loss behavior, not taking into account additional effects like multiple scattering [11]. The typical resolvable track separation in this analysis starts at about 150m.

increased effective volume for detection compared to muons. This can partially compensate for the low branching ratio to exotic particles compared to SM particles.

Due to CHAMPs mimicking the much more numerous muons, particle identification of a single CHAMP is a difficult. The CHAMPs will, however, always be produced in pairs and - at least generally - far from the detector. This results in a signature of *two parallel tracks* with a track separation of up to several hundred meters as seen in Figure 1. SM neutrino interactions producing di-muon tracks with a separation greater than 100 m are extremely rare [3, 9] and so an excess of well separated tracks is an excellent indicator for physics beyond the Standard Model. CHAMPs like this will also generally deposit less energy in the detector than other particles at the highest energies.

2. Search for Double Tracks in IceCube

The IceCube detector is installed in the ice at the geographic South Pole [12] between depths of 1450 m and 2450 m. Detector construction started in 2005 and finished in 2010. Reconstruction of the incoming event energy, position and direction relies on the optical detection of Cherenkov radiation emitted by charged particles in the surrounding ice. This search for double tracks is based on data collected between May 2010 and May 2011 in the 79 string configuration (IC79).

Reconstruction

The double track reconstruction is done in several steps. The reconstruction itself implicitly assumes parallel double track events and does not distinguish between signal (parallel tracks) and background (single or non-parallel tracks) events. Still, important cut variables can be derived from the reconstruction result. The start is the separation of photon pulses seen in the digital optical modules (DOMs) of IceCube and assigning them to one of the tracks based on geometric considerations. This is done in two ways, both of which effectively construct a plane that divides the detector. One way is to construct a *tensor of inertia* of the DOMs in an event by treating their

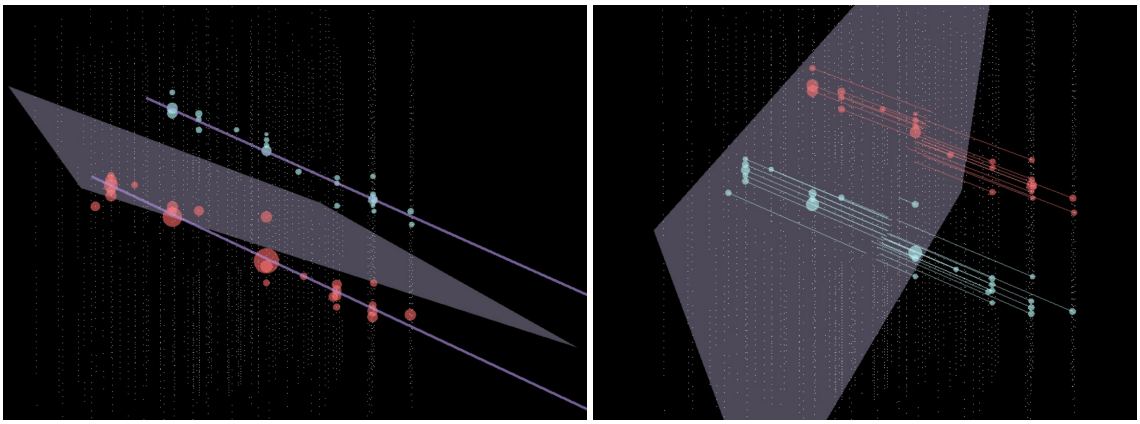

Figure 2: The geometric double track reconstruction - *left:* tensor of inertia based plane; *right:* combination of projection and k-means clustering

charge distribution like masses. The eigenvalues and eigenvectors are then related to the orientation of the parallel tracks within the detector and the correct choice of eigenvectors can be used to construct a dividing plane. The other way used is the application of a k-means clustering algorithm [13] to separate the pulses into two clusters. This is preceded by a projection of the DOM coordinates into a common plane that is perpendicular to the approximate direction of the tracks. This projection-vector is at first obtained via a *single track fit* on the whole event. The procedure minimizes the natural spread of pulses along their trajectory. Both types of reconstructions are illustrated in Figure 2.

The two clusters of DOM pulses can then be used as a basis for a simple (i.e. assuming a plane wave) single track fit each. At least one of these four fits (two for each method) is usually a much more precise estimator for the direction of the double tracks than the initial guess. The clustering algorithm is repeated with a projection in each direction. The clustering attempt showing the smallest spread (i.e. squared mean deviation) of DOM positions around their cluster centers is assumed to be the best. The simple track fits on each of the *best* clusters then form the seed of two separate likelihood reconstructions [14]. The underlying assumptions of these fits are either two infinite tracks with arbitrary location and direction or two tracks that are assumed to be parallel. Whereas the non-parallel fit is done to slightly improve the reconstruction of the opening angle of the tracks, the likelihood parameter of the (more important) parallel fit is used directly in background suppression cuts.

Standard Model Backgrounds and Cuts

Most events in IceCube are muons directly produced in air showers. Since these come from *above* the horizon and exotic double tracks are mostly believed to come from *below* the horizon, simple cuts on the zenith angle of the observed tracks remove the bulk of cosmic ray muons. This leaves two general classes of track-like events: muon tracks related to neutrinos coming from below the detector and mis-reconstructed events actually coming from above.

Double tracks with low track separation are very hard to distinguish from single, up-going muon tracks. The typical horizontal spacing of DOMs in IceCube is 125 m and makes precise

reconstruction of double tracks with separation below this challenging. Removing events with small and unresolvable track separation is done by setting a limit on the minimal reconstructed track separation (150 m). Additionally there is a cut on a variable that effectively works as a likelihood ratio test comparing a single track fit with a parallel double track fit. Only events that look much more like a double track than a single track in this variable are kept.

The most common background for mis-reconstructed events are coincident muons from independent air showers. Most cuts in the IceCube double track search are aimed at them. Note that the actual direction of the muons in these events does not play a large role influencing the mis-reconstructed direction. The misidentification comes from the first event causing a photon signal in DOMs that are - on average - located lower in the detector than the DOMs registering the second event. Simple reconstructions connect these separate events and treat them as a single, up-going, track. Figure 3 (left) shows a typical mis-reconstructed background event of this kind.

There are many ways to remove coincident events from the data. The most effective way is to cut on the (reduced) likelihood variable obtained in the likelihood reconstruction described earlier as can be seen in Figure 3 (right). Yet it is not feasible to do this for every event since the rate of air shower muons is very high and the likelihood reconstruction is computationally intensive. A series of variables for pre-cuts is needed to reduce the data volume to an acceptable level.

The time and geometric distance of the two sets of hits for each muon are not causally connected. Generally, there will be a geometric gap between the hits for coincident events *along the reconstructed track direction* and the hits will also not be very tightly clustered perpendicular to their apparent direction. The reconstructed speed of the tracks will also differ from the speed of light. Often the reconstructed tracks will not be very parallel as seen in their reconstructed opening angle.

If the coincident muons are produced in separate air showers - as is most often the case - their individual tracks will still be down-going. Ordering all DOM hits in time and assuming the two sub-events do not overlap, one gets an *average* downward pattern from one hit to the next apart from the very last hit of the first and the very first hit of the last track.

This is true for both muon tracks and the average pattern is usually retained even if there is some time overlap of both sub-events. Since the situation is reversed for an up-going signal double track this average pattern from one hit to the next is another useful cut. This does not work if one or both of the coincident events is an up-going muon caused by a neutrino interaction near the detector. Fortunately the situation of two (possibly up-going and somewhat parallel) coincident neutrino events is extremely rare (≈ 0.0008 per year) [9]. All these cuts - including the likelihood cut - were optimized to remove all air shower simulation corresponding to $\mathcal{O}(1\%)$ of a year's experimental IceCube data.

There are also some other SM particle interactions that can directly lead to separated tracks. One such possibility is the production of a muon and a charmed hadron in a high energy neutrino interaction. The hadron can then decay into another muon and both muons can possibly show up as double tracks. These double tracks can not lead to high track separations (> 150 m) due to the more limited muon range and thus interaction vertices that are much closer to the detector. They are also much more likely to stop in the detector. They also can have a higher energy deposition and so can possibly be distinguished from exotic double tracks. However, in simulations of more than 10 years livetime such a di-muon background was not dominant at any analysis cut level and

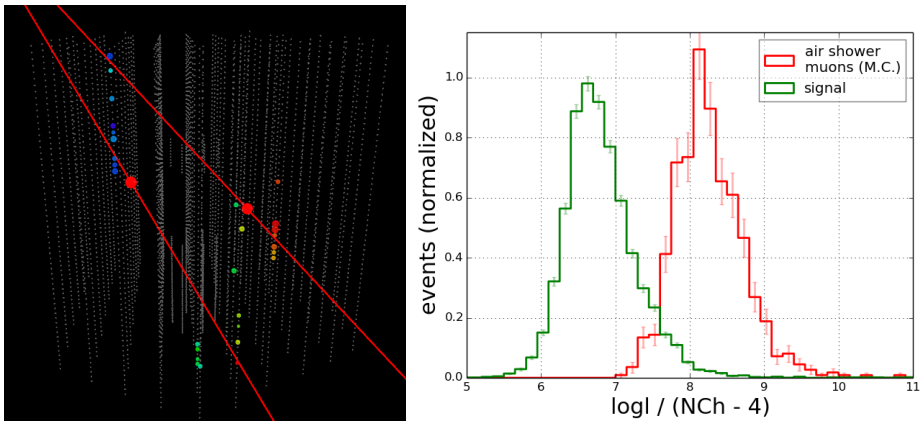

Figure 3: *Left:* A typical mis-reconstructed coincident air shower event - the dominant class of background. Note how the mis-reconstructed track directions do not coincide with the actual direction of the down-going muons. The rainbow palette illustrates the time structure of the DOM pulses (red: early, blue: late); *right:* Cut on a log-likelihood parameter removes most of the coincident air shower background. Distributions shown are at a late cut level.

eventually gets removed completely by cuts also removing single track muon events. This leaves one class of irreducible SM double track background. Two neutrinos produced *in the same* air shower, possibly at the other end of the Earth, are even more penetrating than any charged particle and will also generate parallel tracks with high separation if *both* interact near IceCube. Fortunately this kind of event is also very rare, with a rate ≈ 0.07 events/year [9].

Since the amount of available Monte Carlo data for low energy neutrino and (coincident) air shower muons was much lower than needed to fully characterize the background for the analyzed livetime, some additional cuts were introduced to remove low quality events that show up as either very short tracks or tracks with only a few associated higher quality DOM pulses (i.e. hits that have coincident hits on a nearby DOM). Low quality events that are only seen on very few (i.e. up to four) strings as well as events only clipping the bottom of the detector array are also removed.

3. Simplifications and Model Dependencies

There are many model dependencies that govern the parallel double track flux at the detector:

1. What is the mass of the exotic particles that can be produced in neutrino interactions?
2. What is the size and spectral shape of the neutrino flux most relevant to interactions?
3. How does the mass spectrum of the exotic model in question influence the decay cascade and ultimately the kinematics of the CHAMP?
4. What is the CHAMP's mass?
5. Does the weak interaction play a role in its energy losses?
6. How much does scattering on the way to IceCube change the track separation?
7. Can it decay on its way to the detector?

This renders simulating and analyzing each individual model impossible. On the other hand, the situation is quite easy for a given double track flux *near* the detector. The dependence of the

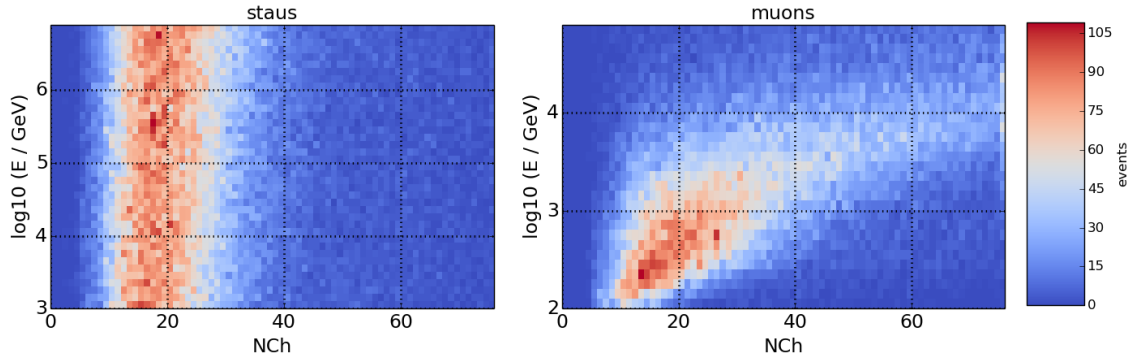

Figure 4: The number of DOM channels *NCh* showing a signal - a very simple energy estimator. For exotic particles like a *stau* in Supersymmetry *(left)* the event-to-event fluctuations dominate over many orders of magnitude in energy unlike for a SM signal like a muon track where the energy dependence is clearly visible *(right)*. Simulation done with the standard IceCube simulation using MMC (Muon Monte Carlo) [15]. Energies shown correspond to the situation when the particles are about to enter the detector volume.

detector signal on the CHAMP energy is extremely weak in many models and can almost be ignored (see Figure 4). The probability that particles with an extremely long range would be starting or stopping within the detector is also very small and can be ignored - it will later be part of the systematic uncertainties of the search. The only relevant parameters which influence the effective area for detection are the zenith angle and the track separation of the two particles.

After performing an analysis and setting a limit on double tracks at the detector one can use the result together with the effective area after all analysis cuts to constrain any specific model. This is done by convolution of the expected zenith and track separation distribution with the effective area. So even any future exotic model that has not been proposed yet can be easily tested this way after the analysis.

4. Results of the IC79 Analysis

None of of the final data sample was used to construct the background separation cuts. Only 1/10 of the data collected in the data taking season served as sample to ensure stable data to simulation rates and develop cuts but these runs are then discarded in the final analysis and the total remaining livetime is 279 days, 17 hours and 54 minutes. Even with an uncertain background rate due to limited Monte Carlo statistics, the data quality cuts proved to be sufficient in eliminating possible background events and there is *no event left* in the final data sample after all cuts. The safest way to interpret this null result is in a *background free pure upper limit* for double tracks at the detector. Exotic models can be easily tested by convolution of the predicted track separation at the detector (e.g. Figure 1) as well as zenith distributions with the limit seen in Figure 5. Since no background expectation was used to compute the limit, it only depends on the effective area after all analysis cuts, the livetime of the data sample and systematic uncertainties of the detector behavior (DOM efficiency, ice models, etc.). Any arbitrary double track model can be tested using this approach. This search is the first of its kind in IceCube and it shows the feasibility of the analysis technique. The analysis is inspired by certain exotic models (i.e. SUSY, UED) but was performed

in a model-independent way, and testing any specific model could benefit from specifically tailored cut variables in order to improve the signal efficiency. Moreover, several years of detector data of the full 86 string IceCube array are still to be analyzed and the double track detection efficiency can be further enhanced with a more detailed background description with larger statistics. The current analysis is based on the IceCube *muon filter* data stream that has a preference for well reconstructed *single* tracks. So a dedicated double track filter is another option to increase the sensitivity.

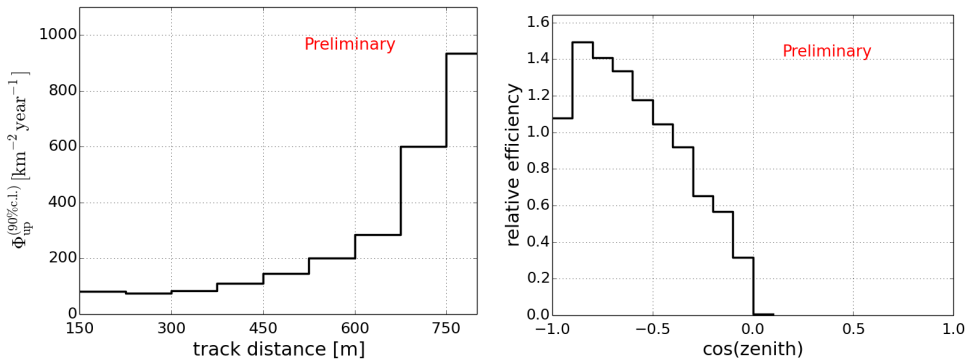

Figure 5: *Left:* The limit (90% confidence level) on up-going double tracks at the detector resulting from the livetime and the double track effective area distribution at the final cut level when assuming a uniform arrival direction from the lower hemisphere. *Right:* The relative efficiency of the analysis when moving from a uniform zenith distribution to a fixed arrival direction. The slightly reduced efficiency closer to the horizon is partially an effect of data quality cuts. There is no notable azimuth dependence.

References

[1] **ATLAS and CMS** Collaboration, G. Aad et al., *Phys. Rev. Lett.* **114** (2015) 191803.

[2] **Super-Kamiokande** Collaboration, Y. Fukuda et al., *Phys. Rev. Lett.* **81** (1998) 1562–1567.

[3] I. F. M. Albuquerque, G. Burdman, and Z. Chacko, *Phys. Rev.* **D75** (2007) 035006.

[4] I. F. M. Albuquerque et al., *Phys. Rev. D* **78** (2008) 015010.

[5] M. Ahlers, J. Kersten, and A. Ringwald, *JCAP* **0607** (2006) 005.

[6] M. Ahlers, J. I. Illana, M. Masip, and D. Meloni, *JCAP* **0708** (2007) 008.

[7] I. F. M. Albuquerque, G. Burdman, and Z. Chacko, *Phys. Rev. Lett.* **92** (2004) 221802.

[8] **IceCube** Collaboration, M. G. Aartsen et al., *Phys. Rev. Lett.* **111** (2013) 021103.

[9] D. van der Drift and S. R. Klein, *Phys. Rev. D* **88** (2013) 033013.

[10] S. Ando et al., *JCAP* **0804** (2008) 029.

[11] I. F. M. Albuquerque and S. R. Klein, *Phys. Rev.* **D80** (2009) 015015.

[12] **IceCube** Collaboration, A. Achterberg et al., *Astropart. Phys.* **26** (2006) 155–173.

[13] J. MacQueen in *Proceedings of the Fifth Berkeley Symposium on Mathematical Statistics and Probability, Volume 1: Statistics*, (Berkeley, Calif.), pp. 281–297, University of California Press.

[14] **IceCube** Collaboration, R. Abbasi et al., *Phys. Rev. D* **87** (2013) 012005.

[15] D. Chirkin and W. Rhode, hep-ph/0407075.

PROCEEDINGS OF SCIENCE

A search for Dark Matter in the centre of the Earth with the IceCube neutrino detector.

The IceCube Collaboration[†]

[†] *http://icecube.wisc.edu/collaboration/authors/icrc15_icecube*

E-mail: Jan.Kunnen@vub.ac.be

Many models predict new particles that have the properties of a Weakly Interacting Massive Particle (WIMP) and could explain the dark matter observed in the universe. Heavy celestial bodies, such as the Earth, could capture these WIMPs and accumulate them. Over time the WIMPs will self-annihilate and may produce standard model particles, including neutrinos. Large scale neutrino telescopes, such as the cubic kilometre IceCube Neutrino Observatory located at the South Pole, can be used to search for such neutrino fluxes.
The dark matter annihilation rate in the centre of the Earth, and thus the resulting neutrino flux depend on the local Dark Matter density and the mass of the Dark Matter particle. This flux could be within reach of a large neutrino detector like IceCube. We present the results of the first search for Earth WIMPs with the IceCube detector.

Corresponding authors: J. Kunnen[*1], J. Lünemann[1],

[1] *Interuniversity Institute for High Energies, Vrije Universiteit Brussel, Belgium*

The 34th International Cosmic Ray Conference,
30 July- 6 August, 2015
The Hague, The Netherlands

[*]Speaker.

1. Introduction

Some of the most promising dark matter candidates are Weakly Interacting Massive Particles (WIMPs). In the Minimally Supersymmetric Standard Model (MSSM), the WIMP can take the form of the lightest neutralino. Dark matter particles from the galactic halo might become bound in the gravitational potential of the solar system as it passes through the galaxy. These particles may then scatter weakly on nuclei in the Earth and lose energy, becoming trapped by the Earth. Over time, this leads to an accumulation of dark matter in the centre of the Earth. The accumulated dark matter may then self annihilate at a rate that is proportional to its density, generating a flux of neutrinos which is spectrally dependent on the annihilation channel and neutralino mass.

Expected neutrino event rates and energies depend on the specific model and distribution of dark matter under consideration and the chemical composition of the Earth. Taking these variables into consideration leads to a neutrino-induced muon flux from the centre of the Earth varying between $10^{-8} - 10^{5}$ per km^2 per year for WIMPs with masses in the GeV$-$TeV range [1]. AMANDA [2] and Super-K [3] already ruled out muon fluxes above $\sim 10^3$ per km^2 per year. The possibility of looking for even lower fluxes due to the increased size of the IceCube neutrino observatory with respect to previous detectors, motivates the continuation of searches for neutrinos coming from WIMP annihilations in the centre of the Earth.

2. The IceCube Neutrino Telescope

IceCube is located in the glacial ice at the geographic South Pole. It consists of an array of digital optical modules (DOMs), designed to collect the Cherenkov radiation produced by high energy, neutrino-induced charged leptons travelling through the detector volume. By recording the number of Cherenkov photons and their arrival times, the direction and energy of the charged lepton, and consequently that of the parent neutrino, can be reconstructed.

IceCube is an approximately 1 km^3 instrumented volume consisting of 86 strings, each containing 60 DOMs, deployed between 1450 m and 2450 m depth in the ice [4]. Of these 86, 8 strings at the centre of IceCube comprise DeepCore, a more densely instrumented sub-array equipped with high quantum efficiency DOMs.

While the large ice overburden provides a shield against downward going, cosmic ray induced muons with energies $\lesssim$ 500 GeV at the surface, most analyses also use the Earth as a filter and focus on upward going neutrinos. Additionally, low energy analyses mainly focus on DeepCore as a fiducial volume and use the surrounding IceCube strings as an active veto to reduce penetrating muon backgrounds. The search for WIMP annihilation signatures at the center of the Earth takes advantage of these two background rejection techniques as the expected signal will be vertically upgoing and of low energy.

3. Dark Matter from the centre of the Earth

WIMPs accumulated in the centre of the Earth will produce a unique signature in IceCube as vertically upgoing muons. The number of detected neutrino-induced muons depends on the neutralino annihilation rate Γ_A. If the capture rate C is constant in time t, Γ_A is given by [1]

$$\Gamma_A = \frac{C}{2}\tanh^2\left(\frac{t}{\tau}\right),\ \tau = (CC_A)^{-1/2}. \tag{3.1}$$

The equilibrium time τ is defined as the time when the annihilation rate and the capture rate are equal, where C_A is a constant depending on the WIMP number density. For the Earth, this equilibrium time is of the order of 10^{11} years if the spin-independent WIMP-proton cross section is $\sigma_p^{SI} \sim 10^{-43}$ cm^2 [5]. The age of the solar system is $t_\circ \approx 4.5$ Gyr and so $t_\circ/\tau \ll 1$, we thus expect that $\Gamma_A \propto C^2$, i.e. the higher the capture rate, the higher the annihilation rate and thus the muon flux.

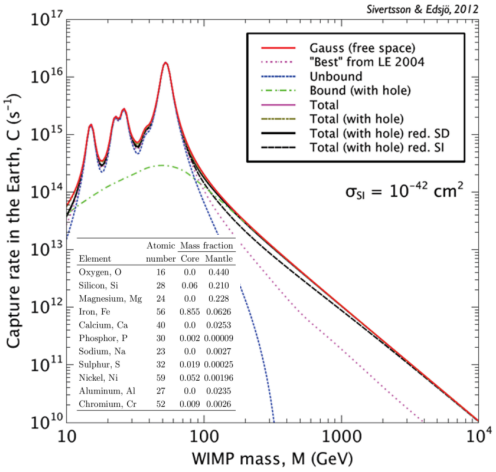

Figure 1: This figure shows the rate at which dark matter particles are captured to the interior of the Earth, for a scattering cross section of $\sigma = 10^{-42}$ cm^2. The peaks correspond to resonant capture on the most abundant elements (listed in the table, abundances are given in weight %) considered in the Earth model [6], ^{16}O, ^{24}Mg, ^{28}Si and ^{56}Fe and their isotopes. A dark matter halo density of $\rho_X = 0.3$ GeV cm^{-3} is assumed [7].

The rate at which WIMPs are captured in the Earth depends on the mass (which is unknown), the local WIMP density (which can be measured) and the velocity of the WIMPs (which cannot be measured observationally, and one has to resort to simulations to try to estimate it). If the WIMP mass is nearly identical to that of one of the nuclear species in the Earth, the capture rate will increase considerably, as is shown in Fig. 1. It should be noted that recent direct detection limits [8] exclude cross sections larger than $\sigma_p^{SI} = 10^{-43}$ cm^2 over a wide range of WIMP masses. This implies that the normalization in Fig. 1 should be corrected downward by about an order of magnitude lower, as the cross section that is assumed in the calculation for the capture rate is $\sigma = 10^{-42}$ cm^2 [7], but it does not affect the overall shape.

The capture rate could be higher if the WIMPs have a low velocity with respect to the Earth due to the small escape velocity, v_{esc}, of WIMPs inside the Earth. This escape velocity varies from 11 km/s at the mantle to 15 km/s at the center of the Earth. WIMPs with high velocities will thus only be captured at the center, whereas low velocity WIMPs may be captured anywhere inside the Earth. As different models for the halo lead to different WIMP velocity distributions, these distributions are very sensitive to theoretical assumptions. The most popular halo model is the Standard Halo Model (SHM), which is a smooth, spherically symmetric density component with a non-rotating Gaussian velocity distribution [9]. Galaxy formation simulations including baryons indicate, however, that there is at least one local macrostructural component beyond the SHM. Some of these simulations show that a thick disc of dark matter, with kinematics similar to the thick disc of stars and a mid-plane density of $0.25-1.5$ times the local dark halo density [10, 11], is formed as the baryonic disc of the Milky Way draws satellites closer to the disc plane by dynamical

friction, where they are disrupted by tides [12]. The particles in this dark disc have a lower relative velocity to the Earth compared to the SHM. Therefore, less scattering is needed for the particles in the dark disc to become gravitationally captured. This dark disk would lead to a higher capture rate and therefore a higher neutrino-induced muon flux at detectors such as IceCube.

4. Analysis

The last published Earth WIMP search was performed with the neutrino data recorded by the AMANDA detector over the three year period 1997 – 99 [2]. No excess above the expected atmospheric neutrino background was found in this search and therefore an upper limit was set on the WIMP annihilation rate Γ_A, in the Earth (dotted line in Fig. 6)

This analysis uses the first year of IC86 data, which has been taken between May 2011 and May 2012. In order to do everything in a blind way, the event selection is optimized by using simulations to estimate the background and signal events. The background simulation consists of atmospheric muons that are simulated with CORSIKA [13] and atmospheric neutrinos that are simulated with GENIE [14] for neutrinos below 190 GeV and NuGeN [15] above. The signal simulations that are used in the analysis are performed using WimpSim [16]. WimpSim is a code that describes the capture and annihilation of WIMPs inside the Sun or the Earth, collects all neutrinos that emerge and lets these propagate out of the Sun/Earth to the detector. The code includes neutrino interactions and neutrino oscillations in a fully consistent three-flavour treatment.

To be sensitive to a wide range of WIMP masses, the analysis is split in two parts, one that is optimised for low masses and the other for higher masses.

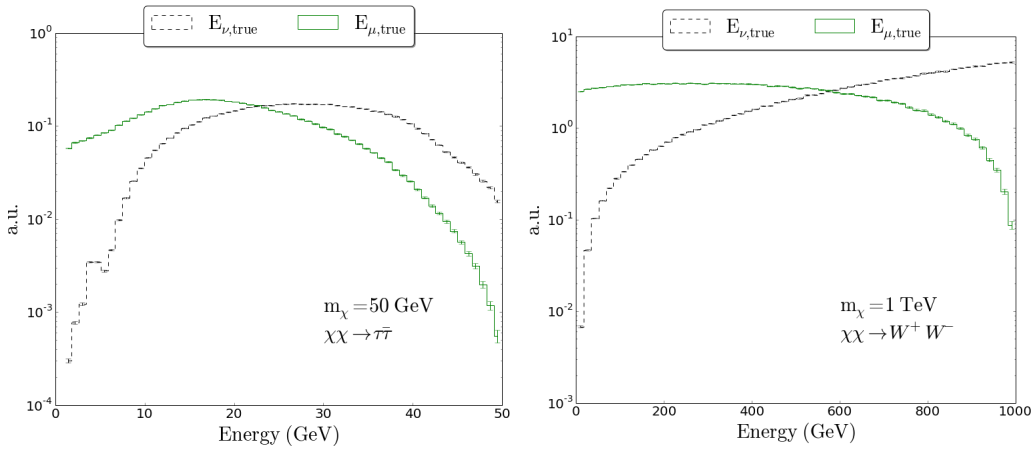

Figure 2: The normalized energy distributions for signal neutrinos and signal neutrino-induced muons, for a WIMP mass of 50 GeV (left) and 1 TeV (right).

The low mass analysis is optimised on WIMPs with a mass $m_\chi = 50$ GeV, that annihilate into $\tau\bar{\tau}$. As the capture rate is highest for WIMPs for this mass (see Fig. 1), the annihilation and thus neutrino rate are also highest. The high mass optimisation is done on WIMPs with a mass $m_\chi = 1$ TeV, that annihilate into W^+W^-. The expected neutrino spectrum (solid lines) and the neutrino-induced muon spectrum (dashed lines) for 50 GeV WIMPs annihilating into $\tau\bar{\tau}$ and

1 TeV WIMPs annihilating into W^+W^- are shown in Fig. 2. Note that the expected muon energy for the 50 GeV WIMPs is lower than 50 GeV, so DeepCore detector will be crucial in this part of the analysis.

The neutrino-induced muon rate in IceCube, coming from WIMPs in the centre of the Earth can not be higher than $\sim 10^3$ muons per year [2, 3], which is a very low rate, compared to the 2.5 kHz rate at which IceCube is taking data. The data are dominated by atmospheric muons (kHz rate), which can be removed via selection cuts, as explained below. These cuts lower the data rate by $\sim$6 orders of magnitude, to get to the level where the data are mainly consisting of atmospheric neutrino events (mHz rate). As atmospheric neutrino events with the same direction and energy as signal neutrino events are irreducible, a statistical analysis is performed on this neutrino sample, to look for an excess from the centre of the Earth.

The first level of cuts are done on the whole sample, i.e. before splitting the data into a low and a high energy sample. This is done to reduce the data rate to $\sim$ 1 Hz, such that more precise (and more time-consuming) reconstructions can be used to calculate the energy on which the splitting will be based. These first cuts consist of a selection of online filters that tag upgoing events, followed by linear cuts on direction and interaction vertex of the lepton. These variables are not correlated with the energy of the neutrino and have thus similar efficiencies for different WIMP masses.

The variables that are used for cuts at this level are the reconstructed zenith angle, the reconstructed interaction vertex and the average drift of hits in the vertical (z) direction. The zenith angle cut can not be too strict, as we aim to retain a signal free control region in which the agreement between data and background simulation will be tested. This is necessary as the detector acceptance is zenith dependent and it is thus not possible to define an off-source region in this analysis. Therefore we need to rely on simulations to understand the background, requiring a detailed understanding of systematic uncertainties. Based on these considerations, the zenith angle cut is chosen such that all events with a reconstructed zenith angle < 120° are removed, and the agreement between data and background simulation can be tested in the region < 150°. The other cut values are chosen by looping over all possible combinations of cut values and checking which combination brings down the background to the Hz level, while removing as little signal as possible.

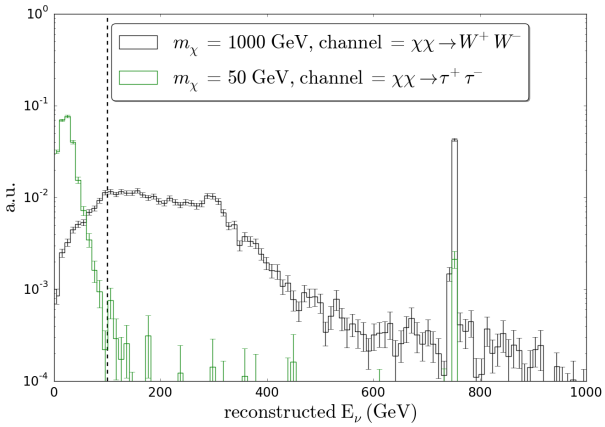

Figure 3: The reconstructed energy distributions for 50 GeV and 1 TeV Earth WIMPs. The vertical dashed line shows where the data sets are split. The peak at $\sim$750 GeV comes from tracks with a reconstructed length of 2 km, which is the value that is set by the algorithm when the length of the muon cannot be reconstructed (e.g. when it is not contained in the detector). As these events are generally bright events, it is a good feature that they end up in the high energy sample.

After this first cut level, the data rate goes down to $\sim$3 Hz, while 30%-60% of the signal

(depending on WIMP mass and channel) is kept. The data is still dominated by atmospheric muons at this level. Now that the data is at this low rate, it can be reprocessed using more precise (and more time-consuming) reconstructions.

One of these reconstructions is an energy reconstruction that is used in oscillation analyses in IceCube [17]. The reconstructed energies for 50 GeV and 1 TeV WIMP neutrinos are shown in Fig. 3. A division at 100 GeV, shown as a vertical line in this figure, is used to split the datasets into low and high energy samples which are statistically independent and will be optimized and analyzed separately.

Both analyses make use of Boosted Decision Trees (BDT), which is a machine learning technique that is designed to optimally separate signal from background [18] by assigning a score between -1 (background-like) and +1 (signal-like) to each event. Before training the BDT, one has to be sure that the simulation is representing the experimental data in a correct way, for this reason some more linear cuts are made prior to the BDT training in order to get good agreement between data and simulation. After this step, the experimental data rates are on the order of 100 mHz, and the data are still dominated by atmospheric muons. The BDTs are then trained on variables that are not too correlated, and that have good data-simulation agreement.

In the low energy optimization, the BDT training samples consist of simulated 50 GeV WIMP neutrinos and experimental data for the signal and background set respectively.

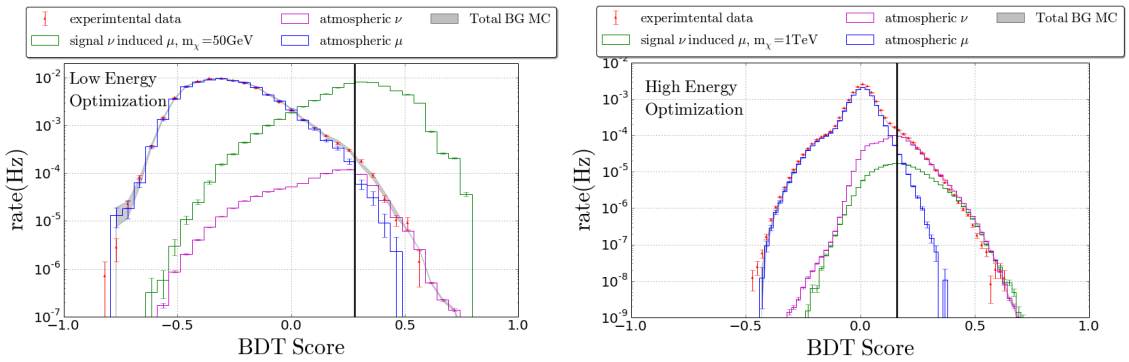

Figure 4: The plot shows the BDT score distributions the low energy analysis (left) and for the high energy analysis using the *Pull-Validation* method (right). Signal distributions are upscaled to be visible in the plot. Signal and backgrounds are compared to experimental data from 10% of the first year of IC86 data. The vertical lines indicate the final cut value used in each analysis, where high scores to the right of the line are retained.

Because the opening angle between the neutrino and its daughter lepton is inversely proportional to the energy of the neutrino, WIMP neutrino-induced muons in the high energy analysis are going to be narrowly concentrated into vertical zenith angles, whereas in the low energy analysis they will be spread over a wider range of zenith angles. To train the BDT in the high energy analysis to find upgoing neutrino-induced candidates generally (rather than straight vertical events specifically), an generic muon neutrino simulation weighted to the energy spectrum of 1 TeV WIMP neutrinos is used to simulate the signal.

The cuts on the BDT score are chosen such that the sensitivities of the analyses are optimal. The sensitivities are calculated with a likelihood ratio hypothesis test based on the values of the reconstructed zenith, using the Feldman-Cousins unified approach [19]. The required probability

densities for signal and background are both calculated from simulations, as this analysis has no off-source region. The background sample that is left after the cut on BDT score mainly consists of atmospheric neutrinos and only has a small amount of atmospheric muon events. Smoothening methods are used to deal with this problem of small statistics.

The high energy analysis uses the *Pull-Validation* method [20], which is a method in which several BDTs (200 in the case of the present analysis) are trained on small subsets that are randomly resampled from the complete dataset. The variation of the BDT output between the trainings can be interpreted as a probability density function (PDF) for each event. This PDF can be used to calculate a weight that is applied to each event instead of making a binary cut decision. With this method not only the BDT score distribution is smoothened (Fig. 4-left), but also the distributions that are made after a cut on the BDT score. In particular the reconstructed zenith distribution used in the likelihood calculation is smooth, as events that would be removed when using a single BDT could now be kept, albeit with a smaller weight.

The low energy analysis tackles the problem of poor statistics of the atmospheric muon background sample in a different way. In this part of the analysis, only a single BDT is trained (Fig. 4-right), and after the cut on the BDT score, the reconstructed zenith distribution is smoothened using Kernel Density Estimation (KDE) [21, 22], which is a method that smoothens each observed data point over a local neighbourhood of that data point.

The reconstructed zenith distributions after the cuts on the BDT scores are shown in Fig. 5. In these plots, the complete dataset of the first year of IC86 data is shown.

5. Results and conclusions

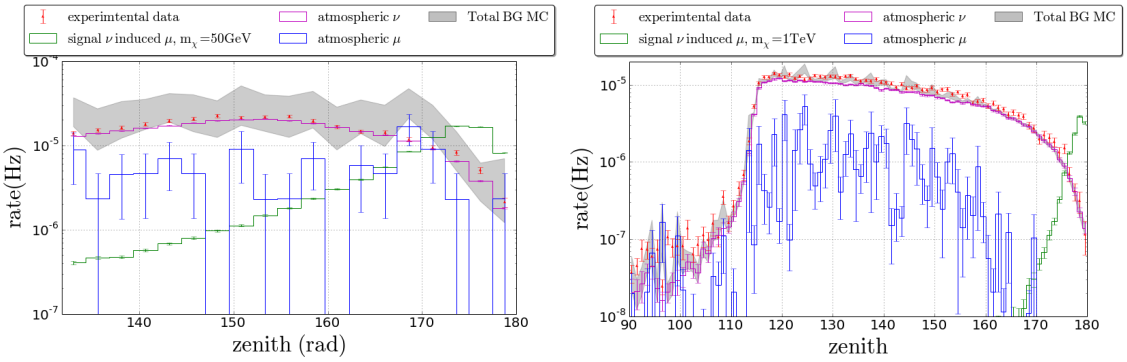

Figure 5: The plot shows the unblinded reconstructed zenith distributions of 1 year of IC86 data for the low energy analysis (left) and the high energy analysis using the *Pull-Validation* method (right). Signal distributions are upscaled to be visible in the plot. The gray areas indicate the background distributions with the 1 sigma uncertainties, including both statistical and systematic uncertainties for the left plot, and statistical uncertainties for the right plot.

As can be seen in Fig. 5, no statistically significant excess is found from the direction of the centre of the Earth, allowing us to set limits on the neutrino flux from the centre of the Earth in the GeV-TeV range. These limits are calculated by using the final reconstructed zenith angle distributions as probability density functions in the likelihood calculation, using the Feldman-Cousins

unified approach [19]. For the signal, the zenith distribution at each WIMP mass is calculated with WimpSim and for the background the smoothened zenith distributions of the remaining simulated atmospheric muons and neutrinos are used.

The limits on the WIMP annihilation rate in the Earth Γ_A for 1 year of IC86 data (2011-2012)[1] are shown in Fig. 6 and are compared with the AMANDA limits [2] which is the last Earth WIMP neutrino search. An improvement of a factor 10 has been found, meaning that a whole new part of the theoretical phase space can be excluded with this analysis.

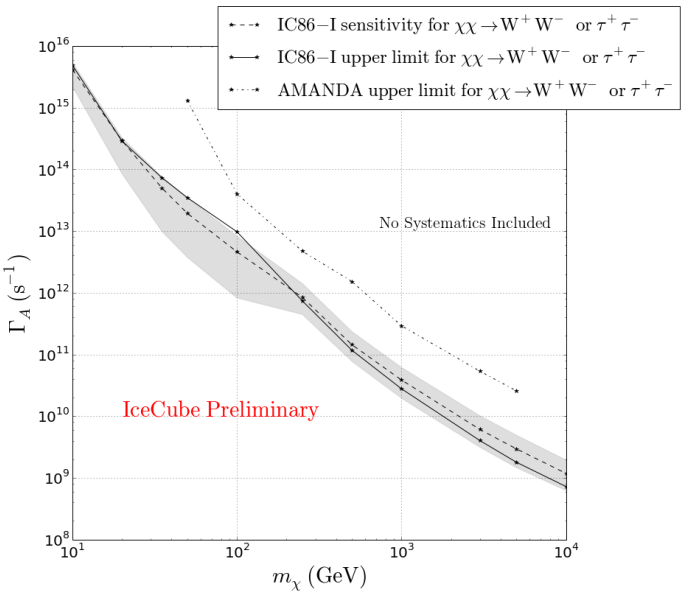

Figure 6: The upper limits (solid line) and sensitivities (dashed line) with 1 sigma uncertainty (gray band, not including systematics) on the annihilation rate in the Earth Γ_A for 1 year of IC86 data as a function of the WIMP mass. The dotted line shows the latest upper limit on the annihilation rate, which was calculated with AMANDA data.

References

[1] T. Bruch et al., *Phys. Lett. B* **675** (2009) 250 [astro-ph/0902.4001].
[2] A. Achterberg et al., *Astropart. Phys.* **26** (2006) 129 [astro-ph/0202370v3].
[3] S. Desai et al., *Phys. Rev. D* **70** (2004) 083523 [hep-ex/0404025].
[4] **IceCube** Collaboration, A. Achterberg, et al., *Astropart. Phys.* **26** (2006) 155 [astro-ph/0604450].
[5] G. Jungman et al., *Phys. Rep.* **267** (1996) 195 [hep-ph/9506380].
[6] W.F. McDonough and S. Sun, *Chemical Geology* **120** (1995) 223.
[7] S. Sivertsson and J. Edsjö, *Phys. Rev. D* **85** (2012) 123514 [astro-ph/1201.1895].
[8] E. Aprile et al., Phys. *Rev. Lett.* **109** (2012) 181301 [astro-ph/1207.5988].
[9] K. Freese et al., *Phys. Rev. D* **37** (1988) 3388.
[10] J. Read et al., *MNRAS* **389** (2008) 1041 [astro-ph/0803.2714].
[11] J. Read et al., *MNRAS* **397** (2009) 44 [astro-ph/0902.0009].
[12] G. Lake, *Astrophys. J.* **98** (1989) 1554.
[13] D. Heck et al., *FZKA Report* **6019** (1998).
[14] C. Andreopoulos et al., *Nucl. Instrum. Meth. A* **614** (2010) 87 [astro-ph/0905.2517].
[15] A. Gazizov et al., *Comput. Phys. Commun.* **172** (2005) 203 [astro-ph/0406439].
[16] J. Edsjö, WimpSim Neutrino Monte Carlo, http://copsosx03.fysik.su.se/wimpsim/.
[17] **IceCube** Collaboration, M. G. Aartsen, et al., *Phys. Rev. D* **91** (2015) 072004 [hep-ex/1410.7227].
[18] A. Hoecker et al., *PoS A CAT* **040** (2007) [physics/0703039].
[19] G. J. Feldman and R. D. Cousins, *Phys. Rev. D* **57** (1998) 3873 [physics/9711021].
[20] **IceCube** Collaboration, *PoS(ICRC2015)1211* these proceedings.
[21] M. Rosenblatt, *The Annals of Mathematical Statistics* **27** (1956) 832.
[22] E. Parzen, *The Annals of Mathematical Statistics* **33** (1962) 1065.

[1] These limits don't contain systematic uncertainties yet.

PROCEEDINGS OF SCIENCE

Search for dark matter annihilations in the Sun using the completed IceCube neutrino telescope.

The IceCube Collaboration[†],

[†]*http://icecube.wisc.edu/collaboration/authors/icrc15_icecube*

E-mail: Mohamed.Rameez@cern.ch

Dark matter particles after scattering off nuclei would be gravitationally captured in the Sun where they may pair-annihilate into standard model particles. Terrestrial neutrino detectors such as IceCube can observe this as an enhanced neutrino flux from the direction of the Sun. We present results from an analysis of 341 days of livetime of IceCube-DeepCore in the 86 string configuration. The sensitivity has improved with respect to previous searches due to better analysis methods and reconstructions. In addition, improved veto techniques using the outer layers of the cubic kilometre array have been used to reduce the atmospheric muon background and thus enhance sensitivity during the austral summer.

Corresponding authors: M. Rameez[*1], T. Montaruli[1], S. Vallecorsa[1],

[1] *Département de physique nucléaire et corpusculaire, Université de Genève, 24 Quai Ernest Ansermet, 1211 Genève, Switzerland*

The 34th International Cosmic Ray Conference,
30 July- 6 August, 2015
The Hague, The Netherlands

[*]Speaker.

1. Introduction

Astrophysical observations provide strong evidence for the existence of dark matter(DM). However the nature of DM is unknown. An interesting and experimentally accessible candidate is the so called 'Weakly Interacting Massive Particle (WIMP)'(see [1] for a comprehensive review) - expected to exist in the mass range of a few GeVs to a few TeVs. If DM consists of WIMPs, they will be gravitationally captured by the Sun [2], where they may pair-annihilate into standard model particles, including neutrinos. Given enough time, the capture and annihilation processes would reach equilibrium [3] and on average only as many WIMPs annihilate as are captured per unit time. This DM-generated neutrino flux may be detected at terrestrial neutrino detectors such as IceCube. As the region at the centre of the Sun where most of the annihilations will occur is very small, the search is equivalent to looking for a point-like source of neutrinos. However, neutrinos above 1 TeV have interaction lengths significantly smaller than the radius of the Sun and are mostly absorbed. As a result all the signal is expected in the range of a few GeVs to $\sim$1 TeV, making this a very low energy point-source search for IceCube. The energies are nevertheless high enough that such neutrinos can never be made by nuclear fusion processes in the Sun.

2. The Detector

IceCube is a cubic-kilometer neutrino detector installed in the ice at the geographic South Pole [8] between depths of 1450 m and 2450 m. Detector construction started in 2005 and finished in 2010. Neutrino reconstruction relies on the optical detection of Cherenkov radiation emitted by secondary particles produced in neutrino interactions in the surrounding ice or the nearby bedrock. At the center of the array, there are 8 more densely instrumented strings containing Digital Optical Modules (DOMs) with higher quantum efficiency photomultiplier tubes, optimized for lower energies. Along with 7 adjacent standard strings, these are defined as the DeepCore sub-array for the purpose of this analysis.

3. Event Selection

Neutrino flux predictions at Earth from WIMP annihilations in the Sun have been widely studied, for example in Ref [4]. We use the flux predictions from DarkSuSy [5] and WimpSim [4] to simulate signals for the IceCube detector according to specific annihilation scenarios. The energy range of the expected signal (a few TeV at maximum) and the properties of IceCube at these energies dictate the event selection strategies. While the principal IceCube array has an energy threshold of $\sim$100 GeV, the more densely instrumented DeepCore infill array has an energy threshold of $\sim$10 GeV. This means that for WIMP masses < 200 GeV, which produce signal neutrinos mostly with energies below the IceCube threshold, only DeepCore[6] will contribute significantly towards the effective volume. However, for higher WIMP masses where a significant fraction of the resultant neutrinos are above the IceCube threshold, the full effective volume of IceCube comes into play. For optimizing the event selections for the analysis and setting upper limits, we consider two scenarios: WIMPs annihilating completely into W^+W^-, a 'hard' channel with emission peaked at neutrino energies close to the WIMP mass, and WIMPs annihilating completely into $b\bar{b}$, a 'soft'

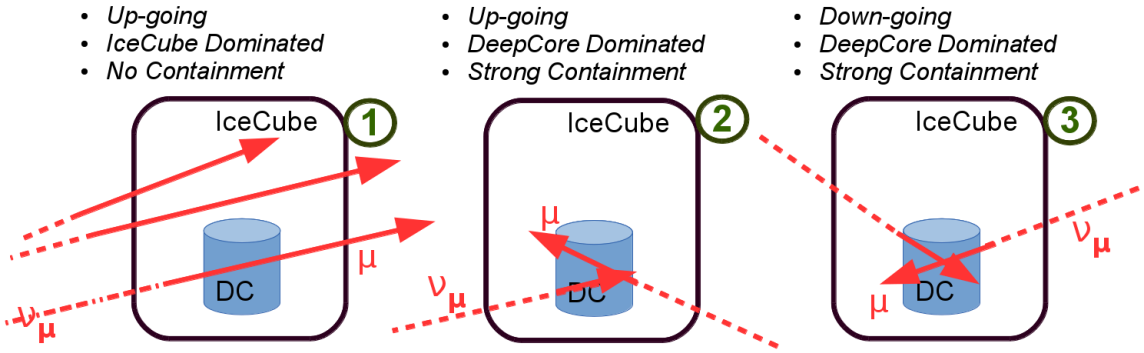

Figure 1: The three event selection strategies for the solar WIMP analysis. Most of the sensitivity for neutrino signals below 100 GeV comes from the DeepCore (DC) dominated low energy samples(2 and 3). During the austral summer (when the Sun is a source of downgoing neutrinos), the very large muon background forces us to use the outer detector as a Veto (see Fig. 2) and consequently there is only a DeepCore dominated-low energy sample (3). This approach is similar to that of earlier IceCube analyses such as [7].

channel with emission peaked at neutrino energies of a few GeV. Since IceCube acceptance is very energy dependent, cuts have to be optimized for the spectral composition of the expected signal flux. For WIMP masses below 80.4 GeV, we also consider a WIMP annihilating into $\tau\bar{\tau}$, since annihilations to W^+W^- are no longer kinematically allowed.

Within IceCube, a standard set of filters are used to pre-select signal-like muon events and reduce the rate of the dominant atmospheric background. This analysis starts with a stream of data from three of these filters, a low-energy DeepCore filter and two filters selecting muon-like events that point upwards; one favouring short low energy tracks and another that favours bright through-going tracks. After these filters the data rate is ~ 100 Hz. From this point onwards, data are treated differently depending upon whether they fall in the austral winter or summer.

During the austral winter, when the Sun is below the horizon, the signal consists of upgoing neutrinos. The background is dominantly made up of downgoing atmospheric muons falsely reconstructed as upgoing. Reconstructed event properties quantifying topology, track length, reconstruction quality etc are used to reject background such as very high energy events or vertical events which obviously cannot come from the Sun and reduce the data to ~ 2 Hz. At this point, a likelihood reconstruction with a prior based on the zenith distribution, which takes into account that the majority of the tracks are downgoing atmospheric muons, is performed to identify and remove falsely reconstructed downgoing events. Depending upon the location of the majority of detected Cherenkov photons (whether within IceCube (1) or within DeepCore (2)), events are split into two streams (see Fig 1). Subsequently, separate instances of a multivariate classification algorithm, known as Boosted Decision Tree (BDT), are used to select signal-like events from both these streams. The BDT of the IceCube dominated sample (1) is optimized for events from a 1 TeV WIMP annihilating into the hard W^+W^- channel while the DeepCore dominated sample (2) is optimized for events from 100 GeV and 50 GeV WIMPs annihilating into W^+W^-, $b\bar{b}$ and $\tau^+\tau^-$ channels. After the selection based on the BDT classifier, event rates of the two samples are ~ 2.9 mHz and ~ 0.34 mHz, respectively, consistent with expectations from a background that is dominated by atmospheric neutrinos.

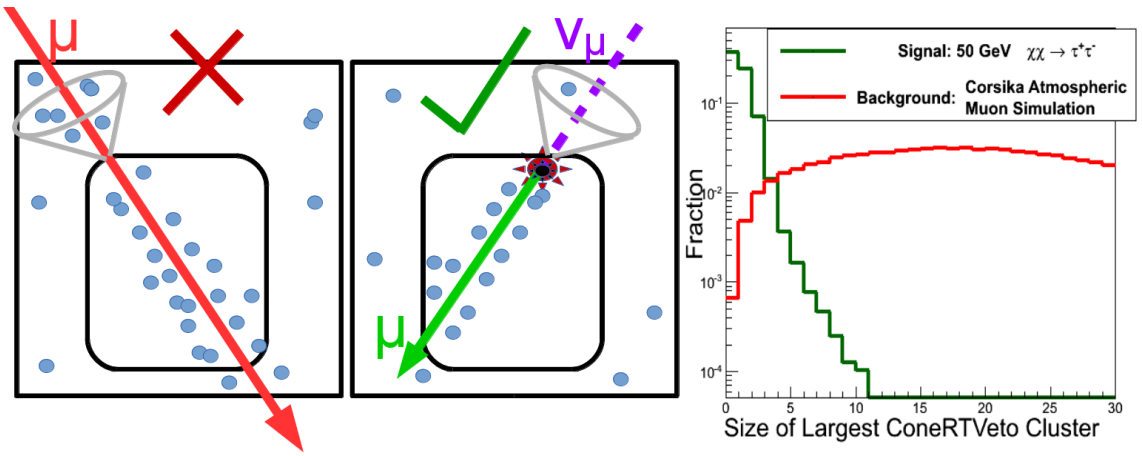

Figure 2: On the left and center: A schematic representation of the veto concept to reject atmospheric muon background and retain neutrinos during austral summer. Only events with their reconstructed vertex near DeepCore are selected. Subsequently, the photon detections within a cone of 40° half-angle at the vertex and aligned along the muon track are sorted into clusters based on whether they are within a specific 'Radius + Time (RT)' radius of each other. The size of the largest of these clusters of hits is reported. On the right: size of this cluster for signal (green) and background (red). Selecting events with cluster sizes ≤ 3 will keep more than 90% of signal while rejecting more than 90% of background of atmospheric muons.

During the austral summer (23rd September 2011 to 16th March 2012), the signal (downgoing) is overwhelmed by a background of downgoing atmospheric muons ($\sim 10^6$ times higher in rate) in addition to the atmospheric neutrinos. A sample of DeepCore dominated downgoing tracks ((3) in Fig 1) can be isolated by using the outer laters of IceCube as a veto (see Fig. 2). This sample is again optimized using a BDT algorithm to select events expected from 100 GeV and 50 GeV WIMPs annihilating into W^+W^-, $b\bar{b}$ and $\tau^+\tau^-$ channels. After the BDT-based event selection the even rate is ~ 0.24 mHz, consistent with the expected residual atmospheric neutrino and muon background.

Fig. 3 summarizes final effective areas and angular resolutions of the three samples.

4. Analysis method

The significance of a cluster of events in the direction of the Sun can be estimated using a modified version of the unbinned maximum likelihood ratio method described in Ref. [9]. Due to the very large point spread function of IceCube at these low neutrino energies, we model the spatial signal p.d.f of Ref. [9] as a Fisher-Bingham distribution from directional statistics [10].

For the fully contained events of the DeepCore dominated samples ((2) and (3) of Figure 1), the energy of the neutrino can be estimated by summing the energy of the muon (obtained by reconstructing the starting and stopping vertex of the muon) and the hadronic cascade from the charged current interaction. Signal and background p.d.f.s are constructed from the signal simulation and datasets randomized in azimuth respectively. Energy weighting is added to the likelihood to enhance sensitivity. Thus the signal p.d.f. is given by:

$$S_i(|\vec{x}_i - \vec{x}_{sun}(t_i)|, E_i, m_\chi, c_{ann}) = \mathscr{K}(|\vec{x}_i - \vec{x}_{sun}(t_i)|, \kappa_i) \times \mathscr{E}_{m_\chi, c_{ann}}(E_i), \tag{4.1}$$

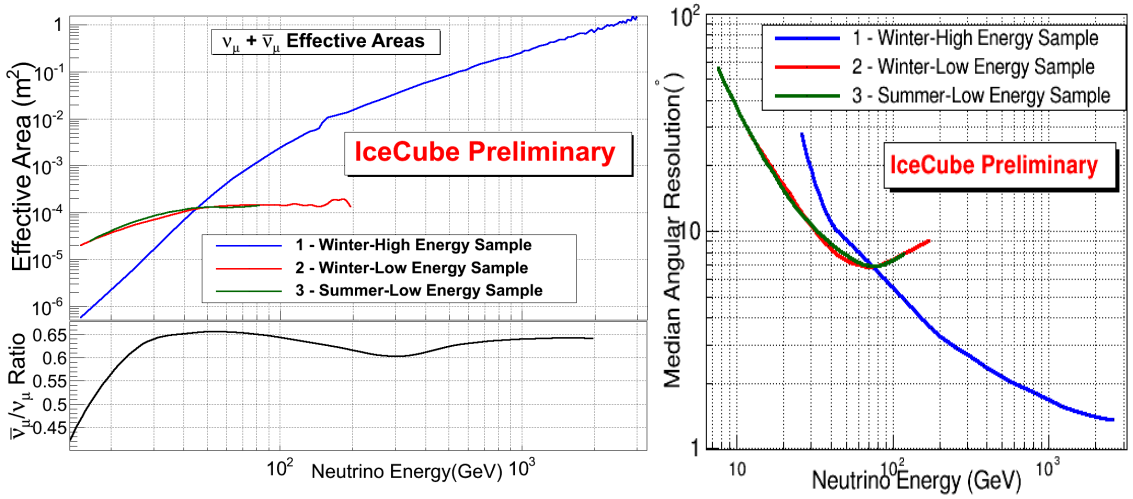

Figure 3: Top Left: $\nu_\mu + \bar{\nu}_\mu$ effective areas for the three different event selections. Bottom Left : Ratio of the $\bar{\nu}_\mu$ and ν_μ effective areas, determined by the relative cross sections and inelasticities of $\bar{\nu}_\mu$ and ν_μ. Right: The angular resolutions of the three samples at different energies, defined as the median of the angular separation between the incoming neutrino and the reconstructed muon.

where $\mathscr{K}$ stands for the spatial and $\mathscr{E}$ for the spectral parts of the p.d.f. and m_χ and c_{ann} stand for the mass and annihilation channel of the WIMP respectively.

$$\mathscr{K}(|\vec{x}_i - \vec{x}_{sun}(t_i)|, \kappa_i) = \frac{\kappa_i e^{\kappa_i cos(\theta_{|\vec{x}_i - \vec{x}_{sun}(t_i)|})}}{2\pi(e^{\kappa_i} - e^{-\kappa_i})} \tag{4.2}$$

where the concentration factor κ_i of the monovariate Fisher-Bingham distribution is obtained from the likelihood based estimate of the angular resolution of the track reconstruction [11].

The backgroung p.d.f. is:

$$\mathscr{B}_i(\vec{x}_i, E_i) = B(\delta_i) \times P(E_i|\phi_{atm}) \tag{4.3}$$

where $B(\delta_i)$ is the declination dependence and $P(E|\phi_{atm})$ indicates the distribution of the energy estimater E of the data sample at analysis level which is consistent with expectations from atmospheric muon and neutrino fluxes and is denoted by ϕ_{atm}.

The spatial p.d.f of the signal and the energy p.d.f of a specific signal and background are illustrated in Fig. 4.

For a sample of N events consisting of n_s signal events from the Sun and $N - n_s$ background events, the likelihood can then be written as:

$$\mathscr{L}(n_s) = \prod_N \left(\frac{n_s}{N} S_i + (1 - \frac{n_s}{N})\mathscr{B}_i\right) \tag{4.4}$$

The best estimate for the number of signal events in the sample is obtained by maximizing the likelihood ratio as defined in Ref. [9]. The significance of the observation can be estimated without depending on Monte Carlo simulations by repeating the process on datasets scrambled in right ascension. As the three separate event selections have no events in common, they can be combined

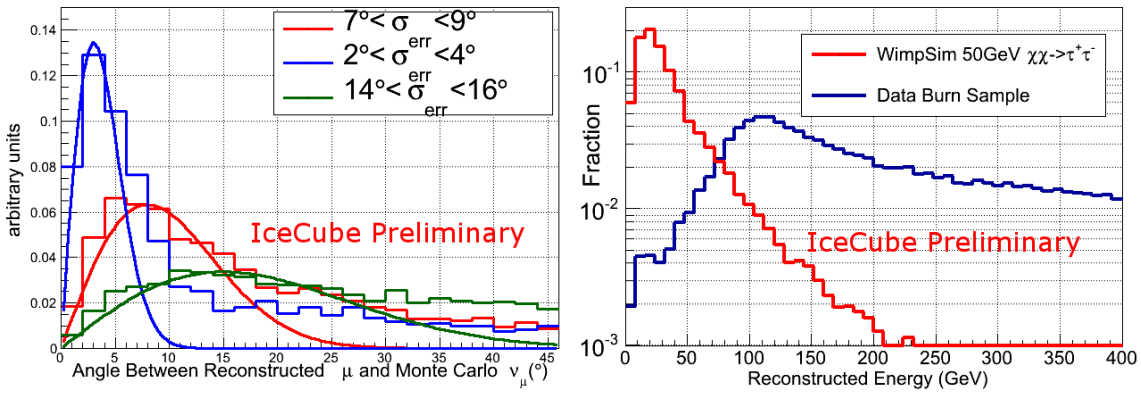

Figure 4: Left: Distribution of the angle between the Monte Carlo neutrino and the reconstructed muon for Monte Carlo events in three different ranges of angular resolutions of the track reconstruction. The histograms denote the observed distribution from Monte Carlo while the smooth curves are the analytical predictions from the Fisher Bingham distribution. While a better description of the tails can improve the sensitivity of this search, the impact will be small due to the small fraction of events present. Right: Normalized distributions of the reconstructed energy observed in real data as well as in signal Monte Carlo for 50 GeV WIMPs annihilating into the $\tau^+\tau^-$ channel. Both plots are for the Winter Low Energy selection.

statistically using the method described in [12]. Confidence intervals on the number of signal events present within the sample are constructed using the method of Feldman and Cousins[13].

5. Results and discussion

No significant excess was found in the direction of the Sun, allowing us to set stringent limits on the neutrino flux from the Sun in the GeV-TeV range. Assuming a local DM density of 0.3 GeV/cm^3, a standard Maxwellian halo velocity distribution and the Standard Solar Model, this limit can also be interpreted as a limit on the WIMP-nucleon scattering cross section. For the spin dependent case, IceCube limits are the most competitive in the region above $\sim$ 150 GeV (Fig. 5). Limits have improved by a factor of $\sim$30% to 60% w.r.t. the previous IceCube analysis [7]. The uncertainties on these limits due to uncertainties in velocity distributions of DM have been quantified in [20] and turn out not to be not greater than $\sim$ 50%. The study also concludes that these limits are conservative with regard to the possible existence of a dark-disk. A second independent solar wimp analysis carried out on the same data set has achieved a consistent level of sensitivity and is presented as separate contribution to ICRC[14].

Two more years of IceCube data are being analyzed using a similar approach and sensitivities are expected to improve further.

In specific supersymmetric models such as the MSSM [21] where the lightest stable state is the neutralino - a good WIMP candidate, these results can be used to constrain the parameter space of such models. More generally, the limits can be interpreted as limits on coupling strengths and mediator masses in certain Effective Field Theories(EFTs), parameter space of which can also be explored at collider searches [23, 24].

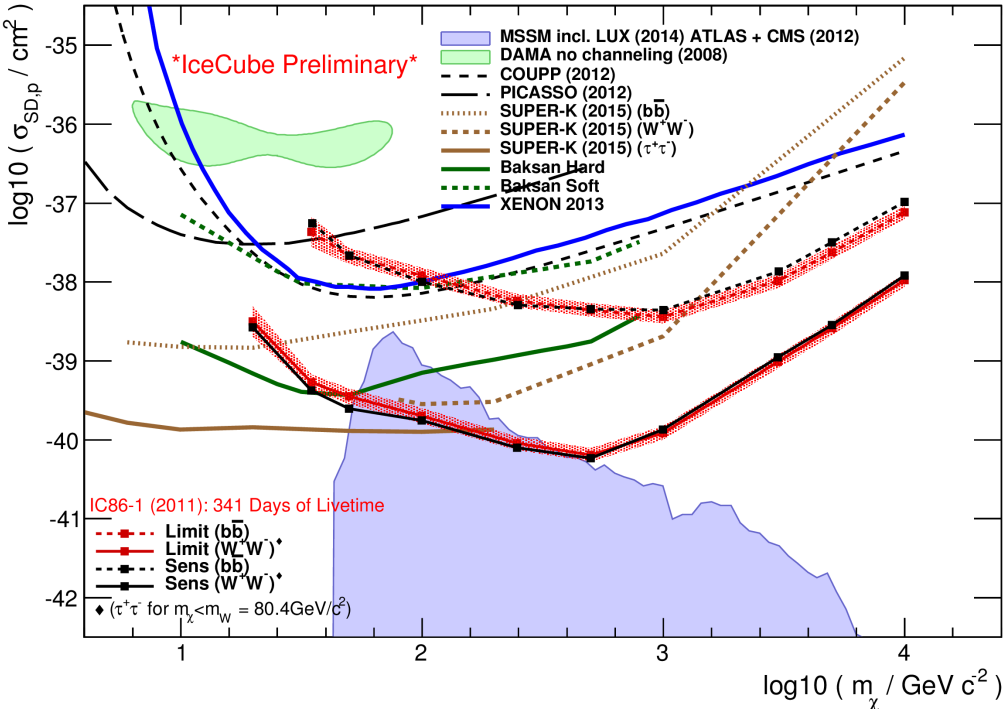

Figure 5: Limits on the spin dependent WIMP-Nucleon scattering cross section as a function of the WIMP mass, derived from this analysis and compared to other experiments' limits from [15, 18, 19, 21, 22]. The red band around the limit signifies systematic uncertainties.

References

[1] G. Bertone *et al*, Phys Rep., **405** (2005) p.279

[2] A. Gould *et al*, 1987 ApJ, vol. **321**, Oct. 1, 1987, p. 571-585.

[3] G. Jungman *et al*, Phys.Rept. **267** (1996) 195-373

[4] M. Blennow, J. Edsjö and T. Ohlsson, JCAP **01**, 021 (2008)

[5] P. Gondolo, J. Edsjö, P. Ullio, L. Bergström, M. Schelke and E.A. Baltz, JCAP **07**, 008 (2004)

[6] R. Abbasi *et al.*, [IceCube Coll.], Astropart. Phys. **35** (2012).

[7] M. G. Aartsen *et al.* [IceCube Coll.], Phys. Rev. Lett. **110**, 131302 (2013)

[8] A. Achterberg *et al.* [IceCube Coll.], Astropart. Phys. **26** 155. (2006)

[9] J. Braun *et al*, Astropart.Phys. **29**, 299-305 (2008).

[10] J.T. Kent, J. Royal. Stat. Soc., **44** 71-80 (1982)

[11] T. Neunhoffer, Astropart.Phys. **25**, 220-225 (2006).

[12] M. G. Aartsen *et al.* [IceCube Coll.], ApJ **796** (2014) 109.

[13] G. Feldman and J. Cousins, Phys.Rev.D **57** 3873-3889 (1998)

[14] IceCube Coll., PoS (ICRC2015) 1099 these proceedings

[15] M. M. Boliev *et al.* JCAP **09**, 019 (2013)

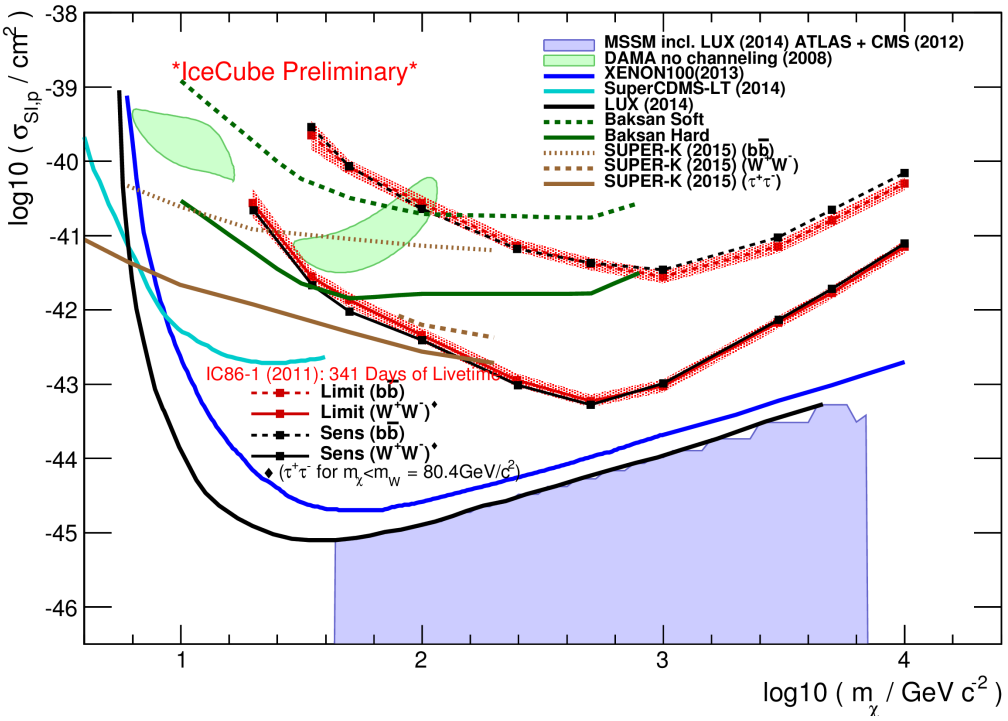

Figure 6: Similar limits on the spin independent WIMP-Nucleon scattering cross section compared to limits from [15, 16, 17, 18, 22]

[16] D. S. Akerib *et al.* [LUX Coll.], Phys. Rev. Lett. **112**, 091303 (2013).

[17] R. Agnese *et al.* [SuperCDMS Coll.], Phys. Rev. Lett. **112**, 241302 (2014).

[18] E. Aprile *et al.* [XENON Coll.], Phys. Rev. Lett, **109**, 181301 (2012).

[19] R. Bernabei *et al.*, Eur. Phys. J. C. **53** (2008), 205.

[20] K. Choi *et al.*, JCAP **05**, 049 (2014)

[21] H. Silverwood *et al.*, JCAP **03**, 027 (2013)

[22] K. Choi *et al.* [Super-Kamiokande Coll.], Phys. Rev. Lett. **114**, 141301 (2015)

[23] J. Blumenthal *et al.*, Phys. Rev. D **91**, 035002, 2015

[24] R. Catena, JCAP **04**, 052 (2015)

PROCEEDINGS OF SCIENCE

Pull-validation: A resampling method to improve the usage of low-statistics datasets

The IceCube Collaboration[†],

[†] *http://icecube.wisc.edu/collaboration/authors/icrc15_icecube*

E-mail: jan.luenemann@vub.ac.be

In high energy physics, many background dominated analyses suffer from limited statistics in simulation: With increasing efficiency of the event selection, the simulated samples are reduced so that in many cases the event number at final analysis level is very low. Due to limited computational resources, the production of more simulation is not always feasible. In these cases, it is helpful to extract more information from the available simulated datasets.
One way to deal with this issue in multivariate analyses (MVA) is by using resampling methods: The MVA is trained many times on small subsets that are randomly resampled from the complete dataset. The variation of the MVA output between the trainings can be interpreted as a probability density function (PDF) for each event. This PDF can be used to calculate a weight that is applied to each event instead of making a binary cut decision. With this procedure, events, that were normally removed by the event selection, can still contribute to the final dataset with a small weight. Another advantage is that pull-validation also provides an estimator for the uncertainty of the multivariate method. As an example of how the method can be used, we present a case-scenario from searches for physics beyond the Standard Model with IceCube.

Corresponding authors: J. Kunnen[1], J. Lünemann[*1], A. Obertacke Pollmann[2], F. Scheriau[3]

[1] *Vrije Universiteit Brussel*

[2] *Bergische Univertität Wuppertal*

[3] *Technische Univertität Dortmund*

The 34th International Cosmic Ray Conference,
30 July- 6 August, 2015
The Hague, The Netherlands

[*]Speaker.

1. Introduction

For typical analyses in high energy physics, very large datasets have to be evaluated. These datasets consist mostly of background, so that an effective event selection must be performed to remove parts of the data that presumably contain no signal. For this task, various multivariate analysis (MVA) tools can be applied, which assign to each event a value that can be interpreted as a probability that the event belongs to the signal or background class. An example are boosted decision trees (BDTs) [1], which assign a score between -1 (background-like) and $+1$ (signal-like) to each event. While the pull-validation technique described in this paper can be applied to different kinds of multivariate analysis methods, all examples provided in this papers are based on boosted decision trees.

In the first step of event selection, the classification algorithm has to be trained on labeled datasets (i.e. data with known class membership) to define efficient decision criteria exploiting differences in the measured variables of background and signal events. These datasets typically consist of simulated signal events and a combination of simulations of all known background types. After training, the decision criteria of the BDT are defined and the algorithm can be used to classify unlabeled data. An example of signal and background score distributions of a BDT is shown in Figure 1.

In analyses where the background rate is estimated from simulation, it can be problematic if the phase space of features for the background class is sparsely populated in the signal region. This will lead to low statistics for high classification scores so that the surviving background rate can be estimated only with large uncertainties. For cuts where no simulated background events survive, background estimation may be impossible. For example, a cut at 0.2 on the BDT score shown in

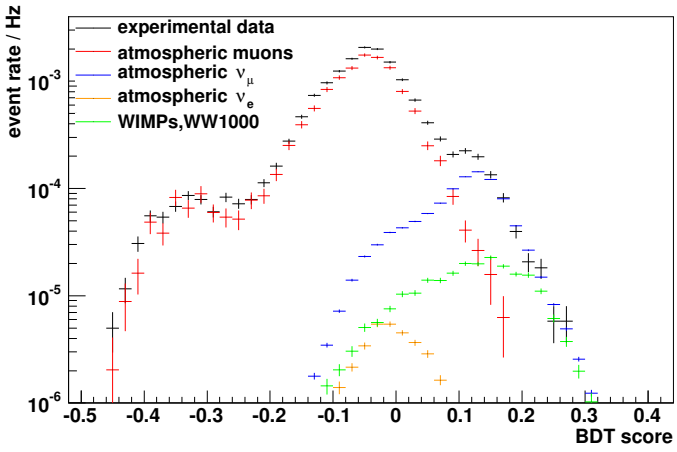

Figure 1: Score distribution for a single BDT, trained on a complete dataset available for training. This example is taken from an IceCube search for annihilating dark matter inside the Earth [2]. The goal of this selection is to achieve a sample with high neutrino purity. Experimental data, background simulations for atmospheric muons and neutrinos, and a neutrino signal from WIMPs with 1 TeV mass that annihilate inside the Earth into W^+W^- are shown.

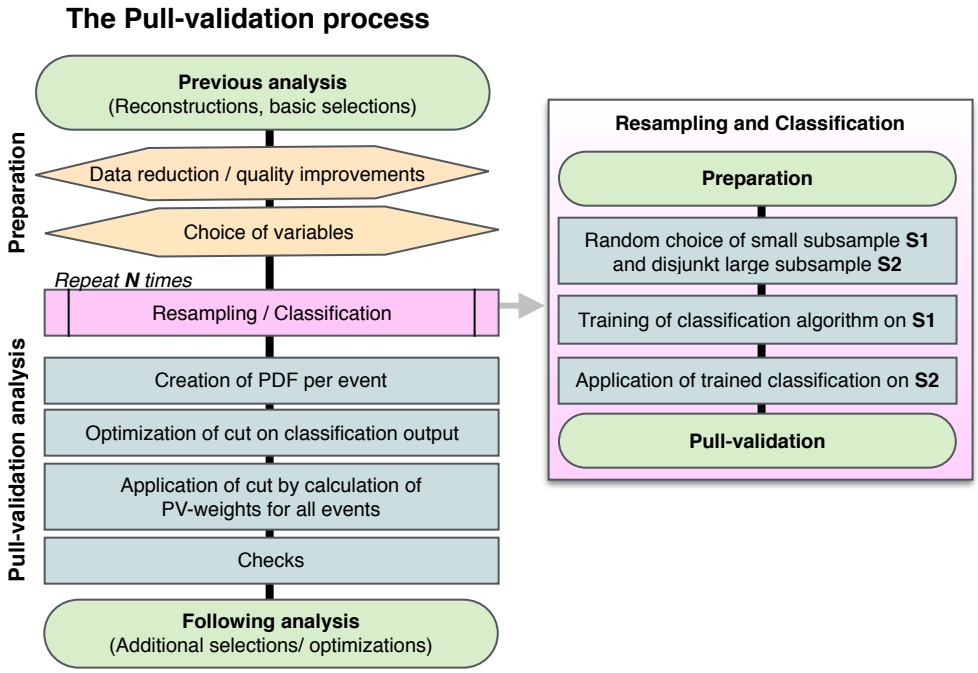

Figure 2: Schematic overview of the pull-validation technique in an analysis chain.

Figure 1 would remove all simulated atmospheric muons, falsely leading to a pure neutrino sample.

An obvious solution is the production of larger Monte Carlo datasets. However, simulation of large background statistics requires large computational efforts and is very inefficient if only the very signal-like tails of the score distributions are of interest. In contrast, the pull-validation technique utilizes the readily available datasets by enlarging the signal-like tail, as will be described in the following section. The term "pull" refers here to the selection of randomized samples and calculation of uncertainties. A schematic overview of this technique is given in Figure 2.

2. Pull-validation

A way to improve the usage of simulation statistics is to make use of uncertainties that can be derived by validation techniques. The most important validation techniques are cross-validation and bootstrapping [3, 4]. For cross-validation, the complete dataset is divided in N disjoint parts and the model is trained on subsamples composed of $(N-1)$ parts. After each training, the model is applied to the remaining subsample. In bootstrapping, events are randomly drawn and replaced for each subsample until these have the same size n as the original sample. Both methods achieve a smoothing of a distribution with insufficient statistics over the whole range. However, the effect is not large enough to compensate a lack of statistics larger than one order of magnitude. Pull-validation on the other hand can enlarge especially the tails of distributions.

Pull-validation includes a validation similar to bootstrapping. Like in bootstrapping, the variability of subsamples is used as an estimator for the variability of the whole sample. Instead of training the classification models with resampled sets of the size n, the subsamples are reduced

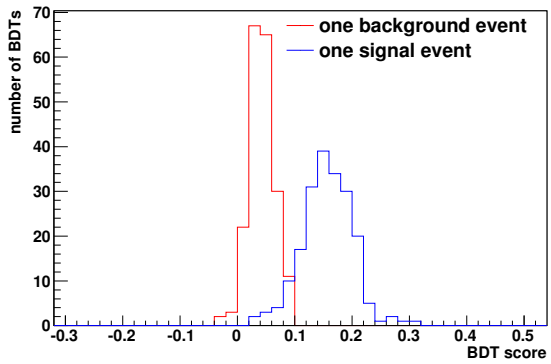

Figure 3: Score distribution of two example events, one of the background class and one of the signal class. As 200 BDTs were trained on different subsamples, the resulting scores for the same events show a variance.

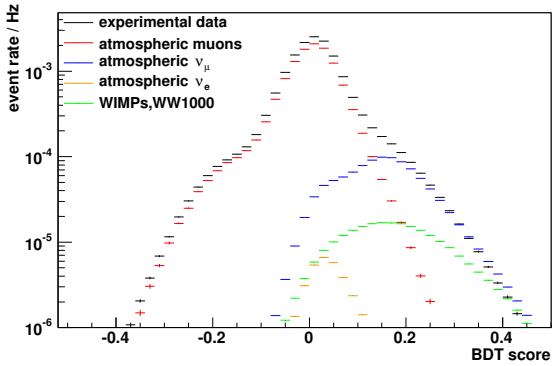

Figure 4: Sum of 200 BDT score distributions for the complete test dataset. Each BDT was trained on 10% of the training data. Compared to Figure 1, the distributions are smoother and broader.

in size (e.g. 10%), which leads to larger uncertainties. Since the subsamples are much smaller, the resampling can be done without replacement. This resampling and training is repeated several times (e.g. 200 times), each with a different subsample. This results in a large number of BDTs that will assign slightly different scores to the same event. The BDT score distribution of one event can be interpreted as probability density function (PDF), which is shown in Figure 3. The sum of all these PDFs (or equivalently the sum of the BDT histograms), shown in Figure 4, is considerably smoother that the single BDT distribution, shown in Figure 1. Note that the tails reach far deeper into the signal-like region.

A relation between pull-validation and kernel density estimation (KDE) is given by the fact that both methods smooth the score distributions. An important difference is that for pull-validation, the weights are derived from the uncertainties of the model while in KDE the smoothing is achieved without taking individual uncertainties into account. Calculating a weight for each event has the advantage that this information can be used in later stages after a cut on the BDT score.

In a classical event selection, a direct cut on the BDT score is applied, which means that an event is either accepted or rejected depending on whether its score is above a threshold or below. With pull-validation, this procedure can be replaced by calculating a weight for each event from its score distribution. This weight is determined by the fraction of scores above a threshold. This means that events with a medium score below the threshold can contribute to the final sample with a reduced weight, instead of being rejected completely. Therefore this procedure gives a higher statistics in the final sample. Figure 5 shows a comparison with a classical event selection, where a cut on a single BDT is applied, with an event selection using pull-validation weights. In this figure, the BDT cut was varied, which results in different final event rates. For each estimated event rate, the statistical uncertainty on the rate is clearly smaller when using pull-validation. Consequently, the distribution of any variable in the final sample will show a smoother behavior than without pull-validation.

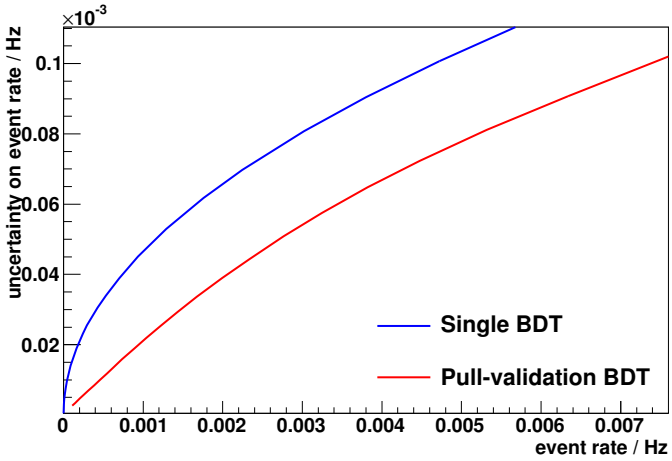

Figure 5: The uncertainty of the background rate versus the rate itself for varying cut values. The uncertainties were calculated as the square root of the sum of the squared weights. Using pull-validation, the uncertainties are significantly smaller than for a cut on a single BDT. The reason is that more events contribute to the final sample.

3. Manual

This section provides some information, that will help implement pull-validation in an analysis.

3.1 Prerequisites

Pull-validation can be used in combination with an MVA that is applied at any stage of an analysis, e.g. for preselections or the final event selection. Of course the computational effort is smaller at later stages, after some preselections have been applied to the data sets. However, some requirements must be fulfilled in all use cases. Then, ideally, pull-validation has the power to handle data with more than an order of magnitude missing simulation statistics. This was successfully tested in the applications described in the next chapter.

At first, the preselection of the events used for pull-validation and the BDT have to be tuned carefully in parallel. A critical issue is that pull-validation, as well as other methods, can not handle unknown (i.e. not simulated) event types. This can be checked by comparing the distributions of physical variables after the pull-validation using the calculated weights.

The interpretation of an MVA output is not straightforward. However, since the input variables have a physical meaning it can be interpreted with some experience. For example, a change of slope in a BDT distribution can be caused by an additional event type. This knowledge can be used to manipulate the result of pull-validation to strengthen its effect even further. This is for example useful if the available statistics for one type of background is much lower than for other background contributions. The event selection and the choice of variables for the BDT can be adjusted to strongly reduce the rate of this background type so that the other event types will compose the

dominating background. Consequently, it is not necessary to calculate the rate of the insufficiently simulated event type directly as this procedure assures that its contribution is negligible.

3.2 Choice of input variables

The variables for pull-validation have to be chosen carefully. The agreement between simulation and data must be excellent since small deviations might be multiplied due to the pull-validation procedure. The optimal number of variables may be higher than without using pull-validation. These training variables should have small correlations and describe the physics well, so that the output is reliable.

3.3 Definition of subsamples

For pull-validation, a comparably small subsample should be chosen (e.g. 10%). The small training sample leads to a large extrapolation of the tails of the BDT score distribution. In addition, this reduces correlation effects because the overlap of the subsamples is smaller. The number of subsamples has to be sufficiently large, so that additional repetitions would not change the result. For the analyses described in Section 4, the choice of 200 repetitions fulfills these requirements.

Once the pull-validation procedure has been applied, typically a cut on the result will be chosen. For the optimal choice of a cut value, a few criteria have to be kept in mind. The looser the cut is, the more reliable is the estimation achieved by pull-validation, i.e. the relative rate uncertainty is smaller. However, uncertainties of the order of 100% are manageable with this method. The number of events contributing at least partially to the final event rate decreases the statistical uncertainty. Another useful statistical check is how much every remaining event contributes to the rate if it had never been simulated. Pull-validation could be sensitive to systematic uncertainties due to the chosen variables which has to be checked and avoided.

3.4 Unblinding test

To prevent bias, the analyses of the IceCube collaboration are built on simulation. Only 10% of recorded data (the so-called burn sample) are typically used to validate the simulation sets. After the event selection is finalized, the remaining 90% of data are unblinded and used to calculate the result. As the optimization of the pull-validation is tested on the burn sample only, it is useful to check with a mock-unblinding if it is valid for the complete dataset. The burn sample is reduced to 10% of the original burn sample. The event selection, pull-validation and sensitivity calculation (including uncertainties) are finalized on this choice and then the other 90% of the sample are unblinded. This should give a rate in the calculated confidence interval, mostly near the estimated rate.

3.5 Overtraining check

Like for all supervised learning techniques, overtraining checks have to be performed when using pull-validation. In general, the risk of overtraining increases when reducing the size of the training data set. However, while individual BDT may be trained on statistical fluctuations, these effects will be averaged out by combining all BDTs. Figure 6 shows the score distributions of 200 BDTs for the complete training set and for an independent dataset. It can be seen that overtraining effects do not appear, if all BDTs are taken into account.

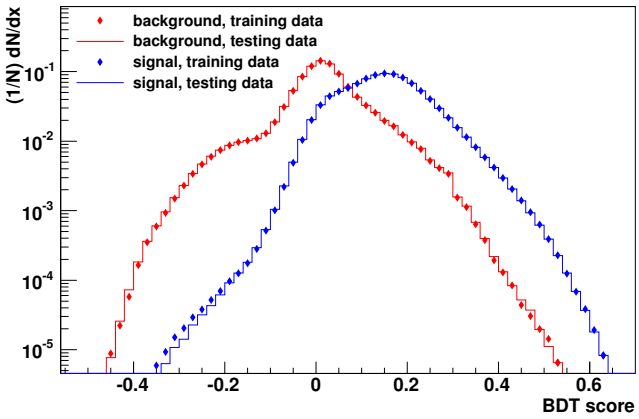

Figure 6: Overtraining test: the combined distributions of all 200 BDTs for the training set and for the testing set do not differ significantly. Possible overtraining in individual BDTs are averaged out.

3.6 Discrimination power

It is expected that the pull-validation technique does not suffer from a reduction in discrimination power compared to a classical training of a single BDT, if for both methods the same features and the same amount of data were used for training. This is indeed the case, as can be seen in Figure 7, which shows the background reduction versus the signal efficiency for a classical cut and for pull-validation event selection.

4. Applications to IceCube analyses

Pull-validation was already used in several analyses within the IceCube Collaboration. The method was first described and used in an IceCube unfolding analysis of the energy spectrum of atmospheric muon neutrinos [6]. In this analysis, a sample of very high signal purity is prepared by the event selection. The the quality of the unfolding that is based on this sample can be improved by smoother input distributions, which is achieved by introducing pull-validation to the analysis. The power of this method could be proven and a comparison with cross-validation showed the sanity of the results.

A second analysis is the search for magnetic monopoles [7], which would be a very rare signal in the IceCube detector. This analysis crucially depends on pull-validation and therefore the method was thoroughly checked as described in section 3. The final background rate after unblinding could be estimated successfully.

Finally, the plots throughout this paper are from a search for neutrinos from annihilating dark matter inside the Earth [2]. As this analysis relies on background simulations, a detailed understanding of systematic uncertainties is required. Therefore large enough statistics are necessary in the simulated data sets. The analysis benefits from the increased usage of background statistics by utilizing pull-validation, as shown in Figure 5.

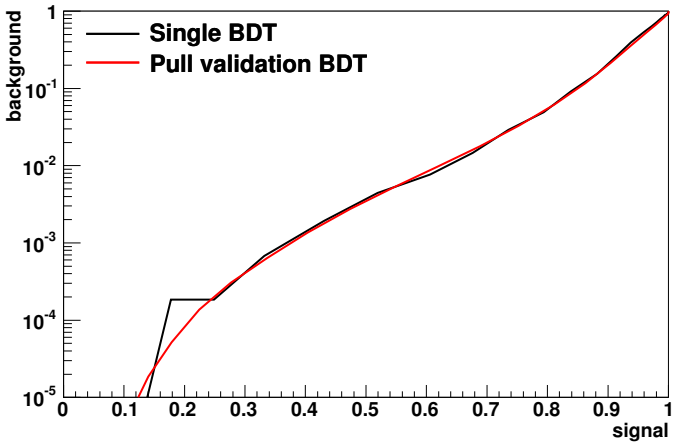

Figure 7: Receiver operating characteristic (ROC) plot. For a given signal efficiency, the background reduction is identical for the classical one BDT and for 200 BDTs. The step at hard cuts for the single BDT is due to low statistics for background estimation. This problem is reduced for pull validation.

5. Summary

Pull-validation is an efficient way to reduce the problem of sparse statistics. By estimating uncertainties of the scores and interpreting their distributions as a PDF, a weight can be calculated that replaces classical binary decisions of event selection. Consequently, more events contribute to the final sample and the statistical uncertainties are considerably reduced without reducing the discriminating power. Additionally, the estimated uncertainties can be taken into account as systematical errors.

References

[1] J. Quinlan, Mach. Learn., Vol.1, No.1 (1986), 81-106.

[2] IceCube Coll., PoS(ICRC2015)1205, these proceedings.

[3] P. Lachenbruch, M. Mickey, Technometrics, Vol.10,No.1 (1968), 1-11.

[4] B. Efron, Annals of Statistics, Vol 7, No.1 (1979), 1-26.

[5] A. Achterberg et al., Astropart.Phys. 26 (2006), 155.

[6] F. Scheriau, Dissertation, Universität Dortmund (2014).

[7] IceCube Coll., PoS(ICRC2015)1061, these proceedings.

PROCEEDINGS OF SCIENCE

Searching for neutrinos from dark matter annihilations in (dwarf) galaxies and galaxy clusters with IceCube

The IceCube Collaboration[†],

[†] *http://icecube.wisc.edu/collaboration/authors/icrc15_icecube*

E-mail: meike.de.with@desy.de

In many models, the self-annihilation of dark matter particles will create neutrinos which can be detected on Earth. An excess flux of these neutrinos is expected from regions of increased dark matter density, like (dwarf) galaxies and galaxy clusters. The IceCube neutrino observatory, a cubic-kilometer neutrino detector at the South Pole, is capable of detecting neutrinos down to energies of the order of 10 GeV and is therefore able to constrain the self-annihilation cross section as a function of the mass of the dark matter particle. This work will present the analysis method and results obtained from the first search for dark matter annihilations in (dwarf) galaxies and galaxy clusters with the complete IceCube detector.

Corresponding authors: M. de With[*1], E. Bernardini[1]

[1] *DESY, D-15735 Zeuthen, Germany*

The 34th International Cosmic Ray Conference,
30 July- 6 August, 2015
The Hague, The Netherlands

[*]Speaker.

1. Introduction

There are many observations which imply the existence of a new type of non-baryonic, non-visible and (meta)stable matter, usually called dark matter (for a review, see e.g. [1]). The currently most favoured candidates are Weakly Interacting Massive Particles (WIMPs), which are predicted by many theories for Beyond the Standard Model physics, for example supersymmetry and theories with extra dimensions. Typical masses are approximately between 10 GeV and 100 TeV.

So far only the gravitational effects of dark matter have been detected, but many experiments are searching for other signatures, both to confirm the gravitational observations and to study the properties of this new type of matter, which are so far mainly unknown. For example, indirect detection experiments search for a flux of stable particles produced in the self-annihilations or decays of WIMPs. The analysis described in these proceedings is a search for neutrinos produced in dark matter annihilations in dwarf galaxies in the Northern Hemisphere, the M31 galaxy and the Virgo cluster, using three years of data from the completed IceCube detector.

IceCube is a cubic-kilometer neutrino detector installed in the ice at the geographic South Pole [2] between depths of 1450 m and 2450 m. Detector construction started in 2005 and finished in 2010, and for this analysis data taken between May 2011 and May 2014 were used, with a total of 982.6 days of livetime. Neutrino reconstruction relies on the optical detection of Cherenkov radiation emitted by secondary particles produced in neutrino interactions in the surrounding ice or the nearby bedrock. The DeepCore subarray as defined in this analysis includes 8 densely instrumented strings optimized for low energies plus 12 adjacent standard strings [3].

2. Signal expectation

The expected differential neutrino flux from dark matter annihilations is given by

$$\frac{d\phi_\nu}{dE} = \frac{\langle\sigma_A v\rangle}{4\pi \cdot 2m_\chi^2}\frac{dN_\nu}{dE}J(\Delta\Omega) \tag{2.1}$$

with $\langle\sigma_A v\rangle$ the velocity-averaged annihilation cross section, m_χ the mass of the WIMP and dN_ν/dE the WIMP annihilation spectrum. $J(\Delta\Omega)$ is the so-called (integrated) J-factor,

$$J(\Delta\Omega) = \int_{\Delta\Omega} d\Omega \int_{l.o.s.} \rho^2(l) dl \tag{2.2}$$

where l is the coordinate along the line of sight, ρ is the dark matter density and $\Delta\Omega$ is the solid angle being integrated over.

The WIMP annihilation spectrum dN_ν/dE depends heavily on the specific annihilation channels of the WIMP and their branching ratios. For this model-independent analysis, we have studied four benchmark channels (neutrinos, muons, W bosons and b quarks) which are typical for many models and in each case assumed a 100% branching ratio to this channel. For each of these channels (where possible) we have considered 19 WIMP masses ranging from 30 GeV to 100 TeV.

For annihilation to neutrinos, dN_ν/dE is a line spectrum at $E_\nu = m_\chi$, since the WIMPs are assumed to annihilate at rest. For the other channels, the annihilation spectra were computed using Pythia 8.1 [4]. Since the region in which neutrinos are produced is much larger than the typical neutrino oscillation length, the spectra at the Earth can be averaged and are no longer dependent on

Targets	Type	RA [deg]	Dec [deg]	Distance [kpc]	$\log_{10}(J_{NFW}$ / GeV^2 cm$^{-5})$
Segue 1	Dwarf galaxy	151.767	16.082	23	19.5 ± 0.29
Ursa Major II	Dwarf galaxy	132.875	61.310	32	19.3 ± 0.28
Willman 1	Dwarf galaxy	162.343	51.051	38	19.1 ± 0.31
Coma Berenices	Dwarf galaxy	186.746	23.919	44	19.0 ± 0.25
Draco	Dwarf galaxy	260.052	57.915	76	18.8 ± 0.16
M31	Major galaxy	10.685	41.269	785	19.2 ± 0.1
Virgo	Galaxy cluster	187.704	12.391	16800	18.5

Table 1: The list of targets considered in the analysis described in these proceedings, including their locations [7] and their distances and J-factors assuming an NFW dark matter profile [8, 9, 10]. For the Virgo cluster, no uncertainty on the J-factor is available.

the exact distance between the source and the Earth [5]. For each annihilation channel, neutrinos of all flavours will arrive at Earth, but for this analysis only muon neutrinos are considered, so only track-like events are used.

As a consequence of equations 2.1 and 2.2, the expected flux is highest in regions with a high dark matter density which are relatively close by. The J-factor will in general depend on the dark matter halo profile, in this analysis we consider the Navarro-Frenk-White (NFW) profile [6], which is given by

$$\rho(r) = \frac{\rho_0}{\frac{r}{R_s}\left(1+\frac{r}{R_s}\right)^2} \tag{2.3}$$

with ρ_0 and R_s the characteristic density and radius.

Dwarf spheroidal galaxies orbiting the Galaxy are interesting targets for indirect dark matter searches because they are close to the Earth (see table 1), highly dark-matter-dominated and have no expected astrophysical backgrounds [11]. In this analysis, the five dwarf galaxies in the Northern Hemisphere with the highest J-factors are considered: Segue 1, Ursa Major II, Willman 1, Coma Berenices and Draco.

In addition to the dwarf galaxies, we also consider the M31 galaxy and the Virgo cluster. As can be seen from table 1, the J-factors for these targets are smaller than for the best dwarf galaxies, leading to a lower sensitivity. However, from N-body simulations [12, 13] it is known that dark matter haloes for major galaxies and galaxy clusters are expected to contain a large amount of substructure, which could increase the expected flux significantly, especially at larger distances from the center of the dark matter halo. Initial estimates for the total size of this increase were of the order of 1000 for galaxy clusters [14], but later studies give more modest estimates [15, 16]. Since the subhaloes are also expected to change the spatial shape of the dark matter profile, we will give limits for the conservative case where there is no significant substructure and the dark matter profile is given by equation 2.3, but we will also search for an extended emission from the direction of M31 and the Virgo cluster.

3. Event selection and reconstruction

The main backgrounds for neutrinos produced in dark matter annihilations are atmospheric muons (triggering the detector at a rate of approximately 2.5 kHz) and atmospheric neutrinos (approximately 20 mHz). Atmospheric neutrinos are an irreducible background, but atmospheric muons can be eliminated from the event sample by removing events which are either downgoing or badly reconstructed. It is also possible to remove atmospheric muons by using the outer layers of IceCube as a veto.

The first set of cuts consists of a number of online filters which select either track-like events, upgoing events or low-energy events where there is no evidence of activity in the detector which would be consistent with an atmospheric muon. These are followed by cuts which remove downgoing events, badly reconstructed events, noise events and events which do not contain enough information for a full direction reconstruction.

The sample is then split in two independent subsamples: one containing events which mostly take place in the DeepCore subdetector (the DeepCore-dominated subsample), and one containing all other events (the IceCube-dominated subsample). For each of these subsamples, a number of further cuts related to the quality of the reconstruction and the light pattern in the detector are made.

The final step of the event selection consists of a cut on the output of a Boosted Decision Tree (BDT) [17]. A BDT is a multivariate machine learning algorithm which is trained to separate signal and background events using training samples of both (which are discarded for the actual analysis). For the DeepCore-dominated subsample, the BDT was trained on 500 GeV WIMPs annihilating to b quarks. For the IceCube-dominated subsample, one BDT was trained on 500 GeV WIMPs annihilating to muons (the 'soft BDT') and one was trained on 10 TeV WIMPs annihilating to muons (the 'hard BDT'). For each target, the final cut on the BDT output score is optimized for the best sensitivity to $\langle \sigma_A v \rangle$. Also, for each combination of a target, a WIMP mass and an annihilation channel, the sensitivities using the hard BDT and using the soft BDT are calculated. In this analysis, we choose whichever one gives the best sensitivity.

The direction reconstruction used for this analysis is described in detail in section 2.1 of [18]. The resulting median angular resolution for different signal samples is shown in figure 1 for simulated signal events passing the event selection up to the final level, using a typical cut on the output of the final-level BDT. A per-event estimation of the angular reconstruction error is also calculated [19].

To reconstruct the energy of the event, different algorithms are used for the IceCube-dominated sample (which contains mainly events above 100 GeV) and the DeepCore-dominated sample (which contains mainly events below 100 GeV). For the IceCube-dominated sample, an algorithm is used which reconstructs the energy loss of the muon in the detector [20], while for the DeepCore-dominated sample, a dedicated low-energy reconstruction algorithm is used [21]. In both cases only the difference in the distributions of output values for signal and background is used, not the absolute output values.

4. Analysis method

After the event selection, the event sample consists mainly of atmospheric neutrinos, with

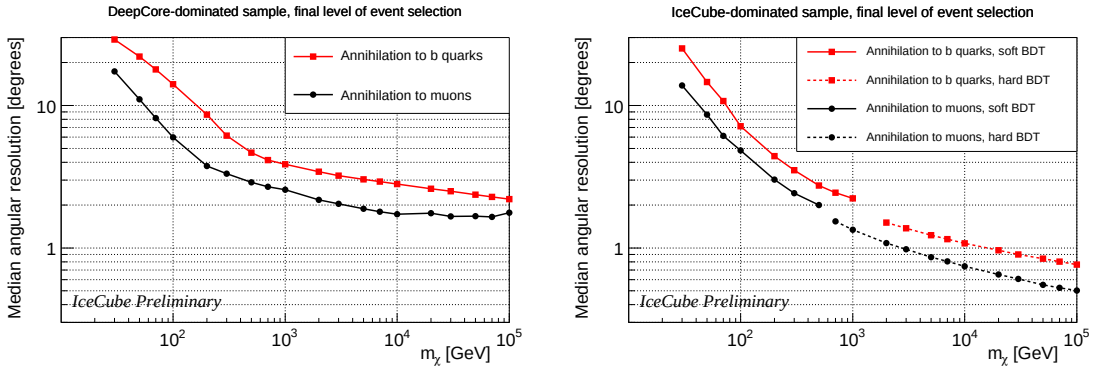

(a) DeepCore-dominated (b) IceCube-dominated

Figure 1: The median angular resolution for different WIMP masses and annihilation channels, using simulated signal events passing the event selection up to the final level, using a typical cut on the output of the final-level BDT. For (b), the sample selected by cutting on the output of the soft BDT is used for masses where the soft BDT gives the better sensitivity to $\langle \sigma_A v \rangle$, otherwise the sample selected by cutting on the output of the hard BDT is used.

a contamination of approximately 10 % (depending on subsample and BDT cut) of atmospheric muons. To determine whether the sample contains neutrinos from dark matter annihilations taking place in the targets that are considered in this analysis, a likelihood method is used which is based on that used in [22], but takes into account the general improvement suggested in [23]. The likelihood for a single sample containing n_{obs} events, of which μ are signal events, can be written as

$$\mathscr{L}(\mu) = \prod_{i=1}^{n_{obs}} \left(\frac{\mu}{n_{obs}} S_i + \left(1 - \frac{\mu}{n_{obs}}\right) B_i \right) \tag{4.1}$$

with the signal PDF S_i for an event with space angle (angle between the reconstructed muon direction and the target direction) ψ_i, reconstructed energy E_i and direction reconstruction error estimate σ_i given by

$$\begin{aligned} S_i(\psi_i, E_i, \sigma_i) &= f_{sig}(\psi_i|\sigma_i) \cdot g_{sig}(E_i, \sigma_i) \\ &= \frac{\psi_i}{\sigma_i^2} \exp\left(-\frac{\psi_i^2}{2\sigma_i^2}\right) \cdot g_{sig}(E_i, \sigma_i) \end{aligned} \tag{4.2}$$

with $f_{sig}(\psi_i|\sigma_i)$ the probability for signal events to have a space angle ψ_i given that the direction reconstruction error estimate is σ_i, which is assumed to follow a two-dimensional Gaussian distribution with a width given by σ_i. $g_{sig}(E_i, \sigma_i)$ is the probability for a signal event to have a reconstructed energy E_i and error estimate σ_i. This is taken from simulated signal events and smoothed using Kernel Density Estimation [24, 25].

The background PDF is given by

$$B_i(\psi_i, E_i, \sigma_i) = f_{bg}(\psi_i) \cdot g_{bg}(E_i, \sigma_i) \tag{4.3}$$

where $f_{bg}(\psi_i)$ and $g_{bg}(E_i, \sigma_i)$ are taken from data events where the azimuth has been randomized, and g_{bg} is smoothed in the same way as g_{sig}. Background events are isotropic, so ψ_i is not correlated with σ_i or E_i.

For this analysis, only events where the difference between the reconstructed zenith and the zenith of the target is less than 2.5 degrees (for the dwarf galaxies) or 5 degrees (for the M31 galaxy and the Virgo cluster) are considered, since events which are further from the target are very unlikely to be signal events. The PDFs are constructed using only events in these zenith bands, and thus are not only different for each WIMP mass and annihilation channel (in case of the signal PDFs) but also for each target.

For multiple independent subsamples, equation 4.1 is adapted to

$$\mathscr{L}(\mu) = \prod_{j=1}^{n_{samp}} \prod_{i=1}^{n_{obs,j}} \left(\frac{\mu_j}{n_{obs,j}} S_{j,i} + \left(1 - \frac{\mu_j}{n_{obs,j}}\right) B_{j,i} \right) \tag{4.4}$$

where j runs over the different subsamples, the PDFs are now (in general) different for each sample, and the total number of signal events in all subsamples combined is $\mu = \sum_j \mu_j$.

For this analysis, the DeepCore-dominated and IceCube-dominated subsamples are independent, as are the three years of data-taking. We also stack the five dwarf galaxies by considering them as subsamples, which are indeed independent since the zenith bands do not overlap.

We obtain a best estimate for μ for each WIMP mass and annihilation channel by maximizing the likelihood given in equation 4.4. Using the method of Feldman and Cousins [26], confidence intervals on the number of signal events present in the total sample and thus on the velocity-averaged annihilation cross section can be constructed.

As mentioned in the introduction, we also search for a more extended emission from M31 and the Virgo cluster, which could be caused by dark matter substructure. As the specific profile and extension are unknown, we consider two-dimensional Gaussian source profiles with widths 0.5, 1, 2 and 5 degrees. In this case, the two-dimensional Gaussian distribution used as $f_{sig}(\psi_i|\sigma_i)$ in equation 4.2 is convolved with the source profile, and the result is used as $f_{sig}(\psi_i|\sigma_i)$ instead.

5. Results and conclusion

For the first time, data from the completed IceCube detector has been used to search for neutrinos produced in dark matter annihilations in nearby extra-Galactic objects. No significant excess of neutrinos was found in the direction of any of the targets that were considered, and upper limits at the 90 % confidence level were calculated. In figure 2a the sensitivities and limits are compared for the stacking of five dwarf galaxies, the M31 galaxy and the Virgo cluster, for annihilation to muons. In figure 2b, the limits for different annihilation channels are compared.

Since the background for this analysis was determined directly from data, only systematic uncertainties on the signal acceptance play a significant role. These are dominated by the uncertainty on the sensitivity of the PMTs used for detecting the Cherenkov light and the optical properties (scattering and absorption lengths) of the ice. To get the total systematic uncertainty, these are varied by 10 % and the resulting uncertainties are added in quadrature. The total systematic uncer-

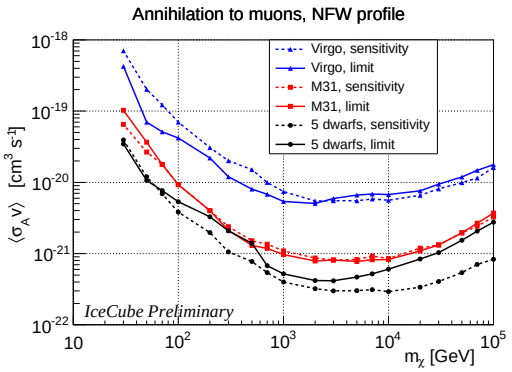

(a) Comparison of upper limits and sensitivities for the stacking of five dwarf galaxies, the M31 galaxy and the Virgo cluster, for annihilation to muons.

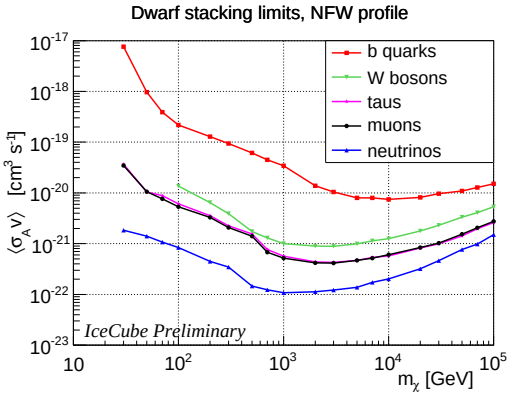

(b) Comparison of upper limits for the different annihilation channels considered in this analysis, for the stacking of five dwarf galaxies.

Figure 2: The 90 % confidence limits on the velocity-averaged annihilation cross section.

tainty which is included in the limits ranges from approximately 15 % to 35 %, depending on the source, WIMP mass and annihilation channel.

For the stacking of five dwarf galaxies, there is an overfluctuation for high WIMP masses which shows up for all channels and a broad range of masses, as the PDFs look relatively similar. To estimate the global significance of this excess, a test statistic is used which is defined as

$$TS = 2\log\frac{\mathscr{L}(\hat{\mu})}{\mathscr{L}(0)} \tag{5.1}$$

with $\hat{\mu}$ the best fit value for μ. A large number of pseudo experiments using data events with randomized azimuths were performed, and for 4.3 % of these background-only pseudo experiments, there was at least one WIMP mass and channel combination with a higher TS. This makes it clear that the excess is not statistically significant.

Searching for an extended neutrino emission from M31 and the Virgo cluster also led to no significant excess, so all results of this analysis are compatible with the background-only hypothesis.

References

[1] G. Bertone, D. Hooper, and J. Silk, *Physics Reports* **405** (2005) 279–390.

[2] **IceCube** Collaboration, A. Achterberg et al., *Astroparticle Physics* **26** (2006), no. 3 155–173.

[3] **IceCube** Collaboration, R. Abbasi et al., *Astroparticle Physics* **35** (2012), no. 10 615–624.

[4] T. Sjöstrand, S. Mrenna, and P. Skands, *Computer Physics Communications* **178** (2008), no. 11 852–867.

[5] S. Bilenky and S. Petcov, *Reviews of Modern Physics* **59** (1987), no. 3 671–754.

[6] J. Navarro, C. Frenk, and S. White, *The Astrophysical Journal* **490** (1997), no. 2 493.

[7] SIMBAD catalog, http://simbad.u-strasbg.fr/simbad/.

[8] **Fermi-LAT** Collaboration, M. Ackermann et al., *Physical Review D* **89** (2014), no. 4 042001.

[9] A. Tamm et al., *Astronomy & Astrophysics* **546** (2012) A4.

[10] J. Han et al., *Monthly Notices of the Royal Astronomical Society* **427** (2012), no. 2 1651–1665.

[11] M. Mateo, *Annual Review of Astronomy and Astrophysics* **36** (1998) 435–506.

[12] V. Springel et al., *Monthly Notices of the Royal Astronomical Society* **391** (2008), no. 4 1685–1711.

[13] J. Diemand et al., *Nature* **454** (2008), no. 7205 735–738.

[14] L. Gao et al., *Monthly Notices of the Royal Astronomical Society* **419** (2012), no. 2 1721–1726.

[15] D. Anderhalden and J. Diemand, *Journal of Cosmology and Astroparticle Physics* **2013** (2013), no. 04 009.

[16] M. Sánchez-Conde and F. Prada, *Monthly Notices of the Royal Astronomical Society* **442** (2014), no. 3 2271–2277.

[17] Y. Freund, R. Schapire, and N. Abe, *Journal - Japanese Society for Artificial Intelligence* **14** (1999).

[18] **IceCube** Collaboration, M. Aartsen et al., *The Astrophysical Journal* **796** (2014), no. 2 109.

[19] T. Neunhöffer, *Astroparticle Physics* **25** (2006), no. 3 220–225.

[20] **IceCube** Collaboration, M. Aartsen et al., *Journal of Instrumentation* **9** (2014), no. 03 03009.

[21] **IceCube** Collaboration, M. Aartsen et al., *Physical Review D* **91** (2015), no. 7 072004.

[22] J. Braun et al., *Astroparticle Physics* **29** (2008), no. 4 299–305.

[23] G. Punzi, *Comments on likelihood fits with variable resolution*, 2004. arXiv:physics/0401045.

[24] M. Rosenblatt, *The Annals of Mathematical Statistics* **27** (1956), no. 3 832–837.

[25] E. Parzen, *The Annals of Mathematical Statistics* **33** (1962), no. 3 1065–1076.

[26] G. Feldman and R. Cousins, *Physical Review D* **57** (1998), no. 7 3873.

PROCEEDINGS OF SCIENCE

All-Flavor Searches for Dark Matter with the IceCube Neutrino Observatory

The IceCube Collaboration[†],

[†] http://icecube.wisc.edu/collaboration/authors/icrc15_icecube

E-mail: klaus.wiebe@uni-mainz.de

Dark matter particles can be trapped in massive celestial bodies, such as the Sun or the Earth and their self-annihilations may produce standard model particles, including neutrinos of all flavors. So far, IceCube dark matter searches have focused on muon neutrinos due to their track-like topology and the resulting good pointing resolution. However, recent developments of reconstruction tools have allowed us to reconstruct electron and tau neutrino interactions with sufficiently good angle and energy resolutions and to estimate the corresponding uncertainties. IceCube's in-fill array DeepCore, when using the outer IceCube detector as a veto, permits us to extend all-flavor dark matter searches to energies well below neutrino energies of 100 GeV. This is particularly important for the search of Weakly Interacting Massive Particles (WIMPs) that accumulate in the center of the Earth, as their annihilation rate is expected to be enhanced for WIMP masses around 50 GeV/c^2. All-flavor neutrino searches, in principle, enhance IceCube's sensitivity with respect to previous searches based solely on muon neutrinos. While this paper primarily focuses on demonstrating the applied methods, we will also present a sensitivity and discovery potential for an Earth WIMP search as well as data selection efficiencies for an ongoing solar analysis. We find that efficient neutrino flavor identification is challenging at low energies given that the signatures for tracks and showers are very similar. For the proposed event selection the signal rate increases by a factor of two. However, the worse angular resolution for cascades gives rise to a larger background in the signal region.

Corresponding authors: Klaus Wiebe*[1], Anna Steuer[1]

[1] *Institute of Physics, University of Mainz, Germany*

The 34th International Cosmic Ray Conference,
30 July- 6 August, 2015
The Hague, The Netherlands

*Speaker.

1. Introduction

The IceCube Neutrino Observatory, located at the geographic South Pole, consists of the IceCube neutrino telescope and the IceTop air shower array [1]. In the ice, a volume of one cubic kilometer is instrumented with 5160 digital optical modules (DOMs), deployed at depths between 1450 m and 2450 m. The denser low energy infill, DeepCore, considerably improves neutrino detection with energies below 100 GeV due to the higher sensor granularity and the veto capacity of the surrounding IceCube strings.

IceCube can detect all flavors of active neutrinos through Cherenkov light emission from secondary particles created when a neutrino interacts in the ice. The primary background in the search for neutrinos originates from cosmic ray hadronic air showers produced in the Earth's upper atmosphere. The decay of pions, kaons (and charmed mesons) results in a continuous stream of neutrinos and penetrating muons. High energy muons are capable of traveling long distances through matter before they eventually decay, resulting in a downgoing muon flux at the IceCube detector. In contrast to earlier solar analyses we do not restrict ourselves to periods where the Sun is below the horizon and the Earth forms a shield against cosmic ray muons. Instead we take advantage of IceCube's veto capabilities, which limits the accessible WIMP mass range below 1 TeV/c^2.

Muon neutrinos with extended track-like topologies are relatively easy to reconstruct with degree pointing precision. The reconstruction of electron and tau neutrino interactions, leaving cascade-like signatures in the detector, is more challenging. Due to this better angular resolution, Earth WIMP searches [2] as well as solar WIMP searches [3] with IceCube have until now aimed at extracting solely ν_μ events from the dataset. However, all-neutrino searches have become more important recently. The reasons are obvious [4]: the measured flux is enhanced, the neutrino energies may be determined to a better precision, backgrounds from atmospheric ν_e and ν_τ are smaller and cosmic ray muons tend to be rejected better by requiring that the events have a cascade-like signature.

This paper discusses a study of IceCube's sensitivity to WIMP annihilations in the centers of the Earth and Sun with an analysis that is sensitive to all flavors of neutrinos. The methods presented in sections 3 and 4 have been developed for application on one year of 86-string configuration IceCube data from the 2011 season. Note that while both Earth and Sun may trap WIMPs, only the Sun is expected to be in an equilibrium making the annihilation rate directly proportional to the WIMP-Nucleon scattering cross section. The lower mass of the Earth prohibits this equilibrium in most cases. Similar to the moderation process in nuclear reactors, WIMPs are most efficiently slowed down if their energy is in the mass range of their nuclear scattering partners. As iron is very abundant in the Earth's core, 50 GeV/c^2 mass WIMPs are most easily captured, thereby enhancing the annihilation rate. For the simulation of a WIMP-induced neutrino signal we use the *WimpSIM* package [5], which takes care of neutrino generation, propagation and oscillations.

2. Low Energy Cascade Reconstruction

Unlike the extended tracks caused by muons from charged-current (CC) ν_μ events, ν_e and ν_τ leave an almost spherical pattern of hit DOMs in the detector. The $e^\pm$ produced in CC ν_e interactions are subject to successive bremsstrahlung energy losses and lead to electromagnetic cascades.

ν_τ interactions and τ decays predominantly produce hadronic cascades, as do neutral-current interactions from all neutrino flavors. While the energy reconstruction benefits from the confined event signature, a good directional reconstruction of the spherically shaped cascade events demands significant computing resources and also an excellent description of the ice properties [6]. Energy E, position and orientation are estimated [7] by minimizing the negative log-likelihood $-\ln L = \sum_i k_i \ln(E\Lambda_i + \rho_i) - (E\Lambda_i - \rho_i) - \ln k_i!$, where ρ_i is the expected number of noise photons. The number of photons per unit energy for an assumed orientation and vertex Λ_i incorporates detailed information on the position dependent absorption and scattering of photons in the ice. This information is available in the form of spline-fitted [8] tables obtained from a photon-tracking simulation using a ray tracing algorithm modeling scattering and absorption. When iterating the minimization chain (in this analysis 32 times) and optimizing minimization parameters, the resulting angular resolutions are similar to the ones seeded by the true direction and vertex.

The energy dependent median spatial angle resolution is shown in Fig. 1. The analyses presented in the following sections focus on rather low energies where the discussed methods are competitive, but an efficient particle identification of cascades and tracks is not possible. Therefore all flavors – including muon (see Fig. 1, solid orange line) – are first reconstructed with a cascade event hypothesis.

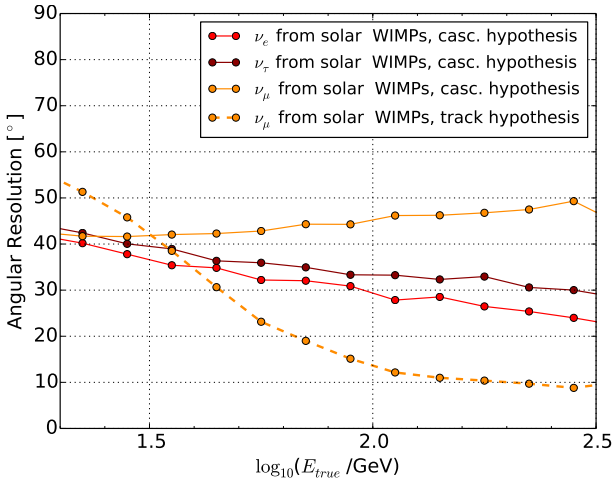

Figure 1: Angular resolution of the cascade reconstruction algorithm versus the energy of neutrinos. The resolution improves with energy for cascade signatures. For comparison, the dashed orange line shows the resolution potential for tracks reconstructed by an algorithm using the correct track hypothesis.

Individual event resolutions may vary from the average resolution (see Fig. 1) dependent on the event's exact topology and the amount of light deposited in the detector volume. Since event-based resolutions allow for a reconstruction quality based event weighting, a resolution estimator, based on the Cramer-Rao upper bound on the variance, was coded. Assuming a set of parameters $\vec{\theta} = (x_0, y_0, z_0, \theta, \phi)$, the vertex and directional angles, we formulate a Poissonian likelihood[1]

$$L(\vec{\theta}) = \prod_{i=1}^{\#\text{hitDOMs}} \left(\prod_{j=1}^{\text{nbins}(i)} \frac{\mu_\text{h}(\vec{\theta}, i, j)^{n(i,j)}}{n(i,j)!} \cdot \exp\left(-\mu_\text{h}(\vec{\theta}, i, j)\right) \right) \cdot \prod_{k=1}^{\#\text{nonhitDOMs}} \exp\left(-\mu_\text{nh}(\vec{\theta}, k)\right) \quad (2.1)$$

with μ_h being the expected number of photons in module i for time bin j (μ_nh for a non-hit module k respectively) and n the actually measured number of photons.

In order to obtain resolution expectations for individual cascades, one can either scan the likelihood around its minimum or take advantage of the Cramer-Rao bound. Under certain conditions,

[1] Similar to the likelihood formulated in the beginning of the section, but without explicit energy formulation and neglecting noise.

the latter provides the relation $(\mathrm{cov}^{-1})_{lm} = F_{lm} = -\left\langle \frac{\partial^2 \log L(\vec{\theta})}{\partial\theta_l \partial\theta_m} \right\rangle$, where F is the Fisher Information matrix, the inverse of the covariance matrix. Applying the second derivative and exploiting $\langle n(i,j)\rangle = \mu_h(\vec{\theta},i,j)$ we obtain:

$$F_{lm} = \sum_{i=1}^{\#\mathrm{hitDOMs}} \sum_{j=1}^{\mathrm{nbins}(i)} \frac{1}{\mu_\mathrm{h}(\vec{\theta},i,j)} \frac{\partial\mu_\mathrm{h}(\vec{\theta},i,j)}{\partial\theta_l} \frac{\partial\mu_\mathrm{h}(\vec{\theta},i,j)}{\partial\theta_m} + \sum_{k=1}^{\#\mathrm{nonhitDOMs}} \frac{\partial^2\mu_\mathrm{nh}(\vec{\theta},k)}{\partial\theta_l\partial\theta_m} \quad . \tag{2.2}$$

The expected value for the number of registered photons for DOM i and time bin j, $\mu_\mathrm{h}(\vec{\theta},i,j)$, is obtained from the spline fitted tables discussed above. In order to accelerate the algorithm, optical modules not hit and the actual amount of detected photons as well as their timing information are currently ignored. Standard deviations calculated from the diagonal entries of the covariance matrix correlate well with the actual resolutions. The estimate on the spatial resolution is approximated by $\sigma_\mathrm{spatial} = \sqrt{\sigma_\theta^2 + \left(\sigma_\varphi \cdot \sin\theta_\mathrm{reco}\right)^2}$, where $\sigma_{\theta/\varphi}$ are the zenith and azimuth uncertainties and θ_reco is the reconstructed zenith angle. Figure 2 shows the relation between the median resolution taken from the difference of reconstructed and true event direction and the estimate.

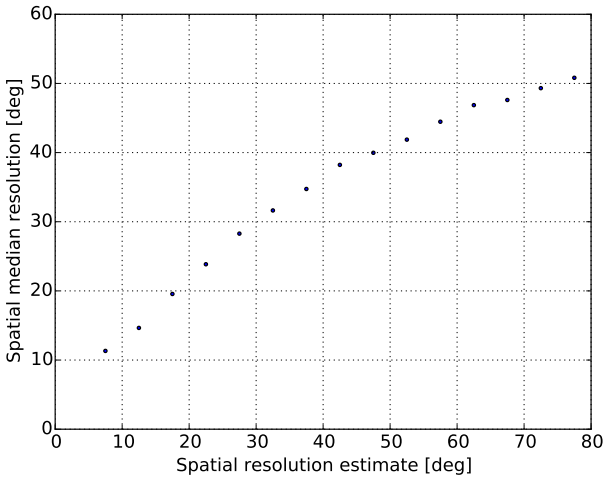

Figure 2: Cascade Resolution Estimator: a successful quantitative modeling of the actually achieved resolution.

3. Search for dark matter annihilation in the center of the Earth

As a test case, we restrict ourselves in this study to 50 GeV/c^2 WIMPs. This has the advantage that we can make use of the enhanced cross section. The disadvantage is that neutrinos from the annihilation are very low in energy and thus are at the threshold of detection. The most energetic neutrinos at these energies stem from the annihilation in tau pairs and for this reason we concentrate first on this channel. In order to extract this signal from the dataset, an event selection favoring potentially well reconstructed, low energetic neutrino events mainly from the northern hemisphere was developed. For example, the reconstructed energy was required to

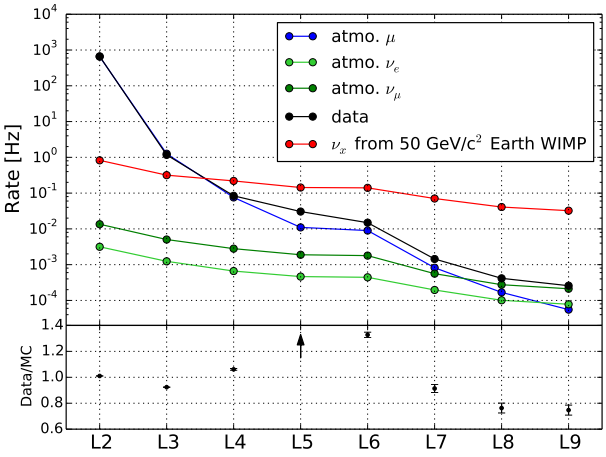

Figure 3: Rates of signal (arbitrarily scaled for comparison), background MC and data versus selection levels. The lower subplot shows the ratio of data over the sum of the background MC rates and its statistical uncertainty. The arrow indicates an outlier not visible at the scale chosen.

be in the 5 to 30 GeV range. This selection is subdivided into *levels*, each combining requirements pursuing a similar objective.

The progress with the selection levels of signal and background rates from Monte Carlo (MC) simulations and the data rates is shown in Fig. 3. *Data* here refers to a subset of the full experimental dataset[2]. The applied event selection achieves a signal efficiency of about 4% while the atmospheric muon background is reduced by seven orders of magnitude. As can be seen in the lower portion of Fig. 3, showing the data-MC-agreement, the data rate falls short of the MC rate by about 25% on the final selection level. Outliers on intermediate levels can mostly be explained by unsimulated noise. This discrepancy is removed by subsequent noise-rejecting vetos. The precise MC description of experimental data in the low energy regime is a non-trivial issue which is currently subject to collaboration-wide investigations.

Since the event simulation and the simulation of the detector response near the detector's energy threshold is challenging, the method to analyze a potential WIMP signal should not rely on precise MC background predictions. A further difficulty is the particle identification at very low energies as well as the directional reconstruction of low energy events in general and cascades in particular. A likelihood fitting procedure takes advantage of distinguishing features of cascade and track signatures and the angular distribution of signal and backgrounds. The basic input for the algorithm are two-dimensional histograms of two reconstructed zenith angles - one developed to reconstruct cascade-like events the other well suited for the reconstruction of tracks. For the case of signal events coming from the direction of the Earth's core, one would e.g. expect the cascade likelihood to recover the direction of the cascade-like events while the algorithm using the incorrect track hypothesis smears this directional peak. This concept also reveals distributional differences between atmospheric electron and muon neutrinos and discriminates the atmospheric muon background. In order to pass this distributional information efficiently to the fitter, the two-dimensional histograms are binned such that signal regions are well resolved while the background dominated parts are merged. For the sake of simplicity and in order to increase the MC statistics, the three signal channels are combined into one all-flavor flux χ. Fig. 4 shows a comparison of the histograms of WIMP-induced neutrinos and atmospheric neutrinos and demonstrates the discrimination potential of this method. The histogram for experimental data is analyzed by an algorithm maximizing the Poissonian likelihood

$$L = \prod_{\text{bins}} \frac{\lambda_i^{k_i}}{k_i!} e^{-\lambda_i} + \text{nuisance terms} \quad , \tag{3.1}$$

with the MC prediction

$$\lambda_\text{i} = \gamma \cdot \lambda_\text{i}^{\text{atmo. } \mu} + \Delta\text{r}_{\pi/\text{K},\nu_\mu} \cdot \mu \cdot \lambda_\text{i}^{\text{atmo. } \nu_\mu} + \Delta\text{r}_{\pi/\text{K},\nu_\text{e}} \cdot \varepsilon \cdot \lambda_\text{i}^{\text{atmo. } \nu_\text{e}} + \alpha \cdot \lambda_\text{i}^{\chi} \tag{3.2}$$

and data k_i in bin i and the physical fit parameter α revealing which annihilation rate is compatible with the experimental data. Nuisance parameters included in this likelihood account for the relevant systematic uncertainties. These are the absolute flux normalizations of the atmospheric backgrounds and the pion to kaon ratio in the generation of atmospheric neutrinos which is contained in the weight $\Delta r_{\pi/K,\nu_\ell}$ in Eq. 3.2. Thus, the final log-likelihood function, including Gaussian

[2] In IceCube, selection criteria are developed on typically 10% of the experimental data to avoid biased results.

penalty factors for the nuisance parameters, reads:

$$-\ln L = \sum_{\text{bins}} \lambda_i - k \cdot \ln \lambda_i + \frac{1}{2} \cdot \left(\frac{(\gamma-1)^2}{\sigma_\gamma^2} + \frac{(\mu-1)^2}{\sigma_\mu^2} + \frac{(\varepsilon-1)^2}{\sigma_\varepsilon^2} + \frac{(r-1)^2}{\sigma_r^2} \right) \quad . \tag{3.3}$$

The incorporated nuisance parameters together with their priors and uncertainties are summarized in Table 1.

uncertainty	nuisance parameter n	default value	σ_n
normalization of atmospheric μ	γ	1.0	0.3
normalization of atmospheric ν_μ	μ	1.0	0.3
normalization of atmospheric ν_e	ε	1.0	0.3
pion-kaon ratio	r	1.0	0.1

Table 1: Summary of the nuisance parameters explicitly implemented in the likelihood function together with their priors and uncertainties.

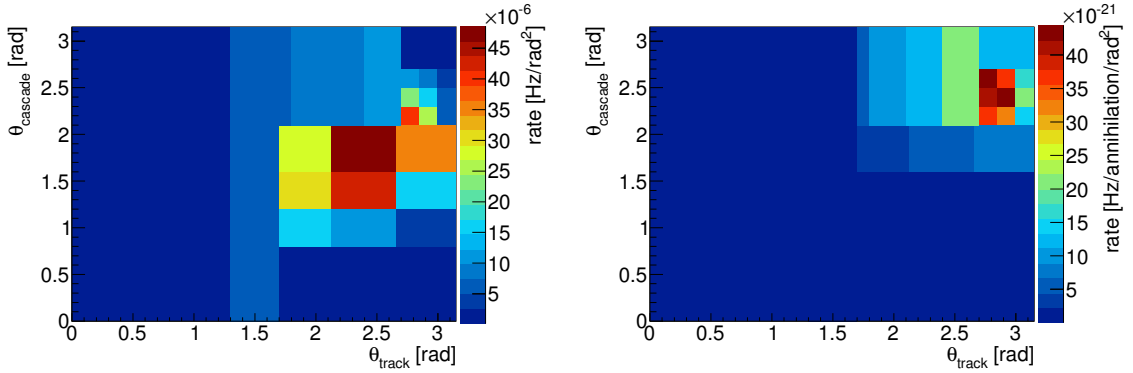

Figure 4: Two-dimensional histogram of reconstructed zenith angles with apt binning for atmospheric electron neutrinos (left) and for WIMP induced neutrinos (right). The bin contents are normalized to the bin size to emphasize the relative contributions.

To determine the sensitivity, evidence and discovery potential, a likelihood-ratio test is performed on simulated data using the test statistic $w = 2 \cdot \ln\left(\frac{\max L}{\max_{H_0} L}\right)$, where $\max_{H_0} L$ denotes the maximum likelihood under the null hypothesis while $\max L$ refers to the maximum likelihood under the alternative, i.e. signal, hypothesis. From the comparison of the test statistic distribution for many simulated data realizations containing a certain signal strength with simulated background only data realizations the sensitivity, evidence and discovery potential were calculated for one year of IceCube data (see Table 2).

Since the Earth is not expected to have reached equilibrium of WIMP capture and annihilation, the annihilation rate is not directly correlated with the WIMP-nucleon scattering cross section. For this reason, the sensitivities are given in terms of annihilation rates which maintains as much model independence as possible.

The sensitivity determined in this analysis is not competitive yet with a dedicated study for Earth WIMPs solely based on ν_μ events [2]. The implementation of multivariate techniques promises the required enhancement of the efficiency, as can be seen in the following section.

	annihilation rate [annihilations/s]
Sensitivity (90% Confidence Level)	$7.7{\cdot}10^{13}$
Evidence (3σ)	$1.7{\cdot}10^{14}$
Discovery Potential (5σ)	$2.2{\cdot}10^{14}$

Table 2: Sensitivity, evidence and discovery potential for one year of IceCube data taken with its 86-string configuration assuming a 50 GeV/c^2 mass WIMP annihilating into $\tau^+\tau^-$.

4. Search for dark matter annihilation in the center of the Sun

The indirect detection of solar WIMP particles with IceCube places some of the most stringent limits on the spin-dependent nucleon-WIMP scattering cross-section [9, 10]. Here we are exploring the capabilities of the all-flavor approach, by taking advantage of the cascade reconstruction methods discussed in section 2.

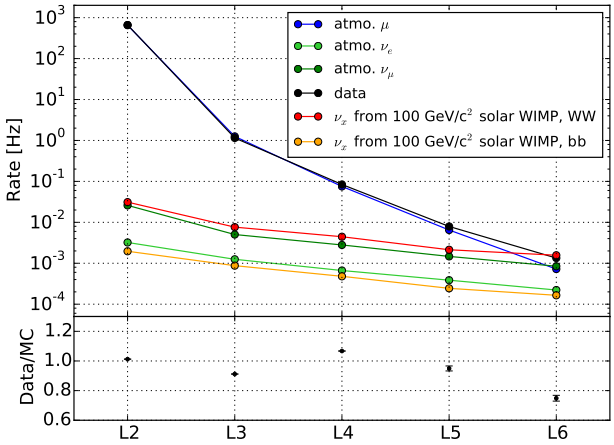

Figure 5: Data and Monte-Carlo (MC) rates versus selection level. The simulated all-flavor signal rate is shown for a 100 GeV/c^2 WIMP mass, arbitrarily scaled assuming 10^{25} annihilations/s. The bottom sub-plot shows the ratio of data and the sum of background MC including statistical uncertainties.

Figure 5 shows the development of data and MC rates throughout the event selection. For the signal MC, a showcase WIMP candidate mass of 100 GeV/c^2 is chosen, while the complete analysis will cover a candidate mass range from 50 to 1000 GeV/c^2. Cut levels 3 and 4 aim at significantly reducing the dominant background from atmospheric muons, followed by filters that effectively remove noise clusters and coincident events. Similar to the Earth WIMP analysis, we see differences between data and Monte Carlo which we suspect to be due to a non-perfect description of the optical module noise for the particular time period. Concerted efforts are under way in the collaboration to remedy this situation.

Candidate mass [GeV/c^2]	Hard channel efficiency (W$^+$W$^-$, $\tau^+\tau^-$ for 50 GeV/c^2 WIMPs) [%]	Soft channel efficiency ($b\bar{b}$) [%]
50	8.6 (ν_e: 7.5, ν_μ: 9.7, ν_τ: 7.5)	12.5 (ν_e: 10.5, ν_μ: 14.4, ν_τ: 9.7)
100	5.0 (ν_e: 4.5, ν_μ: 5.7, ν_τ: 4.5)	8.4 (ν_e: 7.2, ν_μ: 9.7, ν_τ: 7.0)

Table 3: Selection efficiencies

Following level 5, a set of Boosted Decision Trees (BDTs) is trained to discriminate signal-like from background-like events, leading to level 6 by selecting events with a BDT score larger than 0.04 (see Fig. 6). Twelve variables are used as BDT input, including reconstructed direction, energy and vertex, reconstruction quality parameters as well as veto and geometrical quantities. An overtraining check was performed, showing good agreement of training and testing score distributions. The efficiency at level 6, compared to level 2, is $\approx 10^{-6}$ for atmospheric muons and 5.0%

(8.4%) for signal neutrinos from the W^+W^- ($b\bar{b}$) channel. Signal efficiencies are shown in Table 3 and are competitive to the final-level efficiencies obtained with a track-based approach [10]. Ultimately, we want to include WIMP masses up to 1 TeV/c^2, but concentrate here on the low energetic 50 and 100 GeV/c^2 candidates.

For the determination of limits we will choose a likelihood approach [11] that will consider direction, directional uncertainty estimates as well as the reconstructed energy.

5. Conclusions

For the first time, an all-flavor analysis for WIMP searches has been made possible by the development of better angular reconstruction techniques for cascades at low neutrino energies. In order to limit the background from atmospheric muons, the analysis was restricted to events reconstructed in the volume of the DeepCore sub-array by exploiting the veto-capacity of the surrounding IceCube sensors. To maximize the selection efficiency, no flavor-separation – which is very difficult to achieve at low energies – was attempted. In the future, a combination of the different analysis strategies, especially for smaller candidate masses, should be considered.

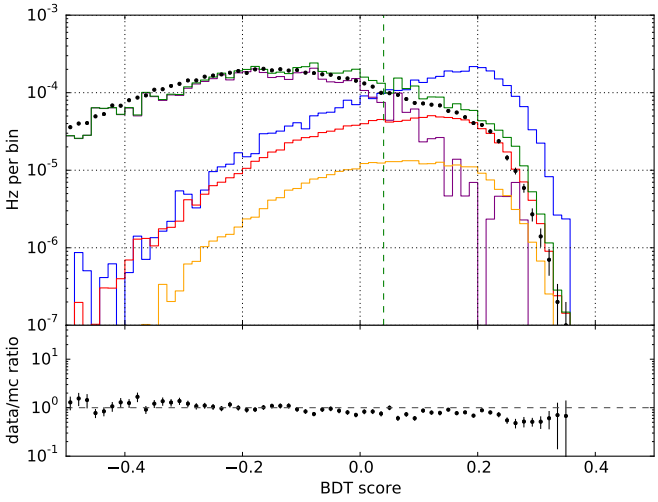

Figure 6: Score distribution after BDT training. Events with a spatial angle deviation from the solar position larger than 40 degrees are defined as "off-source". Such data (black) are used to train against the signal simulation (blue, shown here for a 100 GeV/c^2 candidate). We reserve 50% of the data and the Monte Carlo signal events for overtraining checks. Shown for comparison are atmospheric muons (purple) and ν_μ (ν_e) in red (orange). The total background MC rate is depicted in green. The vertical dashed line shows the applied cut value at a BDT score of 0.04.

References

[1] The IceCube Collaboration: A. Achterberg et al., *Astropart.Phys.* **26** (2006) 155 [arXiv:astro-ph/0604450]
[2] IceCube Coll., *A search for Dark Matter in the centre of the Earth with the IceCube neutrino detector*, PoS(ICRC2015)1205, these proceedings
[3] The IceCube Collaboration: M.G. Aartsen et al., *Phys. Rev. Lett.* **110** (2013) 131302 [arXiv:1212.4097]
[4] C. Rott, T. Tanaka and Y. Itow, *JCAP* **1109** (2011) 029 [arXiv:1107.3182]
[5] M. Blennow, J. Edsjö and T. Ohlsson, *JCAP* **0801** (2008) 021 [arXiv:0709.3898]
[6] The IceCube Collaboration: M.G. Aartsen et al., *Nucl.Instrum.Meth.* **A711** (2013) 73-89 [arXiv:1301.5361]
[7] The IceCube Collaboration: M.G. Aartsen et al., *JINST* **9** (2014) P03009 [arXiv:1311.4767]
[8] N. Whitehorn et al., *Comput.Phys.Commun.* **184** (2013) 2214-2220 [arXiv:1301.2184]
[9] IceCube Coll., *Search for Dark Matter annihilations in the Sun using the completed IceCube neutrino telescope*, PoS(ICRC2015)1209, these proceedings
[10] IceCube Coll., *Improved methods for solar Dark Matter searches with the IceCube neutrino telescope*, PoS(ICRC2015)1099, these proceedings
[11] IceCube Coll., *Results of neutrino point source searches with 2008-2014 IceCube data above 10 TeV*, PoS(ICRC2015)1047, these proceedings